Impacts of phytoplankton radiant heating on ocean structure and climate

A thesis submitted to the School of Environmental Sciences at the University of East Anglia in partial fulfilment of the requirements for the degree of Doctor of Philosophy

Siyu Meng

January 2026

Abstract

Chlorophyll, the primary light-absorbing pigment in phytoplankton, modulates the vertical distribution of solar radiation in the ocean. Despite growing evidence that chlorophyll-induced solar absorption affects ocean physics and climate, this process remains incompletely represented in Earth System Models (ESMs), and its implications for future climate are unclear. This thesis investigates the impacts of chlorophyll-induced solar absorption on ocean structure and climate across multiple spatial and temporal scales.

Contrasting thermal and dynamical responses to chlorophyll-induced solar absorption are found between Pacific and Atlantic eastern boundary coastal upwelling systems, based on an ocean–biogeochemistry coupled model. In the Pacific, shading by high surface chlorophyll reduces solar penetration into the ocean below, leading to colder subsurface waters that are subsequently upwelled and contribute to surface cooling, with enhanced stratification strengthening upwelling. In the Atlantic, solar absorption by a subsurface chlorophyll maximum leads to warmer and weaker upwelling.

Under climate warming, projected future chlorophyll decline reduces solar absorption within the mixed layer, redistributing $0.25\,\mathrm{W\,m^{-2}}$ of global-mean radiative flux below and delaying anthropogenic surface warming by up to 12 years. The uncertainty arises from inter-model differences in both simulated chlorophyll concentrations and their representation of solar absorption. Such differences also contribute to biases in the mean state of ESMs.

Based on ocean model projections, we further show that future chlorophyll decline leads to significant subsurface warming of 0.05–0.2 °C and changes the seasonal cycle of upper-ocean temperature. In addition, chlorophyll decline induces an El Niño–like response in the eastern equatorial Pacific, characterised by thermocline deepening and weakened equatorial circulation.

Overall, this thesis demonstrates that chlorophyll-induced radiative effects play a non-negligible role in regulating mean state and future change of climate, highlighting the need for improved representation of these processes in ESMs.

Contents

List of Figures

List of Tables

List of Abbreviations

AMOC	Atlantic Meridional Overturning Circulation
CDOM	Coloured Dissolved Organic Matter
CMIP	Coupled Model Intercomparison Project
CORE2	Version 2 forcing for the Coordinated Ocean–ice Reference Experiments
DIC	Dissolved Inorganic Carbon
ENSO	El Niño–Southern Oscillation
ESM	Earth System Model
IOD	Indian Ocean Dipole
MEDUSA	Model of Ecosystem Dynamics, nutrient Utilisation, Sequestration and Acidification
MLD	Mixed Layer Depth
MODIS	Moderate Resolution Imaging Spectroradiometer
NAP	Non-Algal Particles
NEMO	Nucleus for European Modelling of the Ocean
piControl	Pre-industrial Control Simulation
RGB	Red–Green–Blue
SeaWiFS	Sea-viewing Wide Field-of-view Sensor
SSH	Sea Surface Height
SSP	Shared Socioeconomic Pathway
SST	Sea Surface Temperature

Acknowledgements

Choosing to pursue my PhD at the University of East Anglia for four years has been one of the luckiest decisions of my life. I have been extremely fortunate to be guided by three supervisors who will continue to support and influence me throughout my life: Benjamin Webber, Manoj Joshi, and David Stevens.

Benjamin Webber has always been thoughtful and supportive, both in my research and throughout my PhD journey. He has guided me with great patience and care, always paying close attention to how I was doing and to my progress. In research, he has a remarkable ability to provide clear direction at the big-picture level, while also offering practical and insightful advice on the details when it matters most. When I first met Manoj Joshi, he came across as very serious, but as I got to know him better, I realised that he is not only an outstanding scientist, but also someone who feels like family. He has a deep understanding of science, and beyond research, he has always made me feel that he truly stands behind me, offering steady and reliable support whenever I need it. David Stevens has taught me an enormous amount through his extensive knowledge of mathematics and numerical modelling. Every discussion with him has been inspiring, and his enthusiasm and positive energy have consistently left me feeling motivated and encouraged.

I am also very grateful to Corinne Le Quéré, Andrew Yool, and Julien Palmieri for providing essential model and data support. I sincerely thank Philip Townsend for patiently teaching me how to run the models and for his continuous technical assistance. I also thank Timothy Osborn and Carol Robinson for their helpful feedback on the manuscript. This PhD was financially supported by the China Scholarship Council (CSC), which is gratefully acknowledged.

I would like to thank my office mates, Jessica Chapman, Beckie George, Manasa Sharma, Louisa Moor, Xiang Weng, Jack Heslop, and Widya Ayuningtiyas. Your companionship has been a tremendous source of motivation throughout my research journey. I am deeply thankful to my friends: Aparna Anitha Reghunathan, Shunan Fu, Amee Gollop, Mingliang Gu, Yunzhu He, Haoyu Jin, Yang Li, Yixuan Li, Eilean MacDonald, Nicole Forstenhaeusler, Chuang Sun, Xueqiong Sun, Qingru Wang, Xiangpeng Wang, Ruoting Xiong, Fulong Yao, Qianyu Zha, and Zhenzhen Zhang. Your friendship, encouragement, and the many experiences we have shared have meant more to me than words can express. I am especially grateful to Xiaoyu Zhu, my best flatmate for four years, who stood by me and supported me through the most difficult times of my PhD.

Finally, I owe my deepest gratitude to my parents and my sister. Your unconditional support has been the greatest source of strength that allows me to move forward without fear.

1

Introduction

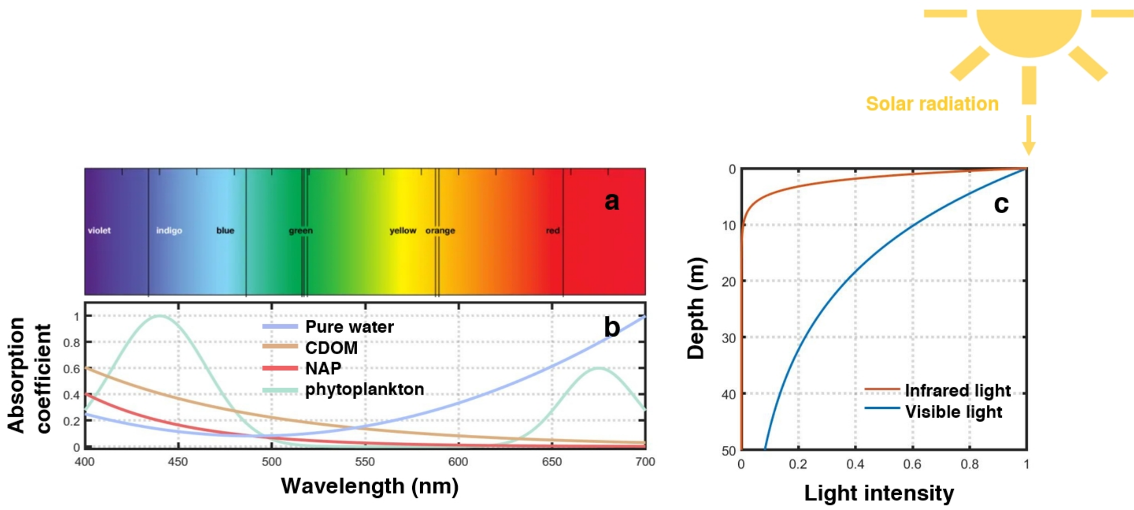

Figure 1.1: Absorption and penetration of solar radiation in the ocean. (a) The solar spectrum in the wavelength range 400–700 nm. (b) Spectral absorption by pure water, CDOM, NAP and phytoplankton, with absorption coefficients normalised by the maximum absorption over the full solar spectrum. (c) Schematic illustration of the depth-dependent attenuation of infrared and visible light in the upper ocean, with light intensity normalised by the surface irradiance. The above schematic is adapted from Bricaud et al. (1981); Sosik and Mitchell (1995); Pope and Fry (1997).

1.1 Phytoplankton and solar radiation absorption in the ocean

1.1.1 The role of the ocean in the Earth's energy budget

The global climate system is fundamentally governed by the balance between incoming solar radiation and outgoing terrestrial radiation. As the largest reservoir of heat on Earth, the ocean plays an essential role in regulating this planetary energy budget (Trenberth and Fasullo, 2010; Trenberth et al., 2014). Covering more than 70% of the Earth's surface, the ocean absorbs the majority of incoming shortwave radiation, particularly at low to mid-latitudes where solar insolation is strongest. In these regions, the low ocean surface albedo ($\approx$ 0.05–0.07) means that more than 90% of incident solar energy is absorbed rather than reflected (Coakley, 2003).

Absorbed solar energy is stored within the ocean's upper layer and redistributed through physical processes such as turbulent mixing (Whalen et al., 2012) and advective transport across multiple spatial scales, from submesoscale and mesoscale flows (Chelton et al., 2011) to large-scale circulation (Buckley and Marshall, 2016). This capacity to store and transport heat makes the ocean a key regulator of weather and climate across a range of temporal and spatial scales. On seasonal to interannual timescales, the ocean modulates surface temperature variability, while on longer timescales it acts as a key component of Earth's heat uptake associated with anthropogenic climate change (Durack et al., 2018).

The ocean's role in the Earth's energy budget is closely linked to its vertical structure. Unlike the land surface, where absorbed solar radiation is confined to a very shallow layer, solar radiation in the ocean can penetrate tens of metres into the water column, depending on water clarity and the presence of absorbing or scattering substances (Paulson and Simpson, 1977; Morel, 1988). In the upper ocean, wind forcing and surface buoyancy fluxes drive efficient vertical mixing, resulting in a layer characterised by a nearly uniform temperature profile known as the mixed layer. The vertical distribution of energy, especially within and below the mixed layer, affects the ocean's thermal structure and stratification (the degree to which density varies with depth and inhibits vertical mixing), thereby influencing ocean dynamics and atmosphere-ocean interactions. Consequently, understanding how the ocean absorbs and redistributes solar radiation vertically is essential for accurately characterising the global climate system and its energy transport.

1.1.2 Phytoplankton, chlorophyll and optical properties of seawater

Phytoplankton are photosynthetic microalgae that form the base of the marine food web and play an essential role in global biogeochemical cycles. Using incoming solar radiation, phytoplankton perform photosynthesis and convert CO_2 into organic carbon, a process commonly referred to as marine primary production. A key pigment that enables photosynthesis is chlorophyll, the primary photosynthetic pigment in marine phytoplankton, which captures light energy to drive the photochemical reactions of photosynthesis. Its concentration is also widely used as a first-order proxy for phytoplankton biomass.

Apart from the small fraction of solar radiation ($< 1\%$) used for photosynthesis, most incident solar energy is absorbed by seawater and converted into heat. The absorption of underwater solar radiation primarily depends on the properties of optically active substances, including pure seawater, Coloured Dissolved Organic Matter (CDOM), Non-Algal Particles (NAP) and phytoplankton pigments such as chlorophyll (Figures 1.1a and b). Pure seawater dominates absorption in the red and near-infrared wavelengths (Pope and Fry, 1997); CDOM absorbs strongly in the ultraviolet and blue part of the spectrum due to its high content of degraded organic compounds, including humic substances and fulvic acids derived from the breakdown of terrestrial and marine organic matter (Bricaud et al., 1981); NAP includes mineral particles (e.g., clays and silts) and organic detritus from the decomposition of phytoplankton and other organic matter, and it contributes a generally weaker absorption spectrum (Babin et al., 2003); Phytoplankton pigments, particularly chlorophyll, display characteristic absorption peaks in the blue (around 440 nm) and red (around 675 nm) wavelengths (Figure 1.1b). In the open ocean, phytoplankton pigments are a major absorber of visible light and therefore exert a dominant control on light absorption and penetration (Bricaud et al., 1995; Jerlov, 1968).

1.1.3 Penetration of solar radiation in the upper ocean

Incoming solar radiation reaching the ocean surface consists primarily of two spectral bands: the visible spectrum (400–700 nm) and the near-infrared spectrum (700–1400 nm). Although both spectral components attenuate exponentially in seawater following the Beer-Lambert law (Lambert, 1760), they differ notably in their attenuation rates and the substances that absorb them. The near-infrared component typically represents around 40–60 % of the total solar radiation flux, depending on the solar zenith angle and atmospheric conditions (Nalli et al., 2008), and is absorbed very rapidly by seawater within the upper few metres (Mobley, 1994). In contrast, the visible component penetrates much deeper into the water column and plays a central role in subsurface heating and marine photosynthesis (Figure 1.1c).

The penetration of visible light shows substantial spatial variability because it is strongly influenced by the concentration and composition of optically active substances in seawater. In coastal regions, where terrestrial inputs exert a strong influence on optical properties, visible light penetration is jointly controlled by CDOM, NAP and phytoplankton pigments (Bricaud et al., 1981; Babin et al., 2003). In the open ocean, however, light attenuation is governed primarily by phytoplankton pigments, with higher chlorophyll concentrations enhancing the absorption of solar radiation and reducing its penetration to depth (Morel, 1988). The chlorophyll-induced absorption of solar energy has important implications for underwater visibility, primary production, upper-ocean physics, air-sea interactions and climate (Paulson and Simpson, 1977; Manizza et al., 2005; Tian et al., 2021b; Asselot et al., 2022). Consequently, understanding the spatial and temporal variability of chlorophyll and its radiative effects is essential for characterising how solar radiation is absorbed in the water column and how this, in turn, influences ocean heat uptake, ocean physics and climate.

1.2 Phytoplankton feedbacks on the climate system

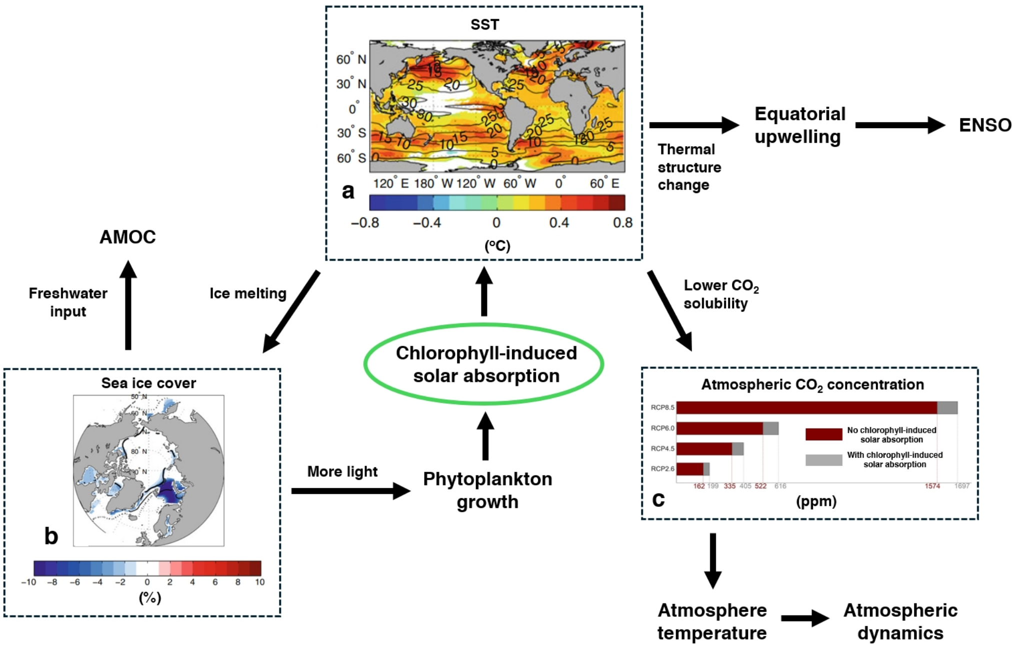

Figure 1.2: Schematic illustration of the impacts of chlorophyll-induced solar radiation absorption on the climate system. (a) Differences in SST between two numerical experiments: one in which simulated chlorophyll by a biogeochemical model modulates solar radiation absorption in an ocean physical model, and another using only an ocean physical model without chlorophyll-induced radiative effects. (b) As in (a), but showing differences in sea-ice cover in the Arctic region. (c) Atmospheric CO_2 concentrations from two ESM simulations, where dark red bars represent experiments without chlorophyll-induced solar absorption and grey bars represent experiments that include this effect. Panels (a-b) are from Patara et al. (2012), and panel (c) is from Asselot et al. (2024).

1.2.1 Ocean physical feedbacks

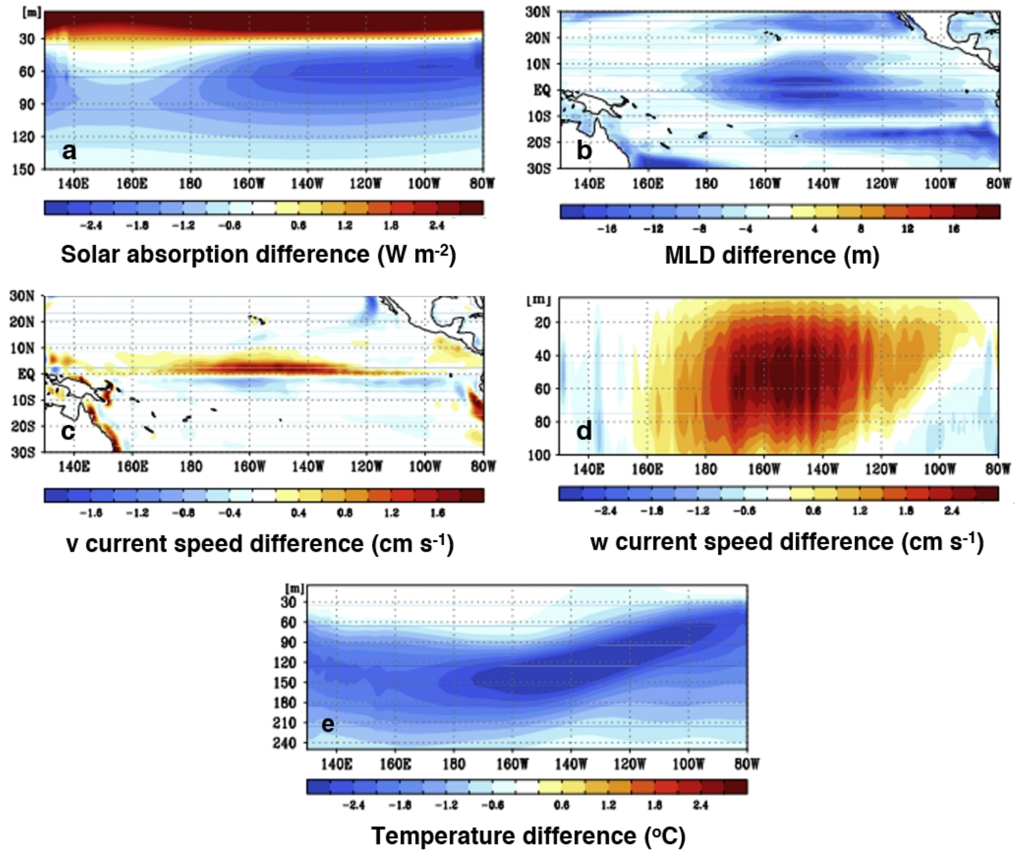

Figure 1.3: Mean differences in the equatorial Pacific between experiments using simulated chlorophyll for solar radiation calculations and experiments with chlorophyll set to zero for (a) absorbed solar radiation, (b) MLD, (c) meridional ocean current averaged over the upper 50 m, (d) vertical velocity and (e) temperature, from Park et al. (2014a). Panels (a), (d) and (e) are shown as zonal cross sections along the equator, and Panels (b) and (c) represent surface quantities.

Chlorophyll-driven solar absorption exerts a basin-scale to global influence on ocean temperature, stratification and dynamical processes. Based on a comparison between simulations with and without chlorophyll-induced solar absorption, Patara et al. (2012) has shown that chlorophyll allows the upper ocean to trap more incoming solar radiation, leading to a global-mean sea surface warming of approximately 0.5 °C (Figure 1.2a). Chlorophyll also modifies the seasonal cycle of upper-ocean properties, increasing the seasonal amplitude of temperature and mixed layer depth (MLD) by roughly 10%. At mid and high latitudes, surface waters warm by 0.1–1.5 °C in spring-summer and cool by 0.1–0.3 °C in autumn-winter of the respective hemisphere, as a response to chlorophyll-induced radiative effects (Manizza et al., 2005).

The chlorophyll-induced changes in the thermal structure of the upper ocean further influence large-scale water mass transformation. One of the most prominent ocean circulation responses is manifested in the Atlantic Meridional Overturning Circulation (AMOC). Lengaigne et al. (2009) has shown that chlorophyll-induced solar absorption increases Arctic surface temperatures, reduces sea-ice cover, and enhances freshwater inputs; together, these changes modify upper-ocean density and weaken the AMOC by around 15%. By prescribing ocean water clarity in an ocean general circulation model, Gnanadesikan and Anderson (2009) highlighted that stronger shortwave penetration warms subsurface waters and increases the supply of lighter water to the Southern Ocean, thereby enhancing mode and intermediate water formation. These adjustments reshape inter-basin density gradients and modify the strength of the southern limb of the AMOC. Chlorophyll-induced solar absorption also affects water mass transformation rates in other basins, including the formation and transport of Pacific subtropical mode water and Arabian Sea mode water (Iudicone et al., 2008; Groeskamp et al., 2019; Ma et al., 2022; Font et al., 2025).

Equatorial upwelling regions are also strongly affected by chlorophyll-induced solar absorption. In the tropical Pacific, chlorophyll-induced solar absorption tends to warm the upper ocean and deepens the thermocline (Murtugudde et al., 2002; Wetzel et al., 2006; Patara et al., 2012). However, contrasting responses have also been reported. Some studies simulate a cooling of equatorial Pacific Sea Surface Temperature (SST) (Figure 1.3e) after including the effects of chlorophyll-induced solar absorption (Figure 1.3a) (Nakamoto et al., 2001; Manizza et al., 2005; Park et al., 2014a), mainly because enhanced near-surface heating leads to a shoaling of the mixed layer (Figure 1.3b). When an ocean-only model keeps the surface wind forcing unchanged, the wind-driven Ekman transport can be regarded as constant. As shown by Sweeney et al. (2005), the meridional transport in the equatorial

Pacific is therefore mainly controlled by the MLD (see their Equation 10). A shallower mixed layer consequently enhances meridional transport away from the equator and the associated divergence of off-equatorial surface currents (Figure 1.3c), thereby strengthening equatorial upwelling (Figure 1.3d). The intensified upwelling brings colder thermocline waters to the surface, resulting in equatorial cooling. This mechanism has subsequently been supported by other studies (Sweeney et al., 2005; Park et al., 2014a; Zhang et al., 2019). These responses highlight the strong sensitivity of equatorial dynamics to the vertical structure of solar radiation and temperature.

Coastal upwelling systems are important to understand because their high phytoplankton biomass and intense dynamical processes make them regions of strong air-sea interaction with significant climatic impacts (Patti et al., 2008; Chavez and Messié, 2009). Previous studies have shown that chlorophyll-driven solar absorption can influence the thermal structure and dynamics of coastal upwelling (Hernandez et al., 2017; Echevin et al., 2021; Meng et al., 2024). In particular, the shading effect of surface chlorophyll reduces solar penetration into the subsurface ocean, leading to cooler subsurface waters that are subsequently upwelled to the surface, resulting in surface cooling (Figure 1.4). Many of these studies used relatively high-resolution regional ocean models (e.g. 10 km horizontal resolution, as shown in Figure 1.4), which are able to capture the fine-scale upwelling structures and the detailed SST responses associated with chlorophyll-induced solar absorption. In contrast, lower-resolution models may not fully resolve such mesoscale and coastal fine structures, but they remain useful for assessing large-scale responses (Lorente et al., 2019). Previous studies have typically focused on specific upwelling systems and used configurations that vary from study to study, including different solar penetration parameterisations, boundary and forcing conditions, making their results difficult to compare and leaving many coastal upwelling regions insufficiently investigated.

In addition, pronounced inter-basin differences in the vertical distribution of chlorophyll have been reported within eastern boundary coastal upwelling systems and their adjacent offshore regions. In the Atlantic, these regions often exhibit relatively strong subsurface chlorophyll maxima due to shallower nutriclines associated with basin-scale circulation characteristics and weaker upper-ocean stratification (Talley et al., 2011), which maintain nutrients closer to the euphotic zone (Wang et al., 2013). Moreover, enhanced iron supply from dust deposition alleviates iron limitation in the Atlantic (Foltz and McPhaden, 2008), allowing phytoplankton biomass to accumulate efficiently where sufficient light and nutrients coexist (Wang et al., 2013). In contrast, Pacific upwelling regions often show relatively high surface chlorophyll concentrations, while subsurface maxima are deeper or less pronounced because stronger iron limitation and more intense stratification constrain phytoplankton biomass accumulation at depth. These basin-scale differences in physical and biogeochemical controls may therefore contribute to systematic contrasts in chlorophyll distribution and the associated chlorophyll-induced solar absorption between Atlantic and Pacific upwelling regions.

At smaller spatial scales, chlorophyll-induced solar absorption also impacts mesoscale and submesoscale processes. In the eastern equatorial Pacific, where chlorophyll concentrations are high, Löptien et al. (2009) found that chlorophyll-induced solar absorption enhances the mean vertical (and to a lesser extent horizontal) shear of the south equatorial current and the equatorial undercurrent system, increasing eddy kinetic energy by nearly 100% and thus intensifying mesoscale eddy activity. Regional coupled model simulations have shown that phytoplankton–light feedbacks can modulate extreme upper-ocean temperature events, delaying the emergence of a permanent marine heatwave state in the Indian Ocean by altering upper-ocean heat uptake and stratification (Dinesh et al., 2025). Furthermore, enhanced near-surface stratification produced by chlorophyll-driven solar absorption can suppress turbulent mixing and modify the depth of the mixed layer, thereby influencing submesoscale instabilities and vertical heat and material exchange (Sweeney et al., 2005; Lengaigne et al., 2007).

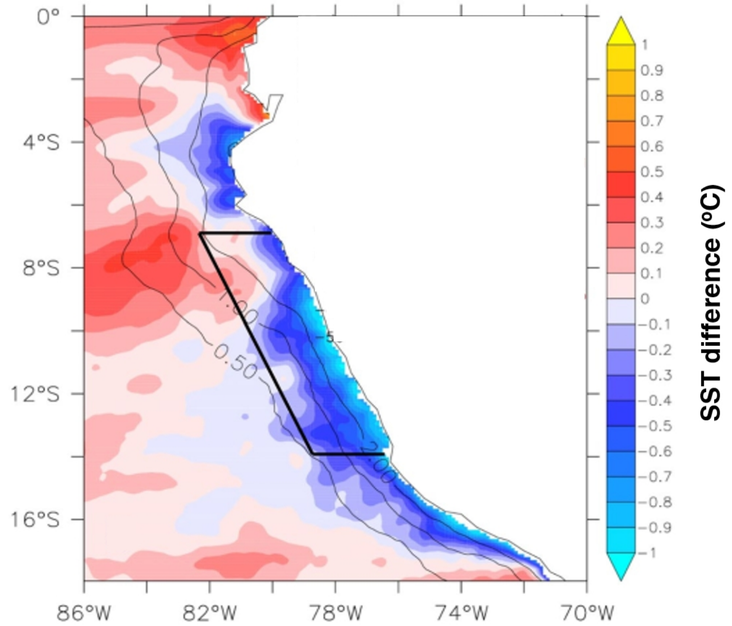

Figure 1.4: Climatological-mean SST difference between experiments using simulated chlorophyll for solar radiation calculations and experiments with chlorophyll set to zero in the Peru upwelling region, from Echevin et al. (2021).

1.2.2 Sea-ice feedbacks

Chlorophyll-induced solar absorption influences sea ice and the associated upper-ocean physical processes in the Arctic region. By trapping more shortwave radiation near the surface, chlorophyll increases SST and reduces sea ice concentration, with annual-mean sea ice cover decreasing by up to 10% in simulations that include chlorophyll effects on solar absorption compared with those that ignore them (Figure 1.2b), particularly in boreal spring and summer (Manizza et al., 2005, 2008; Patara et al., 2012). Locally, the sea ice season can be shortened by nearly one month due to chlorophyll-driven surface warming (Pefanis et al., 2020). Lengaigne et al. (2009) showed that, under climatological mean conditions, chlorophyll-induced near surface heating reduces both sea-ice concentration and thickness, and these reductions strengthen the positive ice-albedo feedback, thereby intensifying seasonal sea-ice melt. The resulting temperature and salinity anomalies alter the upper-ocean density structure, modifying horizontal density gradients and advection; in the Nordic Seas, the chlorophyll-induced dynamical changes reduce winter convection and favour the persistence of surface warming and sea-ice loss, thereby amplifying the overall impact (Pefanis et al., 2020).

Under climate warming, these mechanisms are projected to become more pronounced. Park et al. (2015) suggested that increasing downward longwave radiation associated with rising atmospheric CO_2 accelerates sea-ice melt in the Arctic, allowing more shortwave radiation to penetrate the upper ocean. This enhanced light availability promotes phytoplankton growth in spring, increasing chlorophyll concentrations and thereby intensifying the absorption of solar radiation in surface waters, which further accelerates sea-ice melt and strengthens the overall positive ice-albedo-chlorophyll feedback. However, future changes in CDOM have also been shown to contribute substantially to upper-ocean solar absorption in Arctic regions, with an influence comparable to that of chlorophyll and potentially larger in some coastal and river-influenced regions (Pefanis et al., 2020). Yet many Earth System Models (ESMs) use simplified parameterisations to calculate oceanic solar radiation penetration (hereafter referred to as physical solar schemes), in which the solar spectrum is represented by two or three bands. Such schemes do not account for the spectrally dependent absorption of solar radiation by chlorophyll or CDOM, and in many cases do not even represent their time-varying radiative effects in future climate projections. As a result, under future climate warming, the relative contributions of different light-absorbing constituents for upper-ocean warming and sea-ice melt as well as their combined effects, remain highly uncertain in ESMs.

1.2.3 Atmosphere and climate feedbacks

Chlorophyll-induced solar absorption not only shapes upper-ocean physics but also influences the atmosphere by modifying the ocean-atmosphere thermal and moisture conditions, affecting air-sea carbon fluxes and modulating large-scale atmospheric circulation. Previous studies have shown that chlorophyll-induced ocean surface warming of approximately 0.5 °C can warm the lower atmosphere and increase atmospheric humidity by 2–5% (Patara et al., 2012), in line with the Clausius-Clapeyron relationship. In addition, this chlorophyll-driven sea surface warming reduces CO_2 solubility, thereby enhancing CO_2 outgassing to the atmosphere (Figure 1.2c). This process strengthens the Earth's greenhouse effect and contributes to an atmospheric warming of approximately 0.7 °C. Moreover, Shell et al. (2003) showed that the responses of air-sea heat and moisture exchanges to chlorophyll-induced radiative effects can modify the intensity of the Walker and Hadley circulations.

At regional to local scales, chlorophyll blooms and the resulting SST increases have been linked to intensified rainfall, for example during the onset of the South Asian summer monsoon over the Arabian Sea (Turner et al., 2012). Similar effects have been reported during the southwest monsoon over coastal Myanmar, where SST increases of up to 0.5 °C lead to rainfall increases of up to 3 mm d^{-1} (Giddings et al., 2020).

Beyond its effects on the climate mean state, chlorophyll also exerts an important influence on climate variability. In the tropical Pacific, interannual variations in chlorophyll-induced solar absorption tend to damp the El Niño-Southern Oscillation (ENSO) variability, with reported reductions ranging from 1–15% across different modelling frameworks and configurations (Wetzel et al., 2006; Jochum et al., 2010; Park et al., 2014b). While the interannual variability of chlorophyll could influence ENSO via changing ocean dynamics in the eastern equatorial Pacific (Kang et al., 2017), the dominant effect is through direct thermodynamic processes associated with solar absorption (Marzeion et al., 2005; Jochum et al., 2010; Zhang, 2015). During La Niña conditions, cold SST anomalies coincide with high phytoplankton biomass in the central and eastern equatorial Pacific. The associated increase in chlorophyll traps more incoming solar radiation within the mixed layer, leading to local surface warming and thereby weakening the cold SST anomalies (Jochum et al., 2010; Park et al., 2014b; Zhang, 2015). During El Niño conditions, the opposite response leads to surface cooling and therefore reduces ENSO variability. Moreover, it has been suggested that the magnitude of ENSO response to chlorophyll variability can be modulated by the strength of ocean-atmosphere coupling in ESMs (Jochum et al., 2010; Tian et al., 2021a).

Chlorophyll interannual variability also exerts a notable influence on the Indian Ocean Dipole (IOD). During positive IOD events, enhanced upwelling and thermocline shoaling in the eastern equatorial Indian Ocean increase nutrient supply and favour positive chlorophyll anomalies (Currie et al., 2013). Perturbation experiments show that increased chlorophyll concentrations warm the upper ocean through enhanced solar absorption that can outweigh the cooling from upwelling that is strengthened by chlorophyll anomalies. As a result, the interannual variability in chlorophyll reduces IOD amplitude by 3–6% (Park and Kug, 2014; Ma et al., 2015), indicating that this chlorophyll–radiative effect plays a non-negligible role in shaping Indian Ocean climate variability.

Furthermore, on longer time scales, chlorophyll exhibits a significant response to future climate warming, through shifts in stratification, nutrient supply and phytoplankton community structure and phenology (Dai et al., 2023; Zhao et al., 2025). However, substantial uncertainty exists in future chlorophyll projections across ESMs, and many models do not incorporate chlorophyll-dependent physical solar schemes. As a result, how the radiative effects associated with future chlorophyll changes may affect the ocean and climate system remains poorly understood.

1.3 Approaches to investigate chlorophyll-induced solar absorption

Observational studies have long aimed to quantify how chlorophyll influences the penetration of solar radiation in the upper ocean by modifying its optical properties, and these observed bio-optical relationships have been incorporated into parameterisations used in ocean models (Figure 1.5). The classical

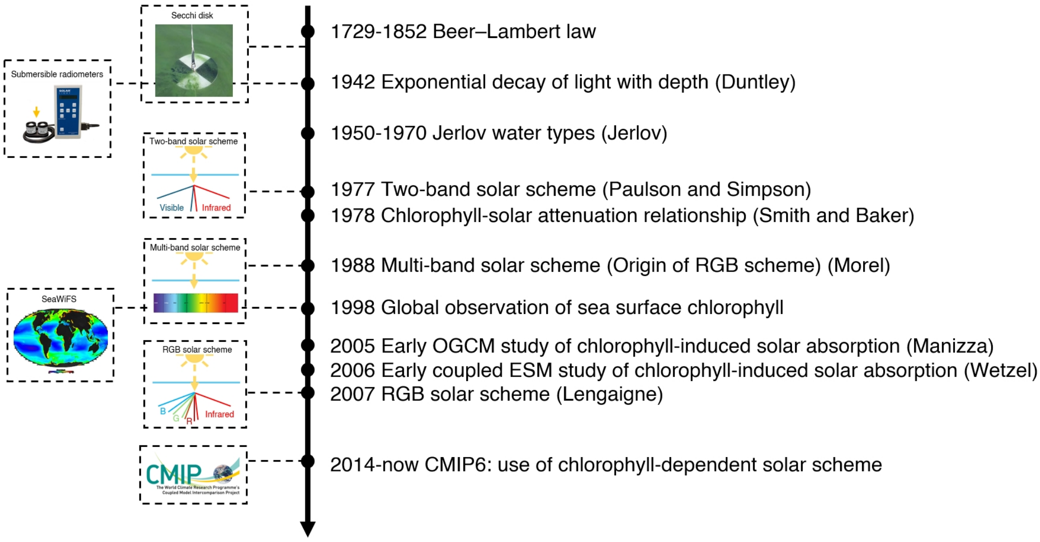

Figure 1.5: Historical development of studies on chlorophyll-induced solar absorption in the ocean. OGCM stands for Ocean General Circulation Model.

Beer-Lambert law (Lambert, 1760), which describes the exponential decay of light in an absorbing medium, provides the theoretical foundation for interpreting observations of light attenuation in the ocean. Early in-situ observations relied on vertical profiles of downwelling irradiance obtained from submersible radiometers (Duntley, 1942), or on simple transparency indicators such as Secchi depth (Poole and Atkins, 1929), to characterise light attenuation with depth and to derive the attenuation coefficient of solar radiation (K_d). Building on these developments, Jerlov (1968) classified global natural waters into several optical water types based on their spectral attenuation characteristics, providing a framework for quantifying spatial variations in water clarity. In the open ocean, where the optical properties of seawater are largely determined by phytoplankton biomass, empirical relationships linking chlorophyll concentration to K_d were established (Smith and Baker, 1978; Morel, 1988; Morel and Maritorena, 2001).

With the advent of satellite ocean-colour remote sensing, global observations of surface chlorophyll (O'Reilly et al., 1998), when combined with established chlorophyll-K_d relationships, enabled global estimates of solar radiation attenuation in the upper ocean (Lee et al., 2005). Subsequent studies further improved these estimates by inferring vertical chlorophyll profiles from surface observations, allowing more realistic depth-dependent representations of light attenuation (Morel and Berthon, 1989; Zhang et al., 2011). Other studies have used in-situ spectral irradiance profiles to refine the parameterisations of chlorophyll-induced solar absorption (Ohlmann and Siegel, 2000; Ohlmann, 2003; Witte et al., 2024).

With the establishment of quantitative relationships between chlorophyll concentration and the attenuation of solar radiation, an increasing number of studies have incorporated these bio-optical dependencies into numerical models. Following the contributions of Morel (1988) and Ohlmann and Siegel (2000), chlorophyll-based physical solar schemes were adopted in a variety of ocean general circulation models, enabling models to represent the biologically induced heating more realistically and thereby to examine the responses of ocean physics to chlorophyll-induced solar absorption (Manizza et al., 2005; Sweeney et al., 2005). In atmosphere-ocean-biogeochemistry coupled ESMs, the physical solar schemes enable atmospheric feedbacks associated with chlorophyll-induced solar absorption while allowing simulated phytoplankton dynamics to directly modify light penetration (Wetzel et al., 2006; Patara et al., 2012; Asselot et al., 2024). Such interactive bio-optical feedbacks have been shown to influence ocean physics, sea-ice dynamics and large-scale climate patterns (Section 1.2). As a result, the integration of chlorophyll-dependent solar absorption has become an essential component for improving realism in modern coupled climate simulations.

Despite these advances, the parameterisation of chlorophyll-induced solar absorption in ESMs remains highly uncertain, with substantial differences across models included in the Coupled Model Intercomparison Project (CMIP). CMIP provides a coordinated experimental framework in which a suite of state-of-the-art ESMs are integrated under common forcing scenarios, enabling systematic comparisons of climate simulations and future climate projections (Eyring et al., 2016). Within the sixth phase of CMIP (CMIP6), some models employ interactive bio-optical schemes in which simulated chlorophyll fields determine the vertical distribution of solar absorption. However, biases in simulated chlorophyll can lead to unrealistic representations of upper-ocean solar absorption (Lim et al., 2018). Some other models instead rely on satellite-derived climatological surface chlorophyll to calculate solar absorption, capturing realistic spatial patterns but lacking information on the vertical structure of chlorophyll, such as ACCESS-ESM and CanESM (Bi et al., 2013). Recent studies have demonstrated that this missing vertical variability can substantially affect the modelled light penetration and heating rates (Shi et al., 2023; Meng et al., 2024). The rest of the models apply constant attenuation profiles that are entirely independent of spatial and temporal variability of chlorophyll, thereby leading to unrealistic representations of upper-ocean radiative heating. Paulsen et al. (2018), using MPI-ESM as an example, demonstrated that the use of constant solar attenuation profiles can lead to significant biases in both the climatological mean state and the interannual variability of SST, ocean dynamics and atmospheric circulation. As a consequence of these disparate approaches, the treatment of chlorophyll-induced solar absorption in CMIP ESMs remains poorly constrained and introduces significant uncertainty into climate simulations and projections.

1.4 Motivation and aims of this thesis

As outlined in Chapter 1, previous studies have investigated chlorophyll-induced solar absorption in detail and demonstrated that it can exert substantial impacts on the climate system, influencing ocean heat uptake, thermal structure, vertical stratification and air-sea interactions. However, several important knowledge gaps remain. First, from a spatial perspective, existing studies have either focused on the global impacts of chlorophyll-induced radiative effects or on regional responses in equatorial upwelling systems and polar oceans. In contrast, the influence of chlorophyll-induced solar absorption in other dynamically active regions, such as eastern boundary coastal upwelling systems, remains poorly understood. Second, from a temporal perspective, most previous work has emphasised the role of chlorophyll-induced solar absorption in modulating large-scale modes of climate variability, such as ENSO and the IOD. Much less attention has been paid to the impacts of chlorophyll-induced radiative changes on the ocean and climate system under future anthropogenic climate change. Finally, given the central role of CMIP ESMs in climate research, it remains unclear how chlorophyll-induced solar absorption is parameterised across these ESMs, and how differences in these representations contribute to inter-model spread in climate simulations and future projections.

In this thesis, the role of chlorophyll-induced solar absorption in shaping ocean temperature, dynamics and climate is examined using CMIP6 model output, idealised radiative calculations and global ocean model simulations. Chapter 2 introduces the numerical models used in this thesis and the parameterisations of chlorophyll-induced solar absorption within the ocean model, and also discusses the limitations and uncertainties associated with these model simulations.

Coastal upwelling systems are critical regions for ocean circulation, marine ecosystems, fisheries and air-sea interactions. However, existing research on the impact of chlorophyll-induced solar absorption on coastal upwelling has been restricted to a few specific regions and lacks a unified global assessment. To address this gap, Chapter 3 employs a global ocean-biogeochemical coupled model to investigate the response of coastal upwelling systems to chlorophyll-induced solar absorption. We further explore the mechanisms underlying the opposite temperature responses found in the Pacific and Atlantic coastal upwelling systems.

An increasing number of studies suggest that chlorophyll-induced solar absorption should be included in contemporary ESMs to achieve more realistic climate simulations. However, the treatment of this process varies considerably across CMIP-class models, reflecting differences in parameterisations (physical solar schemes) and in the chlorophyll fields used as inputs to these schemes. In Chapter 4, we compile detailed information from CMIP modelling groups on how individual ESMs represent solar penetration and quantify the resulting impacts of these differences on upper-ocean energy budgets.

While most previous work has focused on the role of chlorophyll-induced solar absorption in shaping climate variability, much less attention has been paid to its potential influence on long-term anthropogenic climate change. To address this, Chapter 4 also employs an idealised radiative calculation to assess the possible impacts of future chlorophyll changes on the climate energy budget under global warming.

Building on these insights, Chapter 5 uses an ocean general circulation model to examine how projected future changes in chlorophyll may modify radiative heating, upper-ocean physics and climate. The results from this modelling work are compared against the idealised calculations in Chapter 4. Finally, Chapter 6 summarises the main findings of the thesis and discusses their implications and directions for future research.

2

Methods

2.1 Research design overview

The central question addressed in this thesis is how chlorophyll-induced solar absorption influences ocean temperature, ocean dynamics and climate. As this study focuses on its large-scale influences on the climate system, the analysis is mainly based on a global ocean general circulation model, in which prescribed chlorophyll fields used in the calculation of solar radiation are modified to assess their impacts.

In Chapter 3, a $1^\circ \times 1^\circ$ horizontal-resolution global ocean general circulation model (Nucleus for European Modelling of the Ocean, NEMO) coupled with a marine biogeochemical model (Model of Ecosystem Dynamics, nutrient Utilisation, Sequestration and Acidification, MEDUSA) is configured to investigate the response of coastal upwelling systems to prescribed chlorophyll-dependent solar absorption.

Chapter 4 applies an offline radiative calculation driven by chlorophyll fields from multiple CMIP6 ESMs to diagnose mixed layer solar absorption, and to assess the radiative effects of future chlorophyll changes and inter-model differences in chlorophyll simulations and solar penetration parameterisations.

Chapter 5 employs a low-resolution ($2^\circ \times 2^\circ$) version of NEMO to examine how projected future declines in chlorophyll may influence ocean structure and climate.

Because the focus is on global-scale and large-scale responses, this low-resolution configuration is sufficient to capture the key physical signals while remaining computationally efficient for long-term simulations.

2.2 Data and model description

This study uses CMIP6 model output, with the relevant variables summarised in Table 2.1, taken from experiments including piControl (a pre-industrial control simulation), historical (forced by observed climate drivers) and future scenarios following the Shared Socioeconomic Pathways (SSPs), including SSP3-7.0 (a medium-to-high emissions pathway) and SSP5-8.5 (a high-emissions pathway representing the strongest warming scenario) (Figure 2.1). For consistency across models, all output fields were horizontally regridded using two-dimensional linear interpolation when necessary.

This study uses NEMO, a widely used global ocean circulation model designed for climate and biogeochemical applications (Madec and NEMO team, 2016). NEMO solves the primitive equations on a structured horizontal grid with a z-coordinate vertical discretisation. Vertical mixing is represented by a turbulent kinetic energy (TKE)-based scheme, which provides a physically based formulation for vertical diffusivity and turbulent mixing processes. Lateral mixing follows a Laplacian or biharmonic operator depending on the configuration. Owing to its numerical stability, flexibility and comprehensive physical parameterisations, NEMO has become one of the most widely adopted ocean components in CMIP6 ESMs.

Solar radiation in NEMO is attenuated using the RGB (red-green-blue) physical solar scheme (Lengaigne et al., 2007), which separates incoming radiation into an infrared wavelength band and three visible wavelength bands, each with distinct attenuation coefficients. The model allows three-dimensional chlorophyll fields to be prescribed externally as input to the solar scheme, providing a framework for assessing the radiative effects of different chlorophyll distributions on the ocean.

Two versions of NEMO are used in this thesis. Chapter 3 employs a 1° horizontal-resolution, 75-layer version to investigate the influence of chlorophyll on coastal upwelling systems. The dominant ocean circulations associated with coastal upwelling extend over spatial scales of several degrees (Patti et al., 2008; Chavez and Messié, 2009), so a 1° horizontal resolution is sufficient to capture their structure. This 30-year simulation is forced with atmospheric fields from the version 2 forcing for coordinated ocean-ice reference experiments (CORE2) (Griffies et al., 2009), including wind stress, surface heat fluxes, freshwater and momentum fluxes, and is coupled with a biogeochemical model (MEDUSA).

Chapter 5 uses a lower-resolution version of NEMO (2° horizontal resolution with 31 vertical levels), forced by the atmospheric fields of historical and SSP3-7.0 scenarios from UK Earth System Model version 1.0 (UKESM1.0), to examine how projected future declines in chlorophyll may influence large-scale ocean structure and climate.

In Chapter 4, observed climatological chlorophyll used as input to the physical solar scheme is derived from the 1998–2007 Sea-viewing Wide Field-of-view Sensor (SeaWiFS) dataset (O'Reilly et al., 1998). Because satellite observations provide only surface chlorophyll, the chlorophyll concentration within the water column used to calculate solar radiation attenuation is assumed to be vertically constant, following common practice in such applications (Table 4.1).

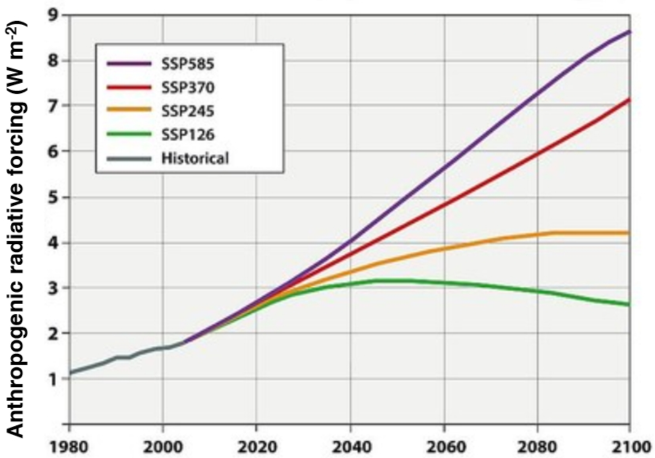

Figure 2.1: Anthropogenic radiative forcing pathways of historical and selected CMIP6 SSP scenarios (SSP1-2.6, SSP2-4.5, SSP3-7.0 and SSP5-8.5). Coloured curves show the time series of radiative forcing ($\mathrm{W\,m^{-2}}$) relative to pre-industrial conditions, from O'Neill et al. (2016).

2.3 Heat budget calculation

In Chapters 3 and 5, the upper-ocean heat budget is diagnosed offline for selected regions to explain the temperature responses to chlorophyll-induced solar absorption following the formulation below:

$$\underbrace{\frac{\partial T}{\partial t}}_{\text{Temperature tendency}} = \underbrace{-\mathbf{u}\cdot\nabla T}_{\text{Advection}} + \underbrace{\mathcal{M}(T)}_{\text{Mixing}} + \underbrace{\frac{Q_{\text{SW}}^{\text{abs}}}{\rho_0 c_p h}}_{\text{Shortwave absorption}} + \underbrace{\frac{Q_{\text{ns}}}{\rho_0 c_p h}}_{\text{Air-sea heat flux}} + \underbrace{R}_{\text{Residual}} . \tag{2.1}$$

T denotes seawater temperature (°C) and $\partial T/\partial t$ is the temperature tendency. $\mathbf{u} = (u, v, w)$ is the three-dimensional ocean velocity vector (m $\mathrm{s^{-1}}$), representing the zonal, meridional and vertical components, respectively. $\mathcal{M}(T)$ represents vertical mixing processes. $Q_{\text{SW}}^{\text{abs}}$ is the shortwave radiative flux ($\mathrm{W\,m^{-2}}$) absorbed within the layer of thickness h. Q_{ns} denotes the non-shortwave air-sea heat flux ($\mathrm{W\,m^{-2}}$), given by the sum of longwave, sensible and latent heat fluxes. ρ_0 is a reference seawater density ($\mathrm{kg\,m^{-3}}$), and c_p is the specific heat capacity of seawater at constant pressure ($\mathrm{J\,kg^{-1}\,K^{-1}}$). The residual term R represents contributions from undiagnosed physical processes, such as horizontal mixing and any remaining imbalance in the heat budget.

All data used in this analysis are derived from NEMO model output. The heat budget terms are first calculated at each grid cell on an interpolated, horizontally regular grid and at the NEMO vertical levels. The results based on the interpolated horizontal grid are similar to those based on the original model grid. In Chapter 5, these heat budget terms are then vertically averaged over the selected depth range and spatially averaged over the selected regions. The mixing term here represents only vertical mixing calculated offline using the K-Profile Parameterisation (Large et al., 1994), while horizontal mixing is not explicitly considered and is included in the residual term.

2.4 Uncertainties and limitations

First, all ocean models exhibit systematic biases in their representation of the mean ocean state, including biases in SST and circulation (Zhang et al., 2023). For example, overly strong upwelling in NEMO (Yool et al., 2011) may lead to faster vertical transport of heat absorbed by chlorophyll, potentially influencing the simulated thermal structure response to chlorophyll-induced solar absorption. In addition, the NEMO configurations used in this study do not explicitly resolve mesoscale features such as eddies, which play an important role in redistributing heat in the upper ocean (Oglethorpe et al., 2025). As a result, any influence of chlorophyll changes on mesoscale eddy activity and the subsequent feedback of these eddies on upper-ocean structure cannot be captured, introducing an additional source of uncertainty into our results (Löptien et al., 2009).

Second, substantial differences exist among CMIP6 ESMs in their projections of future chlorophyll changes (Ryan-Keogh et al., 2025). This spread introduces uncertainty into the analysis of the climate feedbacks driven by future chlorophyll changes in Chapters 4 and 5. In addition, this study does not account for the spatial and temporal variability of other light-absorbing constituents such as CDOM and NAP, which may play an important role in modulating shortwave attenuation and radiative heating in some nearshore regions.

Finally, the ocean-only simulations used in Chapters 3 and 5 are not coupled with an atmospheric model, and therefore any atmospheric response to chlorophyll-induced solar absorption, such as changes in air-sea fluxes or surface wind stress, is not represented. These feedbacks could in turn influence ocean temperature and circulation (Shell et al., 2003; Asselot et al., 2021). Although coupling to an atmospheric model could capture such processes, it would also introduce additional complexity and further uncertainty into the mechanisms analysed here.

Table 2.1: Summary of outputs from CMIP6 ESMs used in this thesis.

Model	**Institution**	**Variant label**	**Variables**	**Experiments and time period**
CESM2	NCAR	r1i1p1f1	chlorophyll, MLD, solar radiation	piControl:last 30 years, historical:1850–2014, SSP3-7.0:2015–2100, SSP5-8.5:2015–2100
CMCC-ESM2	CMCC	r1i1p1f1	chlorophyll, MLD, solar radiation	piControl:last 30 years, historical:1850–2014, SSP3-7.0:2015–2100, SSP5-8.5:2015–2100
CNRM-ESM2.1	CNRM-CERFACS	r1i1p1f2	chlorophyll, MLD, solar radiation	piControl:last 30 years, historical:1850–2014, SSP3-7.0:2015–2100, SSP5-8.5:2015–2100
IPSL-CM6A-LR	IPSL	r1i1p1f1	chlorophyll, MLD, solar radiation	piControl:last 30 years, historical:1850–2014, SSP3-7.0:2015–2100, SSP5-8.5:2015–2100
GFDL-ESM4.1	NOAA-GFDL	r1i1p1f1	chlorophyll, MLD, solar radiation	piControl:last 30 years, historical:1850–2014, SSP3-7.0:2015–2100, SSP5-8.5:2015–2100
ACCESS-ESM1.5	CSIRO/BOM	r1i1p1f1	chlorophyll, MLD, solar radiation	piControl:last 30 years, historical:1850–2014, SSP5-8.5:2015–2100
CanESM5	CCCma	r1i1p2f1	chlorophyll, MLD, solar radiation	piControl:last 30 years, historical:1850–2014, SSP5-8.5:2015–2100
MIROC-ES2L	MIROC	r1i1p1f2	chlorophyll, MLD, solar radiation	piControl:last 30 years, historical:1850–2014, SSP5-8.5:2015–2100
MPI-ESM1.2-LR	MPI-M	r1i1p1f1	chlorophyll, MLD, solar radiation	piControl:last 30 years, historical:1850–2014, SSP5-8.5:2015–2100
NorESM2-LM	NCC	r1i1p1f1	chlorophyll, MLD, solar radiation	piControl:last 30 years, historical:1850–2014, SSP5-8.5:2015–2100
UKESM1.0-LL	UK Met Office	r1i1p1f2	chlorophyll, MLD, solar radiation, wind speed, cloud fraction, w (vertical velocity)	piControl:last 100 years, historical:1850–2014, SSP5-8.5:2015–2100

3

Diverse responses of upper ocean temperatures to chlorophyll-induced solar absorption across different coastal upwelling regions

---

The results presented in the following chapter have been published in *Geophysical Research Letters*, **51**, e2024GL109714 (https://doi.org/10.1029/2024GL109714). The main text and supporting information from the published article are included here, with Figure 3.11 and an associated short discussion added for this thesis.

The work presented in this chapter was led by Siyu Meng. Julien Palmieri and Andrew Yool performed the model simulations. Benjamin Webber, David Stevens and Manoj Joshi contributed to the data analysis and manuscript preparation.

3.1 Abstract

Chlorophyll in phytoplankton absorbs solar radiation and affects the thermal structure and dynamics within upwelling regions. However, research on this process across global-scale coastal upwelling systems is still lacking. Here, we use a coupled ocean-biogeochemical model to investigate differing responses to chlorophyll-induced solar absorption between Pacific and Atlantic coastal upwelling regions. Chlorophyll-induced solar absorption leads to colder Pacific coastal upwelling but warmer Atlantic coastal upwelling. In the Pacific, the shading effect of the surface chlorophyll maximum leads to colder subsurface water, which is then upwelled, contributing to cooling. The more stratified upper ocean leads to shallower mixed layer depth, intensifying offshore transport and upwelling. In the Atlantic, the absorption of solar radiation by the subsurface chlorophyll maximum causes warmer and weaker upwelling. The processes described, in turn, trigger positive feedback to ocean biogeochemistry and potentially interact with climate dynamics, underscoring the necessity to incorporate them into Earth system models.

3.2 Introduction

Phytoplankton, the primary photosynthetic organisms in the ocean, play a crucial role in regulating the vertical distribution of solar radiation through absorption by chlorophyll and related pigments (Lewis et al., 1990; Morel, 1988). Previous research has established a connection between chlorophyll-induced solar absorption and the thermal structure of the upper ocean, based on observations (Huan et al., 2021; Mercado and Gómez-Jakobsen, 2022), in situ data (Parida et al., 2022; Patil et al., 2023) and numerical models (Park et al., 2014a; Asselot et al., 2021). For instance, solar radiation absorption by chlorophyll has been proposed as a significant contributor to the upper ocean heat balance in the open ocean, manifesting in the increase of upper ocean heating rate ranging from 2–20 $\mathrm{W\,m^{-2}}$

(Timmermann and Jin, 2002; Park et al., 2015; Parida et al., 2022). Thus, higher phytoplankton biomass generally leads to a warmer ocean surface layer and exerts a significant influence on global climate (Manizza et al., 2005, 2008). However, some state-of-the-art climate models, such as the UKESM, still lack a realistic representation of this process, relying on a spatially constant chlorophyll value for solar radiation penetration calculations (Sellar et al., 2019). This constraint, along with the significant implications of chlorophyll-induced solar absorption for ocean physics and climate processes, emphasizes the need for a comprehensive investigation into this biophysical interaction.

Solar radiation absorption by chlorophyll has been suggested to impact the large-scale climate variability (Jochum et al., 2010; Zhang et al., 2019; Tian et al., 2021b), and studies on this effect have mainly centred on the Pacific equatorial upwelling region, due to its potential feedbacks to the ENSO. For example, the interannual variations in the upper ocean thermal structure induced by chlorophyll-absorbed solar radiation in the Pacific equatorial upwelling significantly influence the magnitude (Lengaigne et al., 2007) and asymmetry (Timmermann and Jin, 2002) of ENSO. However, the thermal structure in the coastal upwelling regions, situated along the eastern boundaries of mid-latitude ocean basins, can also influence the formation of stratocumulus clouds by changing the ocean-atmosphere fluxes of heat and moisture, and can thus indirectly impact tropical or broader climate (Wood, 2012; Richter, 2015). Hence, it is essential to understand the modification of chlorophyll on the thermal structure of coastal upwelling, as it may exert a substantial impact on climate system.

Previous studies have explored the chlorophyll-induced temperature variations within specific upwelling systems. As indicated by Echevin et al. (2021), increased surface chlorophyll concentrations in the Peru upwelling can absorb more solar radiation in the upper ocean, thereby limiting its penetration into the subsurface. This process leads to a cooling of the upper ocean, attributed to the subsurface cooling of source waters that are upwelled. Furthermore, Hernandez et al. (2017) suggests a comparable surface cooling impact by chlorophyll in the Benguela and

Canary upwelling systems. This cooling effect is associated with not only the redistribution of solar radiation but also the modifications in horizontal ocean advection. However, Hernandez et al. (2017) uses an empirical parameterisation (Morel and Berthon, 1989) to estimate a vertical profile of chlorophyll from satellite-observed surface chlorophyll, which introduces uncertainty into the vertical structure of solar radiation absorption by chlorophyll in the subsurface ocean.

While chlorophyll-induced solar absorption has been associated with ocean thermal structure and dynamics in specific coastal upwelling regions, there remains a need for a comprehensive understanding and comparison of these processes across global coastal upwelling regions, using the same model and assumptions for each region. In this study, we use a global ocean model coupled with a biogeochemistry model to investigate the influence of chlorophyll-induced solar absorption on upper ocean temperatures and dynamics in five coastal upwelling regions (Figure 3.1), with a specific focus on exploring the discrepancies between them.

3.3 Data and methods

3.3.1 Model description

Numerical experiments in this study make use of the NEMO (Madec and NEMO team, 2016) ocean physics model coupled with the MEDUSA marine biogeochemistry model (Yool et al., 2013). The model domain is approximately 1° × 1° in horizontal resolution, with 75 vertical levels and an explicit nonlinear free surface. In NEMO, solar radiation absorption down the water column depends on the chlorophyll concentration at each model level, using a three-waveband RGB light scheme (Morel, 1988; Lengaigne et al., 2007). Operationally, the model permits this chlorophyll concentration to be directly driven by MEDUSA or to be specified independently. In MEDUSA, the solar absorption is calculated separately from NEMO based on a two-waveband light scheme to represent the self-shading by phytoplankton within the water column (Yool et al., 2013). In Section 3.4.2, MLD is used to explain the response of upwelling dynamics to chlorophyll-induced solar absorption. Here, MLD is defined as the depth where the vertical profile of potential temperature decreases by 0.5 °C relative to the near-surface temperature.

Here, the configuration of NEMO-MEDUSA has been made consistent with that of the UKESM1.0 (Sellar et al., 2019). UKESM is a fully-coupled ESM that is built upon the HadGEM3-GC3.1 (Kuhlbrodt et al., 2018) physical climate model, adding interactive atmospheric chemistry and terrestrial and marine biogeochemistry (MEDUSA). HadGEM3-GC3.1 omits marine biogeochemistry, and instead utilizes a spatially-uniform chlorophyll value when calculating the absorption of downwelling radiation in the ocean. To remain consistent with HadGEM3-GC3.1, UKESM1.0 also uses this approach, despite MEDUSA including chlorophyll dynamics. As a result, this may lead to unrealistic model behaviour, especially in regions where MEDUSA's chlorophyll differs significantly from this constant value. For example, where simulated chlorophyll is much lower, as in the low productivity oligotrophic gyres (Meng et al., 2021; Dai et al., 2023), or much higher, as in the highly productive upwelling regions (Ferreira et al., 2021). Consequently, by contrasting model behaviour when this constant value is used with that when MEDUSA's dynamic chlorophyll concentrations are used, this study aims to provide insights for future ESM development.

3.3.2 Case settings

The two case simulations in this study only differ in the chlorophyll inputs of the RGB scheme, the component for calculating solar absorption in NEMO. In the reference simulation (Case.Con), the solar radiation penetration is based on a horizontally and vertically constant chlorophyll concentration set to $0.1\,\mathrm{mg\,m^{-3}}$, which is the default value in NEMO. In Case.MED, solar radiation penetration depends on the time-varying output of chlorophyll concentrations from MEDUSA. Both cases are forced at the ocean surface by identical atmospheric forcing, including solar radiation, heat, freshwater and momentum fluxes, provided by CORE2 (Griffies et al., 2009).

3.3.3 Observational data

Observed sea surface chlorophyll concentration data are used to evaluate the model performance. Monthly mean chlorophyll concentrations are derived from Moderate Resolution Imaging Spectroradiometer (MODIS) satellite data spanning 2005 to 2022 (NASA OBPG, 2022). For ease of computation, the raw data are interpolated to the model grids.

3.3.4 Calculations of net offshore transport

An offline calculation of net offshore transport is applied to both Case.MED and Case.Con by Equation 3.1, following Equation 10 in Sweeney et al. (2005). This equation incorporates two components—Ekman transport and geostrophic transport—to estimate meridional transport away from the equator. In our study, we adapt this equation to calculate transport in the zonal direction and apply it along the coast of upwelling regions:

$$\int_{MLD}^{\eta} -\frac{1}{\rho_o}\frac{\partial p}{\partial y}dz + \frac{\tau_y}{\rho_o} = fM_X, \tag{3.1}$$

where $\left(\frac{1}{\rho_o}\right)\frac{\partial p}{\partial y}$ is the meridional pressure gradient, f is the Coriolis force, η is the sea surface height, ρ_0 is the reference seawater density, and MLD is the mixed layer depth. The first term is the geostrophic component, $\int_{MLD}^{\eta} -\frac{1}{\rho_0}\frac{\partial p}{\partial y}\,dz$, the second term is the Ekman component, $\frac{\tau_y}{\rho_o}$, and the third term is the net zonal transport, fM_X.

Three specific calculations are performed: 1. The first calculation involves quantifying the MLD-induced difference in zonal transport between two configurations that are identical to Case.Con, except that the MLD from

Case.MED is applied in one of them. 2. The second calculation compares the zonal transport calculated from the full outputs of Case.Con and Case.MED. 3. The third calculation analyses the modelling components of zonal transport in Case.Con and Case.MED.

The Ekman transport within the MLD is assumed to be consistent between Case.MED and Case.Con due to identical wind forcings between two cases. By comparing the first and second calculations, we can assess the contribution of MLD changes to geostrophic transport. Comparing the second and third calculations allows us to evaluate the contribution of geostrophic transport to the overall net offshore transport.

3.4 Results

3.4.1 Modifications of chlorophyll-induced solar absorption on upper ocean temperatures in coastal upwelling regions

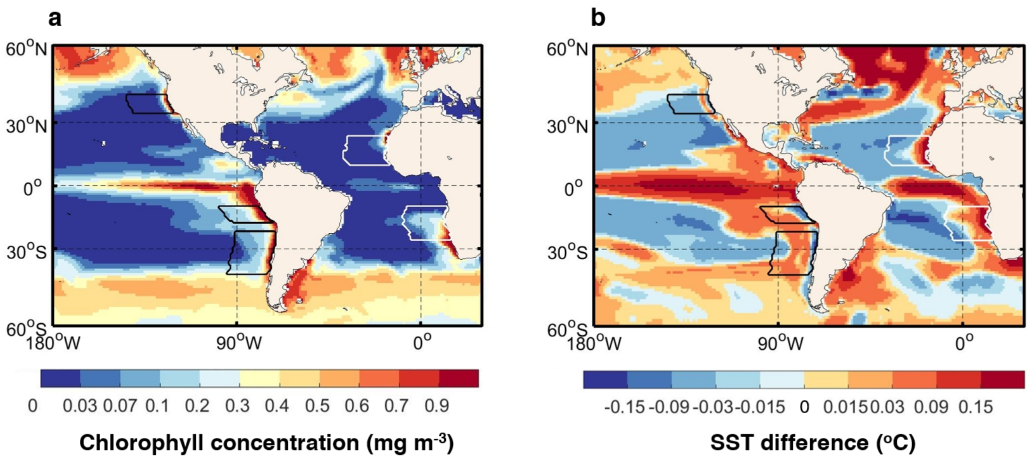

Figure 3.1: Response of SST to chlorophyll-induced solar absorption in coastal upwelling regions. (a) Distribution of surface chlorophyll concentration in Case.MED. (b) SST difference of Case.MED minus Case.Con. Black lines indicate Region.Cold, denoting coastal areas exhibiting surface cooling induced by chlorophyll, and white lines indicate Region.Warm, denoting coastal areas exhibiting surface warming induced by chlorophyll.

Chlorophyll concentrations simulated by MEDUSA within global coastal upwelling regions consistently exceed $0.1\,\mathrm{mg\,m^{-3}}$, the reference value to calculate solar radiation penetration in Case.Con (Figure 3.1a). However, higher chlorophyll levels exhibit a contrasting impact on SSTs between different coastal upwelling regions, producing a surface cooling in Pacific upwelling regions but a surface warming in Atlantic upwelling regions (Figure 3.1b).

To understand the different responses of SSTs to chlorophyll between Pacific and Atlantic coastal upwelling regions, we have categorized global coastal upwelling regions (Patti et al., 2008; Chavez and Messié, 2009) into two zones: Region.Cold and Region.Warm (Figure 3.1). Region.Cold is defined as the coastal upwelling regions where the enhanced chlorophyll-induced solar absorption leads to colder surface temperatures in Case.MED compared with Case.Con. These regions include California, Peru and Chile upwelling zones in the Pacific Ocean. Conversely, Region.Warm, situated along the eastern coasts of the Atlantic, experiences warmer surface temperatures due to enhanced chlorophyll-induced solar absorption.

In Region.Cold, high near-surface chlorophyll concentrations simulated by MEDUSA (Figure 3.2a) lead to increased absorption of solar radiation within the upper 20 m depth (Figure 3.2f) in Case.MED. This, in turn, restricts the penetration of solar radiation into the subsurface ocean (Figure 3.2f), resulting in subsurface cooling below 20 m depth (Figure 3.2j). Subsurface colder water is subsequently transported to the surface via upwelling (Figure 3.3e), while the solar heat accumulated in the near-surface ocean is transported away from the coast via horizontal advection (Figure 3.3i). This mechanism leads to the surface cooling within approximately 300 km of the coast within the upwelling regions and simultaneous warming farther offshore (Figure 3.1b).

In Region.Warm, the modification of the vertical distribution of solar radiation by chlorophyll is similar to that of Region.Cold, i.e. more solar radiation absorbed in the upper ocean and less penetration into the subsurface (Figure 3.2h). However,

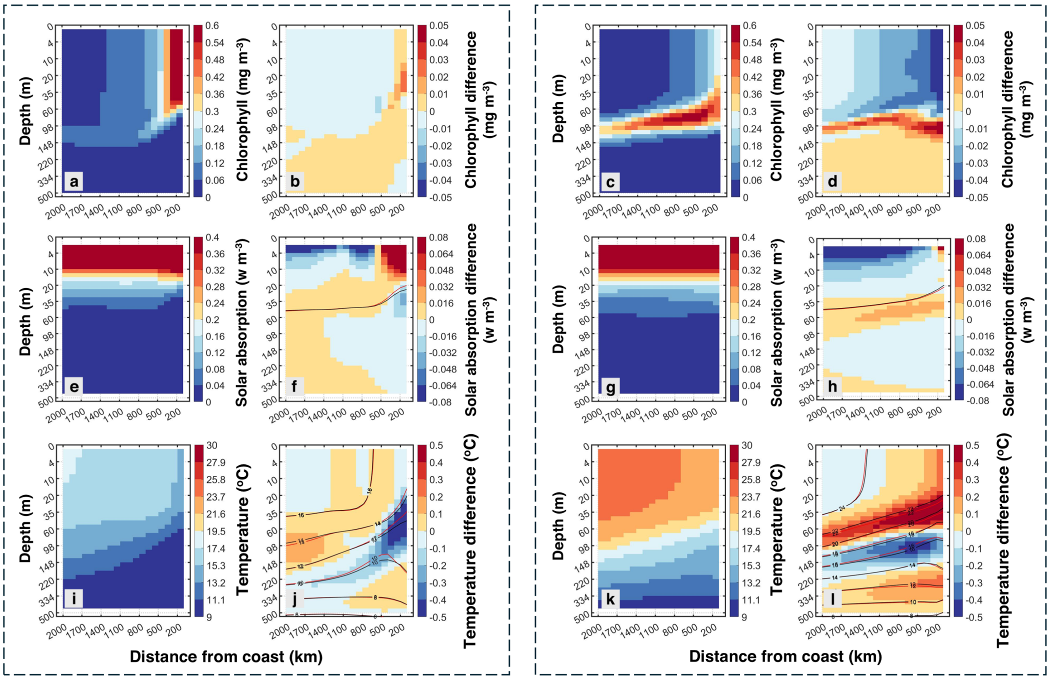

Figure 3.2: Mean cross-shore structures of chlorophyll concentrations (a, c), solar radiation absorption per unit depth (e, g) and potential temperature (i, k) in Case.MED and their differences of Case.MED minus Case.Con (b, d, f, h, j and l) in Region.Cold (left dashed box) and Region.Warm (right dashed box) as indicated in Figure 3.1. Red lines in (f) and (h) indicate the MLD in Case.MED, and black lines indicate the MLD in Case.Con. Red lines in (j) and (l) indicate the isotherms in Case.MED, and black lines indicate the isotherms in Case.Con.

.

this effect is less pronounced in Region.Warm, primarily due to the lower chlorophyll concentrations in the near-coast surface ocean (Figure 3.2c). Notably, within the range of 200–1500 km away from the coast in Region.Warm, more solar radiation is accumulated in the subsurface ocean (at around 60 m depth) (Figure 3.2h), driven by the presence of a subsurface chlorophyll maximum (Figure 3.2c). As a result, additional solar heat is transported towards the coast at depth (Figure 3.3k) and then upwelled (Figure 3.3g), leading to an upper-ocean warming in the coastal upwelling regions (Figure 3.2l).

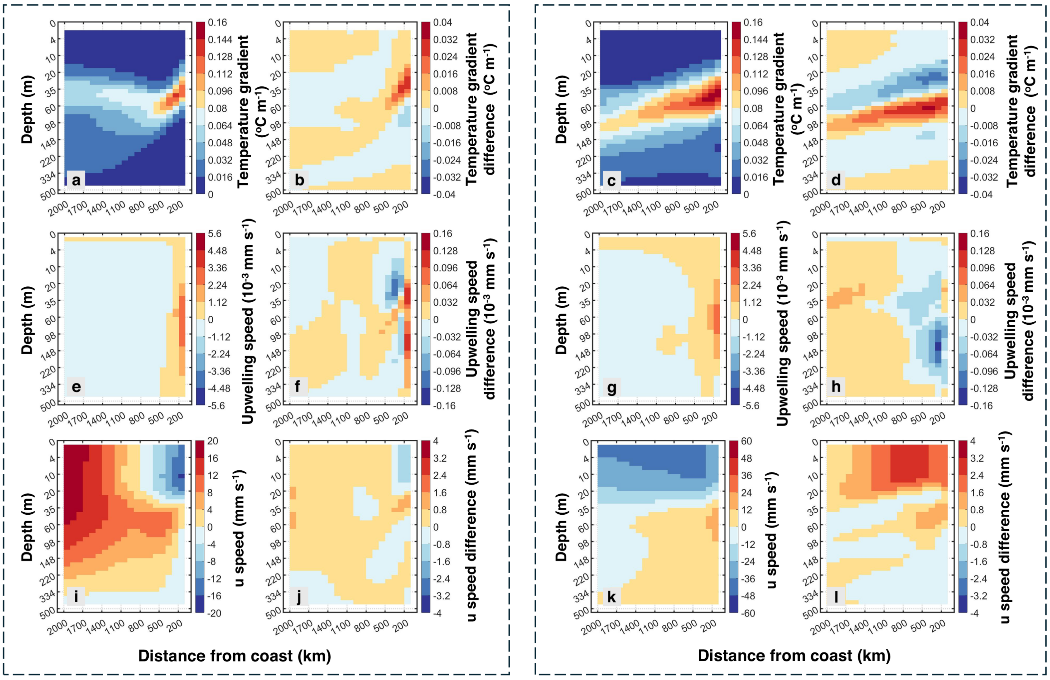

Figure 3.3: Mean cross-shore structures of vertical temperature gradient (a, c), upwelling speed (e, g) and eastward (u-ward) current speed (i, k) in Case.MED and their differences of Case.MED minus Case.Con (b, d, f, h, j and l) in Region.Cold (left dashed box) and Region.Warm (right dashed box) as indicated in Figure 3.1.

3.4.2 Impacts of chlorophyll-induced temperature variations on ocean dynamics

Aligned with the differing temperature responses to chlorophyll-induced solar absorption between the different upwelling regions, the subsequent effects on ocean dynamics differ and are described in this section. The wind forcing, acting as the atmospheric driver of coastal upwelling, remains constant in both cases. However, physical changes in the ocean resulting from chlorophyll-induced solar absorption could potentially influence the offshore transport and thus the upwelling dynamics.

In Region.Cold, the reduction in subsurface temperatures (20–140 m depth) resulting from the chlorophyll shading effect intensifies the vertical stratification in the upper ocean (Figure 3.3b) and leads to a shallower MLD in Case.MED (Figure 3.2f). The change of MLD only has a small impact on the solar absorption within the mixed layer. However, based on the calculation of net offshore transport (Section 3.3.4) following Sweeney et al. (2005), a shallower MLD intensifies offshore geostrophic transport, which largely explains the stronger net offshore transport in the mixed layer in Case.MED (Figure 3.4a). This leads to an intensified upwelling, peaking just below the enhanced offshore velocity anomalies (Figure 3.3j), to compensate the water transported away from the coast in the mixed layer (Figure 3.3f). Moreover, in Case.MED, the additional water transported away from the coast at the ocean surface is subsequently transported back to the coast through more pronounced downwelling between 200–500 km offshore, and subsurface coastward currents at around 60 m depth (Figures 3.3f and j). This process enhances the existing mesoscale zonal overturning circulation in these upwelling regions, characterized by an 'upward-offshore-downward-onshore' flow pattern (Figures 3.3f and j). The intensified upwelling near the coast contributes to cooling the near-coast water column, whereas enhanced downwelling farther offshore leads to the off-coast warming. This process, along with the chlorophyll-induced redistribution of solar heat (Figure 3.2f), collectively contributes to the negative temperature anomalies in near-coast regions and positive temperature anomalies in off-coast regions (Figure 3.2j).

In Region.Warm, the less stratified upper ocean (above 60 m depth) leads to a deeper MLD in Case.MED (Figure 3.2h). This weakens the offshore transport (Figures 3.3l and 3.4b), resulting in a reduced upwelling speed (Figure 3.3h). The circulation anomalies (Figures 3.3h and l) are broadly opposite to those in Region.Cold, indicating a weakening of the zonal overturning circulation consistent with a slower offshore current.

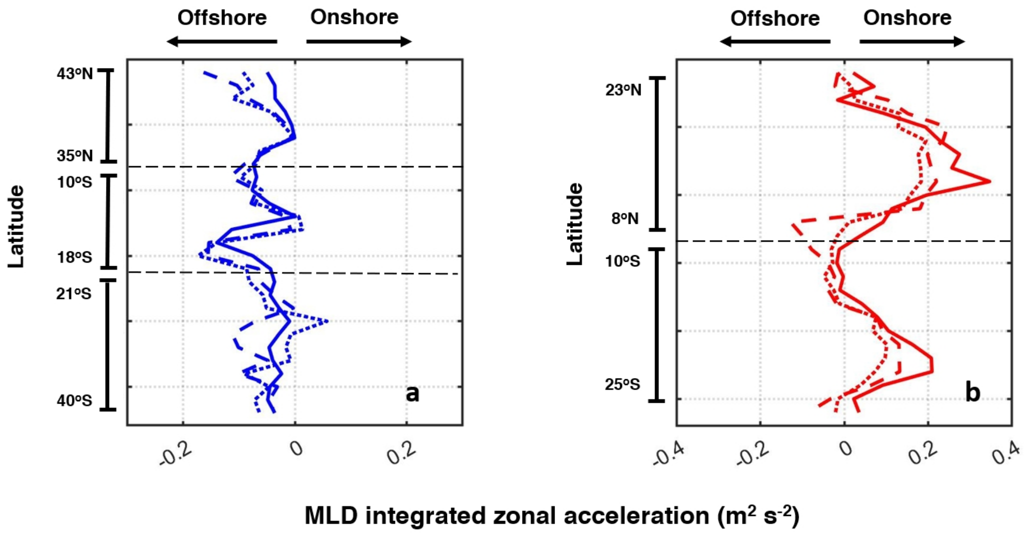

Figure 3.4: The differences of total calculated MLD integrated zonal acceleration between Case.MED and Case.Con along the coasts in Pacific coastal upwelling regions (a) and Atlantic coastal upwelling regions (b) as shown in Figure 3.1 based on the calculations in Section 3.3.4. Dotted lines represent the zonal transport difference induced by MLD change. Dashed lines represent the zonal geostrophic transport difference. Solid lines represent the zonal net transport difference obtained from NEMO modelling output.

3.5 Discussion and conclusions

The responses of the thermal structure and dynamics to chlorophyll-induced solar absorption vary between the Pacific and Atlantic coastal upwelling regions. In the Pacific coastal upwelling regions, increased chlorophyll-induced solar absorption produces cooling in the near-coast areas but simultaneous warming farther offshore. This is in line with Echevin et al. (2021), who proposed a cooling impact of chlorophyll-induced solar absorption in the near-coast Peru upwelling region. However, the maximum surface cooling reported in their study, up to 1 °C, is larger than the 0.3 °C in our study (Figure 3.1b). One possible reason is that the reference simulations of Echevin et al. (2021) are based on no chlorophyll as opposed to 0.1 mg m^{-3} in our study, accentuating the chlorophyll-induced cooling which is calculated based on the chlorophyll differences between reference and experimental simulations. Additionally, Echevin et al. (2021) used a fine-resolution regional ocean model (10 km horizontal resolution), enabling a more accurate simulation of the fine structure of the cooling effect caused by near-coast high chlorophyll concentrations (Hilt et al., 2020).

In the Atlantic coastal upwelling regions, solar heat absorbed by the subsurface chlorophyll maximum is transported coastward by the subsurface eastward currents and then upwelled, resulting in an upper-ocean warming (above 80 m) of the near-coast upwelling region. As a result of increased absorption of solar radiation at a depth of 60–80 m, there is a reduction in the penetration of solar radiation into the deeper ocean. Consequently, the negative anomaly of solar heat input below 80 m depth (as shown in Figure 3.2h) is trapped in the stratified deep ocean, leading to a cooling effect within 80–150 m depth (Figure 3.2l). This finding contrasts with Hernandez et al. (2017) who proposed a surface cooling caused by chlorophyll-induced solar absorption in the Benguela and Canary upwelling systems. The difference might arise from the unrealistic vertical profile of chlorophyll in their study, which was calculated by an empirical parameterisation (Morel and Berthon, 1989) combined with satellite-observed surface chlorophyll concentrations. This approach may not accurately capture the chlorophyll-induced temperature change if the empirical parameterisation only alters the distribution of solar radiation within the mixed layer in response to varying chlorophyll concentrations (see Figure 2 in Hernandez et al. (2017)), and it may fail to represent the warming effect induced by the Atlantic subsurface chlorophyll maximum which is below the mixed layer (Figure 3.2h). Therefore, we emphasize the importance of simulating chlorophyll vertical distribution especially relative to the mixed layer when evaluating the effect of chlorophyll-induced solar absorption (Zhang et al., 2018a; Du et al., 2024).

Furthermore, these results have been compared with the studies in equatorial upwelling regions. In the Pacific Ocean, similar cooling responses to chlorophyll-induced solar absorption are found in both coastal and equatorial upwelling regions, as supported by the majority of studies focused on equatorial upwelling (Zhang et al., 2019; Shi et al., 2023). This similarity is attributed to the

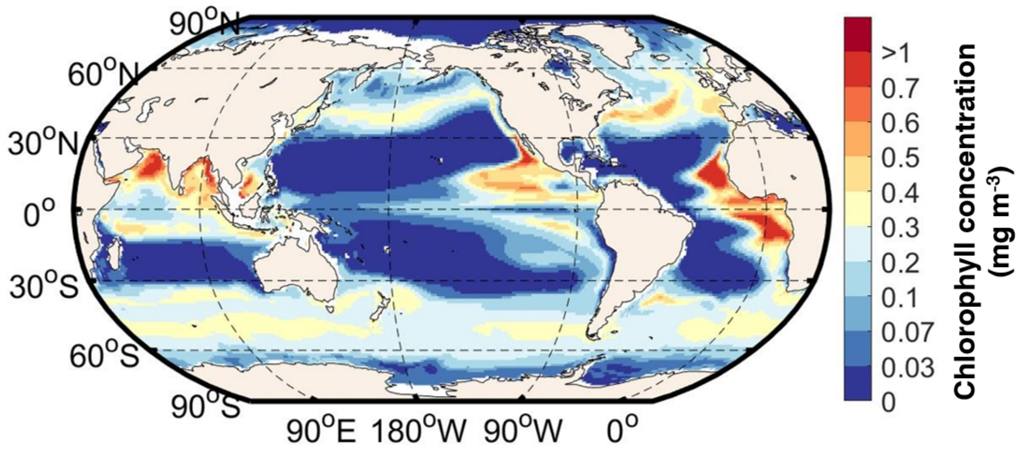

Figure 3.5: Distribution of chlorophyll concentration at 77m depth simulated by MEDUSA.

redistribution of solar radiation caused by chlorophyll (less penetration into subsurface and then upwelled) and resultant stronger surface divergence and upwelling (Murtugudde et al., 2002; Shi et al., 2023). However, the cooling effect in the Pacific coastal upwelling regions is more pronounced due to the higher upwelling speed which can transport more of the colder water affected by the chlorophyll shading effect (see Figure 2 in Shi et al. (2023)). In the Atlantic Ocean, SST responses to chlorophyll-induced solar absorption differ between coastal and equatorial upwelling regions due to varying dynamic and biogeochemical conditions. In equatorial upwelling regions, the variations in complex ocean currents induced by chlorophyll result in negative feedback on SST (Murtugudde et al., 2002), while in coastal regions, more pronounced subsurface chlorophyll maximum leads to positive feedback on SST (Figure 3.5).

We further assess the uncertainties in the results introduced by the methods used in this study. A comparison of surface chlorophyll concentrations between modelling output and satellite observations (Figures 3.6a and b) shows that the chlorophyll distribution in the Pacific upwelling regions is well captured by MEDUSA, although it overestimates chlorophyll concentrations in the Peru upwelling region. In Atlantic coastal upwelling regions within 10°S–10°N, MEDUSA exhibits a negative bias in surface chlorophyll concentrations (Figure 3.6). Nevertheless, MEDUSA accurately

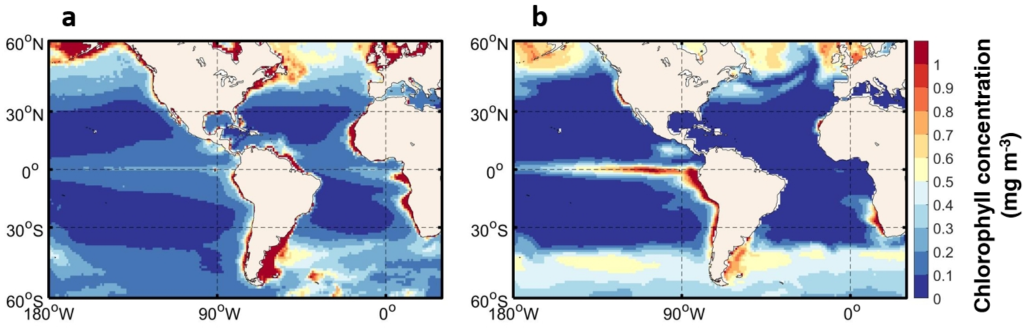

Figure 3.6: Distributions of surface chlorophyll concentrations in MODIS satellite observations (a) and MEDUSA (b).

reproduces the subsurface chlorophyll maximum in this region, which is a key feature contributing to the Atlantic upwelling warming (Figure 3.5 and Yasunaka et al. (2022)). Due to the inaccurate simulation of nutrient availability in MEDUSA (Yool et al., 2021), the positive bias in surface chlorophyll of Pacific coastal upwelling and negative bias in the Atlantic may exaggerate the findings of this study. However, the primary aim of this research is to understand the response of ocean physics to chlorophyll-induced solar absorption, rather than to reproduce precisely the observed ocean conditions. Furthermore, the key results of this study are all statistically significant at the 95% level, based on a Student's t-test analysis of the anomalies (Figure 3.7).

The chlorophyll-induced variations in upper ocean temperatures can further alter the ocean dynamics of upwelling regions. Following Sweeney et al. (2005), the net offshore transport, which governs upwelling strength, is determined by two components: Ekman transport and geostrophic transport (Section 3.3.4). The Ekman transport within the mixed layer remains consistent between the Case.MED and Case.Con simulations due to identical wind forcings in both cases. Therefore, changes in upwelling dynamics are governed by any variations in the geostrophic transport, in line with Ding et al. (2021) and Jing et al. (2023). In Pacific coastal upwelling regions, the enhanced stratification in the upper ocean associated with chlorophyll-induced solar absorption leads to a shallower MLD. This intensifies the offshore geostrophic transport and can largely explain stronger

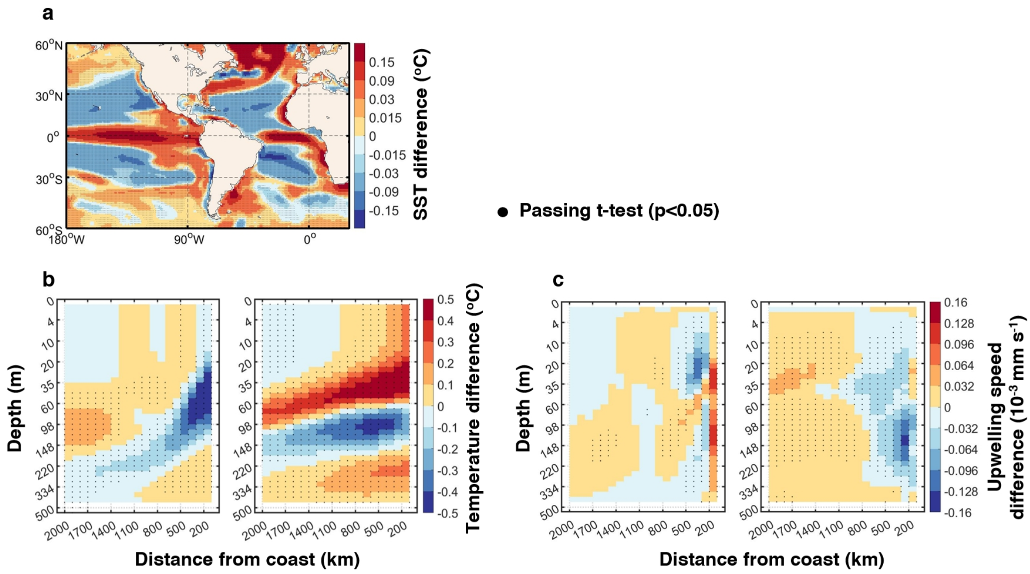

Figure 3.7: T-test results for Figure 3.1a (a), Figures 3.2j and l (b), and Figures 3.3f and h (c).

net offshore transport in Case.MED (Figure 3.4a). Finally, the intensification of offshore transport contributes to a stronger upwelling in the upper ocean (Figure 3.3f). The same mechanism produces the opposite response in Atlantic coastal upwelling regions due to the deeper MLD produced by the deep chlorophyll maximum here (Figure 3.4b).

In this study, the MLD is defined as the depth at which temperature decreases by 0.5 °C relative to the local SST. This temperature-based definition is appropriate in coastal upwelling regions, where upper-ocean density variations are primarily controlled by temperature rather than salinity (Talley, 2007; Koltermann et al., 2011). However, the thermocline transition is gradual in the real ocean rather than sharply defined, so the diagnosed MLD and consequently the geostrophic transport derived from it may depend on the chosen threshold. To assess this sensitivity, we conducted a series of experiments in which the MLD was defined using temperature criteria ranging from 0.1 to 0.5 °C. The resulting changes in the calculated cross-shore transport shown in Figure 3.4 are smaller than 5%. This limited sensitivity arises because our analysis focuses on the difference between Case.MED and Case.Con; therefore, systematic biases associated with the MLD definition largely cancel out between the two simulations.

However, the calculations of net offshore transport only provide an incomplete dynamical interpretation for coastal upwelling, as it may overlook the remote effects of larger-scale circulation, which is an important component in coastal upwelling systems (Lee et al., 2024). Hence, we present the difference of horizontal currents between two cases within coastal upwelling regions in Figure 3.8. In Pacific coastal upwelling regions, the horizontal currents in Case.MED show a 10% increase compared to Case.Con (Figures 3.8e and f), attributed to stronger geostrophic transport, aligning with stronger offshore transport and upwelling caused by chlorophyll-induced solar absorption. However, in Atlantic upwelling regions, variations in ocean currents caused by chlorophyll-induced solar absorption appear to be part of a broader pattern of surface current anomalies, likely correlated with other dynamical changes, such as equatorial currents and larger-scale circulations (Figures 3.8g and h), although these must ultimately be driven by the difference in chlorophyll between the two simulations. Therefore, future research should investigate both local and remote processes driven by changes in chlorophyll-induced solar absorption and resultant impacts on ocean dynamics.

The variations in ocean dynamics caused by chlorophyll-induced thermal structure change potentially feedback to the upper ocean temperatures (Figures 3.3e-l). To quantify the relative contribution of changes in ocean currents on chlorophyll-induced temperature variations, a heat budget analysis has been applied to Case.MED and Case.Con (Figure 3.9). The heat budget differences between the two cases align with our results, revealing a solar heating effect in the upper ocean but a cooling effect from the transport of colder subsurface water in Pacific coastal upwelling regions (Figures 3.9a, b and d), and a warming effect in subsurface water of Atlantic coastal upwelling regions (Figure 3.9c) which is then upwelled (Figures 3.9d and h). We also conduct sensitivity tests by calculating the heat budget difference between Case.MED and Case.Con under the assumptions that either the ocean currents are kept constant or the temperatures are kept

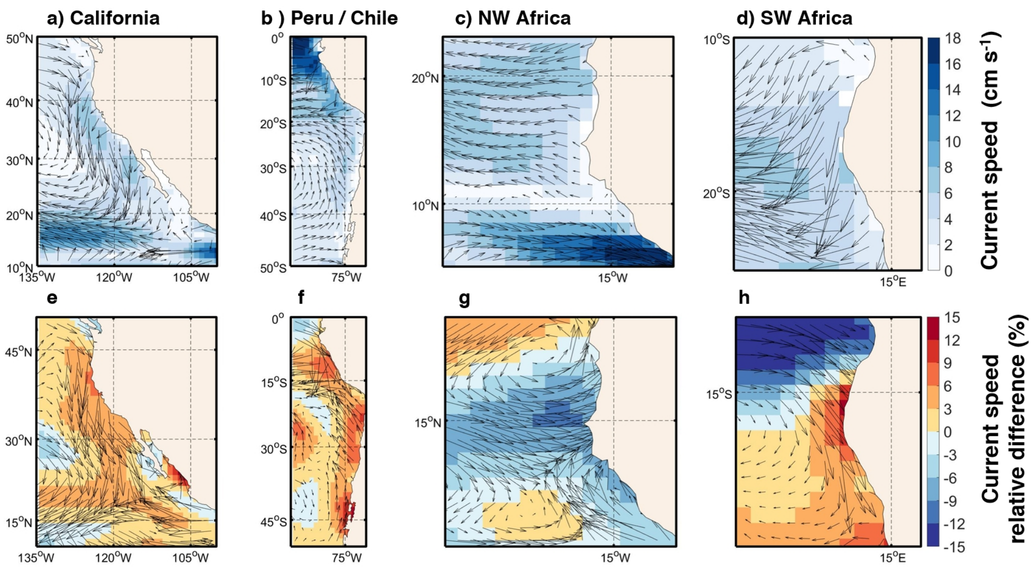

Figure 3.8: Changes in surface ocean current speed in major eastern boundary upwelling systems associated with chlorophyll-induced radiative effects. (a-d) Ocean current speed in California (a), Peru and Chile (b), NW (c) and SW (d) Africa upwelling regions based on the modelling output of Case.MED. (e-h) The relative difference of current speed between Case.MED and Case.Con.

constant (Figure 3.10). Qualitatively, the heat budget difference patterns between the two cases align closely with those caused by temperature changes (Figures 3.10a-d). Quantitatively, in Pacific coastal upwelling regions, the cooling effect of -0.06 °C month^{-1} induced by changes in ocean advection within the mixed layer of near-coast regions (primarily due to stronger upwelling), accounts for only 9 % of the cooling effect of -0.68 °C month^{-1} induced by upward transport of colder water induced by chlorophyll shading. In Atlantic coastal upwelling regions, the weaker upwelling contributes to 12 % of the total warming effect caused by chlorophyll-induced solar absorption.

The simulation of phytoplankton growth in the biogeochemistry model (MEDUSA) is based on the temperature, nutrients and solar radiation availability, influenced by the physical conditions provided by the ocean model (NEMO). Therefore, the variations in ocean physics caused by chlorophyll-induced solar absorption may initiate a feedback effect on chlorophyll concentrations. In Pacific upwelling regions, the stronger upwelling in Case.MED supplies more nutrients to the upper ocean, resulting in increased chlorophyll concentrations in the surface ocean

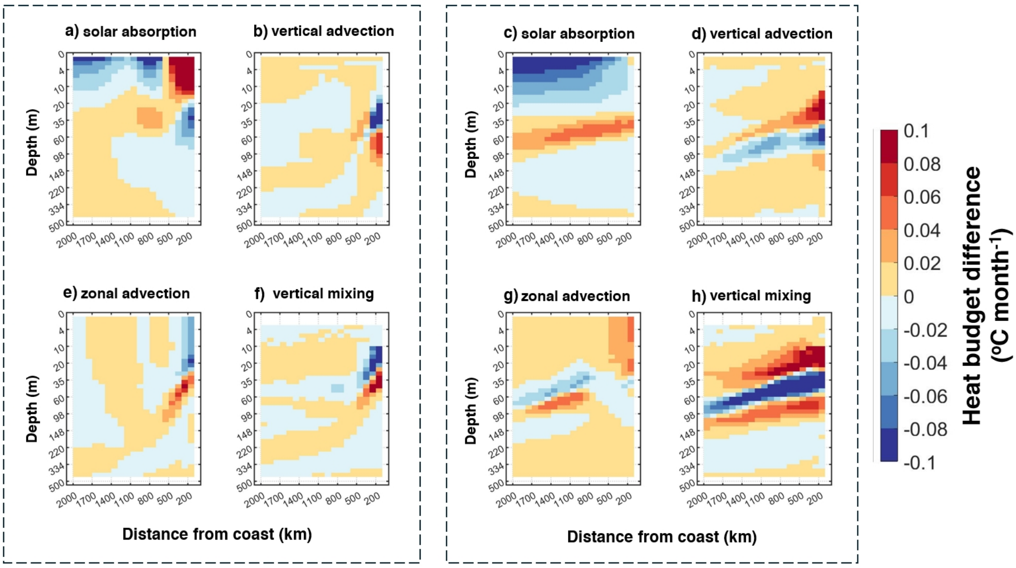

Figure 3.9: Heat budget differences between Case.MED and Case.Con in Pacific coastal upwelling regions (left box) and Atlantic coastal upwelling regions (right box), following Equation 2.1.

(Figure 3.2b). Conversely, in Atlantic coastal upwelling regions, weaker upwelling leads to lower chlorophyll concentrations at the ocean surface (Figure 3.2d) (Messié and Chavez, 2015). However, in the areas away from the Atlantic coast, the penetration of more solar radiation into the subsurface ocean in Case.MED contributes to higher subsurface chlorophyll concentrations (Figure 3.2d). Overall, the surface chlorophyll maximum in Pacific coastal upwelling regions and subsurface chlorophyll maximum in Atlantic coastal upwelling regions can significantly impact ocean thermal structure and dynamics. These effects, in turn, trigger a positive feedback that reinforces the chlorophyll distribution pattern in each coastal upwelling region (Figures 3.2a-d).

In addition, in some ESMs, the light availability for phytoplankton growth in the biogeochemical component is determined by the solar radiation calculated by the physical ocean model. As a result, substantial differences can arise in the simulated light environment throughout the water column when using a constant chlorophyll concentration (e.g. 0.1 mg m^{-3}) compared with using simulated, spatially and temporally varying chlorophyll. For example, the maximum light penetration depth in Case.MED differs from that in Case.Con by up to ∼60 m (Figure 3.11). These

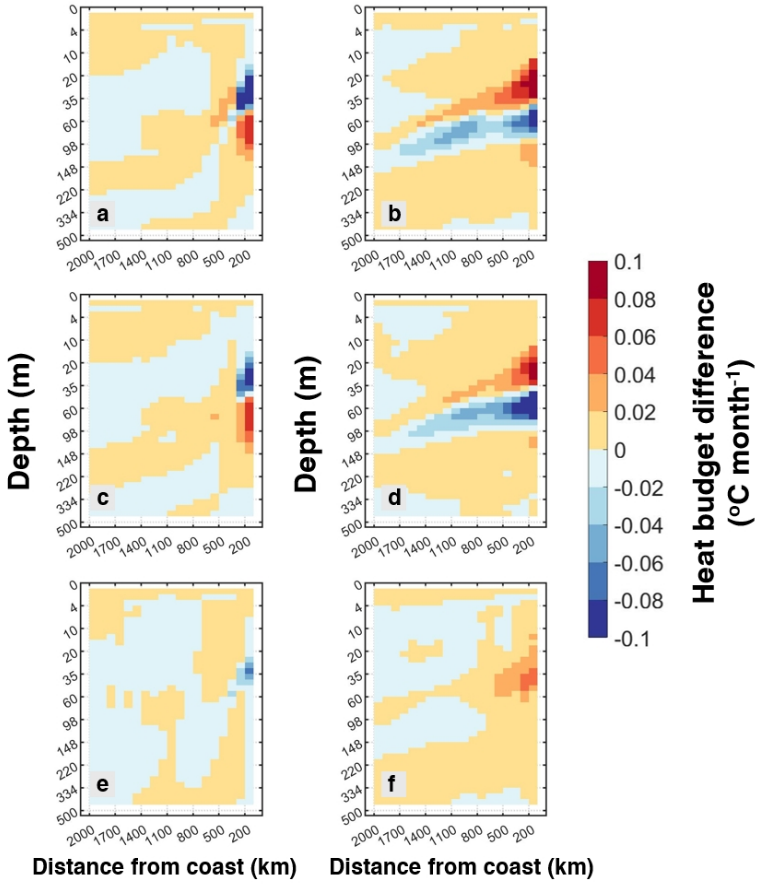

Figure 3.10: Differences in vertical heat advection between Case.MED and Case.Con in Pacific coastal upwelling regions (a, c, e) and Atlantic coastal upwelling regions (b, d, f). (a-b) The heat budget differences between Case.MED and Case.Con. (c-d) The heat budget differences between the two cases, assuming constant ocean currents. (e-f) The heat budget differences between the two cases, assuming constant temperature fields.

results highlight the importance of accurately representing chlorophyll-induced light attenuation in ESMs in order to more realistically simulate phytoplankton growth conditions and the associated biogeochemical cycling.

Figure 3.12 summarises the different mechanisms behind chlorophyll-induced variations in ocean thermal structure and dynamics between Pacific and Atlantic coastal upwelling regions. This discrepancy arises from different chlorophyll distributions in these two regions (green boxes in Figure 3.12). In Pacific coastal upwelling regions, the high surface Chl concentrations near the coast induce a shading effect in the subsurface ocean that is then upwelled, consequently leading

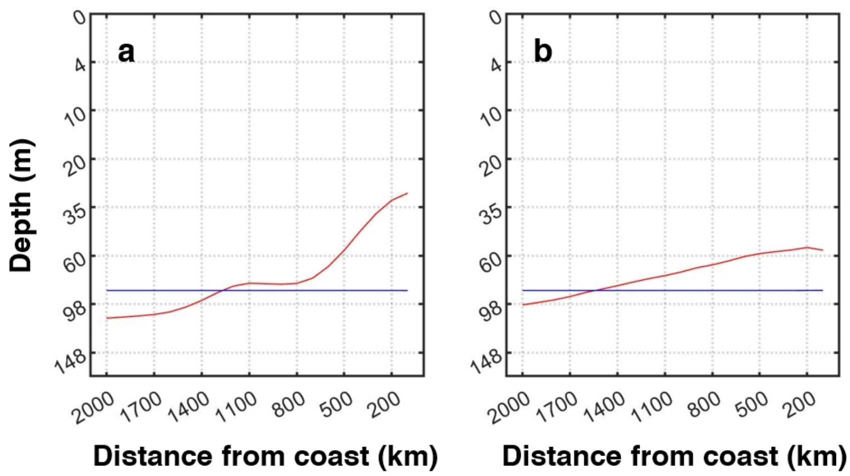

Figure 3.11: Differences in maximum light penetration depth between Case.MED (red lines) and Case.Con (blue lines) in Pacific coastal upwelling regions (a) and Atlantic coastal upwelling regions (b). The maximum light penetration depth is defined as the depth at which downwelling shortwave radiation is reduced to 1% of its surface value.

to colder near-surface waters, a more stratified upper ocean and stronger circulation associated with the upwelling (Figure 3.12a). In Atlantic coastal upwelling regions, the subsurface chlorophyll maximum absorbs solar radiation and leads to a warmer upper ocean and weaker circulation (Figure 3.12b). This study highlights the importance of considering the spatial distributions of chlorophyll when analysing its effect on coastal upwelling.

Compared to the impact of chlorophyll-induced solar absorption in equatorial upwelling, which has been shown to significantly influence large-scale circulation (Nakamoto et al., 2001; Shi et al., 2023) and climate variability such as ENSO (Zhang et al., 2009; Kang et al., 2017), the effect in coastal upwelling regions appears to be more localized. However, the variations in ocean thermal structure driven by chlorophyll in coastal upwelling have the potential to impact stratocumulus clouds in the atmosphere over the upwelling regions and also the climate on a broader scale. SST changes in coastal upwelling regions could alter the lower tropospheric stability, thereby impacting the formation and persistence of oceanic stratocumulus clouds. The response of stratocumulus clouds to SST variations varies widely among models. Some models suggest a decrease in cloud cover (positive feedback), while others indicate an increase (negative feedback) in response to warmer surface in coastal upwelling regions (Zhang and Bretherton, 2008; Brient and Bony, 2012; Qu et al., 2014). Nevertheless, it is undeniable that temperature variations driven by chlorophyll-induced solar absorption can influence the formation and equatorward propagation of stratocumulus clouds and subsequently impact the tropical climate (Yu and Mechoso, 1999; Hu et al., 2008).

In this paper, we have shown that the variability in chlorophyll-induced solar absorption has a crucial role in regulating the ocean thermal structure, dynamics and climate, yet is absent in some physical ocean models and coupled climate models such as UKESM. Therefore, this biophysical feedback needs to be incorporated into future versions of UKESM and other ESMs to achieve a more realistic simulation of ocean physics and improve our understanding of climate dynamics.

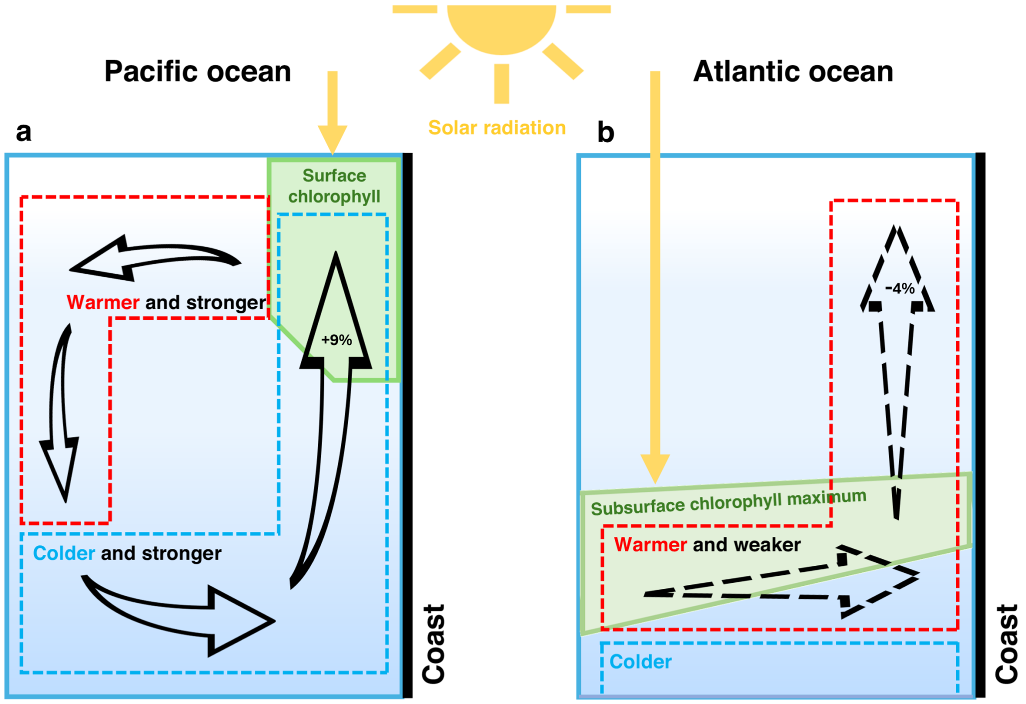

Figure 3.12: Schematic figure of the oceanic responses to chlorophyll-induced solar absorption in Pacific (a) and Atlantic (b) coastal upwelling regions. Black arrows represent the mean state of ocean currents in coastal upwelling regions, with solid arrows indicating stronger currents and dashed arrows representing weaker currents resulting from enhanced chlorophyll-induced solar absorption. The red dashed boxes and blue dashed boxes indicate warmer and colder temperature zones respectively caused by chlorophyll-induced solar absorption. The percentages inside the arrows quantify the variations in upwelling speed attributed to chlorophyll-induced solar absorption.

4

Redistribution of light absorption by chlorophyll decline delays warming by up to a decade

The results presented in the following chapter have been submitted to *Journal of Geophysical Research: Oceans* and are under peer review.

The work presented in this chapter was led by Siyu Meng. Manoj Joshi contributed to the conceptual design of the study. Benjamin Webber, David Stevens and Manoj Joshi contributed to the data analysis and manuscript preparation.

4.1 Abstract

Chlorophyll regulates solar radiation absorption in the upper ocean, influencing the ocean's mean state and climate. However, its response to climate change in Earth System Models (ESMs) remains unclear. Here, we show that in addition to well-known effects on the carbon cycle, projected chlorophyll decline reduces the absorption of solar radiation within the ocean's mixed layer, effectively redistributing $0.25\,\mathrm{W\,m^{-2}}$ of globally-averaged radiative flux to the upper thermocline underneath it, delaying climate warming by up to 12 years under the Shared Socioeconomic Pathway 5-8.5 scenario. The uncertainty arises from inter-model differences in the simulation of chlorophyll and its solar absorption in ESMs that simulate these processes. Such differences also contribute to biases in the mean pre-industrial state of ESMs. Our findings highlight the need to reduce uncertainty in physical, not just biogeochemical, feedbacks associated with chlorophyll in ESMs.

4.2 Introduction

Solar radiation that reaches the sea surface penetrates the upper ocean, with its shortwave component decaying exponentially with depth (Jerlov, 1968). In the ocean, phytoplankton are the primary agents influencing radiation attenuation, as they absorb shortwave radiation through chlorophyll and related pigments (Morel, 1988). Such absorption determines the vertical distribution of solar heating in the ocean, which has been shown to influence the global upper ocean heat budget (Ohlmann, 2003), thermal stratification (Manizza et al., 2005), ocean dynamics (Sweeney et al., 2005) and the broader climate system (Turner et al., 2012; Zhang et al., 2018b; Giddings et al., 2020).

Generally, an increase in surface chlorophyll concentrations would warm the topmost ocean layer (Manizza et al., 2005; Park et al., 2015).

Ocean-biogeochemistry models suggest that chlorophyll concentrations can induce global SST warming of approximately 0.5 °C, compared to an idealised optically clear ocean (Patara et al., 2012). However, in certain regions, such as coastal upwelling regions, the shading effect of high surface chlorophyll concentration cools the subsurface water, which is subsequently upwelled and drives net surface cooling (Hernandez et al., 2017; Echevin et al., 2021; Meng et al., 2024).

Chlorophyll-induced variations in upper ocean temperatures influence climate dynamics across multiple timescales. For instance, interannual variations of chlorophyll concentration in the equatorial upwelling region of the Pacific Ocean significantly influence both the magnitude (Lengaigne et al., 2007; Park et al., 2014a) and asymmetry (Timmermann and Jin, 2002) of the ENSO. On longer timescales, climate warming is projected to decrease near-surface chlorophyll concentration through mechanisms such as enhanced nutrient limitation (Dai et al., 2023; Yang et al., 2023; Zhao et al., 2025) and changes in phytoplankton photoacclimation responses (Behrenfeld et al., 2016). These changes can, in turn, influence oceanic carbon sequestration and hence atmospheric CO_2 concentrations, changing the future rate of ocean warming (Laufkötter et al., 2016). However, our understanding of how future chlorophyll changes will impact solar radiation absorption, and the partitioning of heat between the surface and subsurface ocean, remains very limited.

Earth system models exhibit considerable diversity in their approaches, including both the modelling of chlorophyll itself, and the parameterisations representing the effect of chlorophyll on the vertical profile of solar absorption (physical solar schemes). For instance, some ESMs use the spatially and temporally constant chlorophyll in their physical solar schemes despite simulating dynamic chlorophyll in their ocean biogeochemistry models. Despite numerous studies highlighting the importance of accurately representing chlorophyll-induced solar absorption in climate simulations (e.g. Anderson et al., 2009; Kang et al., 2017; Zhang et al., 2018a; Paulsen et al., 2018; Echevin et al., 2021; Asselot et al., 2021; Meng et al., 2024; Witte et al., 2024), the methodologies currently employed by CMIP6 ESMs for this purpose, and the implications of their differences, remain poorly studied.

The diverse representations of chlorophyll, combined with differences in physical solar schemes between ESMs, are expected to introduce substantial uncertainties into ESM simulations of ocean physics, climate and global change. Here, we show how future changes in chlorophyll modify the amount of solar radiation absorbed in the mixed layer, effectively redistributing energy beneath the mixed layer, and delaying warming. We show how the mechanism occurs and quantify uncertainties introduced by the diverse methodologies used in CMIP6 ESMs in simulating chlorophyll-induced solar absorption.

4.3 Methods

The information on the physical solar schemes, along with the chlorophyll inputs of physical solar scheme used in ESMs, is summarised in Table 4.1. These details have been compiled either from relevant literature or through personal communication with the modelling groups responsible for developing and maintaining the respective ESMs.

4.3.1 Physical solar schemes

Current ESMs employ six physical solar schemes to calculate solar absorption in the ocean, including Jer68 (Jerlov, 1968), PaS77 (Paulson and Simpson, 1977), Ohl03 (Ohlmann, 2003), Man05 (Manizza et al., 2005), CSIRO (Bi et al., 2013) and RGB (Lengaigne et al., 2007) schemes (Table 4.1). Among these schemes, Jer68 and PaS77 are relatively simplified approaches, calculating the exponential attenuation of solar radiation with depth without considering the spatial and temporal variations in chlorophyll concentrations in the open ocean. The CSIRO shortwave scheme uses an attenuation coefficient at a specific wavelength. Man05 divides solar radiation into one infrared band and one visible band, while Ohl03 separates it into one infrared and two visible bands (red and blue). The RGB scheme further refines this spectral division into infrared, red (R), green (G) and blue (B) bands. These physical solar schemes quantify the attenuation effects of chlorophyll on different wavelength bands by measuring the attenuation coefficients, which are then used to calculate the vertical attenuation of total solar radiation. Theoretically, dividing solar radiation into finer wavelength bands can improve the accuracy of radiation attenuation calculations but also increases computational costs. As a result, the RGB scheme, which strikes a balance between accuracy and computational efficiency (Lengaigne et al., 2007), has been adopted by most ESMs (Table 4.1) and is used as a reference physical solar scheme in this study.

4.3.2 Chlorophyll input of physical solar scheme

The chlorophyll data used as input for physical solar schemes vary between ESMs, including prognostic chlorophyll, satellite-observed chlorophyll and spatially and temporally constant chlorophyll values (Table 4.1). This divergence arises because current ESMs often retain the configurations of their previous generations to maintain consistency across model versions and to avoid introducing additional biases in upper ocean heat budget due to biases in simulated chlorophyll. For the models considered here that use satellite-observed chlorophyll data as input for physical solar schemes, the chlorophyll concentrations are derived from SeaWiFS satellite observations averaged over the period 1998–2007. Although satellite observation is unable to capture the vertical distribution of chlorophyll, it still provides the most realistic representation of near-surface chlorophyll, which largely determines the absorption of solar radiation in the upper ocean. Models that use constant chlorophyll values typically adopt a fixed concentration of $0.05\,\mathrm{mg\,m^{-3}}$, a default value in NEMO that is significantly lower than global observed mean concentration (Madec and NEMO team, 2016). However, the UK Meteorological Office recently updated this value to $0.1\,\mathrm{mg\,m^{-3}}$ in the latest version of the NEMO (Guiavarc'h et al., 2025), better aligning simulations with observational data.

4.3.3 Solar absorption calculation

To isolate the role of chlorophyll concentration on upper ocean solar absorption, we use a constant incoming solar radiation field throughout this study, based on the monthly climatological mean over the last 30 years of piControl simulations from a multi-model average (referred to below as the reference incoming solar radiation). If we used the simulated time-varying solar radiation instead then future changes would be strongly influenced by changes in cloud cover, which would obscure the important feedbacks from chlorophyll studied here.

In this study, the solar absorption in the upper ocean is calculated based on the climatological seasonal maximum MLD at each location. This approach accounts for the process whereby, in physical ocean models, heat in the upper ocean is typically set to be fully mixed within the mixed layer (Large et al., 1994), making the total solar energy absorbed within the mixed layer more important than its vertical distribution. It also captures the influence of seasonal mixing processes: for example, in the open ocean of the mid-latitude Northern Hemisphere, chlorophyll concentrations are lower and the mixed layer is shallower in summer (Figure 4.1a), allowing more solar radiation to penetrate below the summer mixed layer, which is later entrained into the mixed layer during winter deepening (Figure 4.1d). Using a climatological value allows us to remove the effect of time-varying MLD, which tend to shoal with climate change and would therefore introduce a large signal of reduced mixed layer radiative heating. This simplification will neglect some spatial and temporal variability in the amount of this sub-mixed layer solar absorption that actually gets entrained into the mixed layer, but we expect the net global effect to be small.

For analysing the impact of future chlorophyll changes on solar absorption in the mixed layer, we regridded the ESM outputs to a 1°×1° horizontal grid and applied the RGB scheme to the depth levels of each model in Section 4.4.1. This was done using chlorophyll outputs from piControl and SSP5-8.5 simulations of five ESMs, which use prognostic chlorophyll data as input for their physical solar schemes (Table 4.1).

The piControl scenario represents a simulation with constant external forcings, while the SSP5-8.5 scenario projects future conditions under a high-emissions pathway (Eyring et al., 2016). The change in response to global warming is defined as the mean of the 2071–2100 period under the SSP5-8.5 scenario minus the mean of the last 30 years of the piControl scenario.

Uncertainty assessment in Section 4.4.2 involved two components: (1) Physical solar scheme difference, which applies reference incoming solar radiation and satellite-observed climatology chlorophyll (1998–2007) to six physical solar schemes, and (2) chlorophyll input difference, which uses the RGB scheme with three chlorophyll inputs: 1998–2007 SeaWiFS observations, contemporary ESM outputs (historical runs) and spatially and temporally constant values of $0.05\,\mathrm{mg\,m^{-3}}$ and $0.1\,\mathrm{mg\,m^{-3}}$. In this study, uncertainty refers to the range between different models (inter-model spread) or physical solar schemes (inter-scheme spread). Where applicable, only differences that are statistically significant at the 95% confidence level are shown.

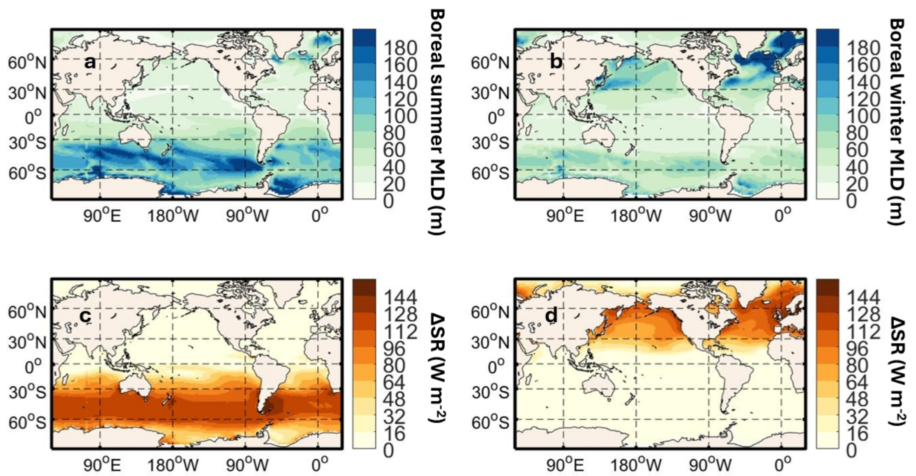

Figure 4.1: Seasonal variations of MLD and their impact on solar radiation absorption within the mixed layer. (a) Boreal summer MLD. (b) Boreal winter MLD. (c) Difference in solar radiation absorbed within the mixed layer under boreal winter solar radiation conditions, calculated as the absorption using the deeper MLD in boreal summer minus that using the shallower MLD in boreal winter. (d) Difference in solar radiation absorbed within the mixed layer under boreal summer solar radiation conditions, calculated as the absorption using the deeper MLD in boreal winter minus that using the shallower MLD in boreal summer. Only positive values are shown, representing the additional solar radiation absorbed by a seasonally deeper mixed layer.

4.4 Results

4.4.1 Chlorophyll effect on future warming

To isolate the role of chlorophyll in future warming, we calculate the solar absorption within mixed layer by fixing the MLD to its climatologically-averaged seasonal maximum and using time-varying chlorophyll from five ESMs that incorporate prognostic chlorophyll into their physical solar schemes (Table 4.1). The seasonal maximum of MLD is used in order to account for the annual cycle of MLD entraining deeper water whose warming is communicated to the surface within a year, while heating beneath this is isolated from the surface for at least several years, thus delaying climate warming. We carry out this calculation using the RGB scheme (Lengaigne et al., 2007).

Over the ocean, the future overall decline in mixed layer chlorophyll concentration (Figure 4.2) is projected to redistribute solar radiation below the mixed layer (Figure 4.3a). As an ocean average, $0.43\,\mathrm{W\,m^{-2}}$ of solar radiation is redistributed below the mixed layer in the period 2071–2100 of the SSP5-8.5 scenario, when compared to the piControl period. To turn this into a global value, we define a global mixed layer chlorophyll forcing (GMF) as the global average anomaly of chlorophyll-induced solar absorption within the ocean mixed layer relative to piControl, assuming that this anomaly is zero over land. Reduced chlorophyll concentrations decrease the GMF by $0.3\,\mathrm{W\,m^{-2}}$ (Figure 4.3b). Such a reduction is of considerable significance, being equivalent to roughly half of the radiative forcing from projected increases in N_2O under the SSP5-8.5 scenario by 2100, while the most pronounced response, in the GFDL model, is more than the full radiative forcing from N_2O changes by this time (Meinshausen et al., 2020).

Chlorophyll-induced changes to the surface heat budget of this nature are neglected by the other ESMs since they rely on temporally constant or climatological chlorophyll concentrations to calculate solar absorption (Table 4.1), even though they simulate dynamic chlorophyll. Given that most of these ESMs also project future declines in chlorophyll concentrations (Figures 4.2f-k), incorporating the radiative effects of prognostic chlorophyll would result in a negative GMF (Figure 4.4), delaying their projected global temperature increase by 2071–2100, which is consistent with the results shown in Figure 4.3. The negative GMF effectively delays the human-induced global warming signal by approximately 3 years on average, with a maximum delay of 12 years across models (Figure 4.5a), based on the chlorophyll output of eleven ESMs.

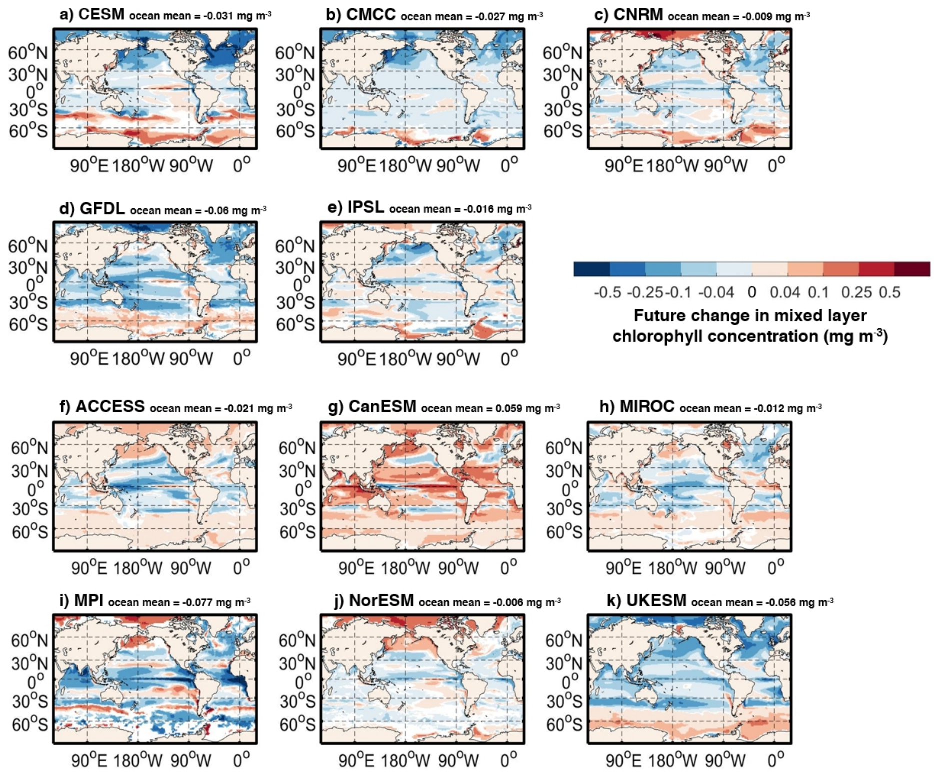

Figure 4.2: Projected changes in mixed layer chlorophyll concentration in each ESM. (a-k) Differences in mixed layer chlorophyll concentration calculated as the period 2071–2100 under the SSP5-8.5 scenario minus the last 30 years of the piControl simulation. The number shown after each panel label represents the global ocean mean value.

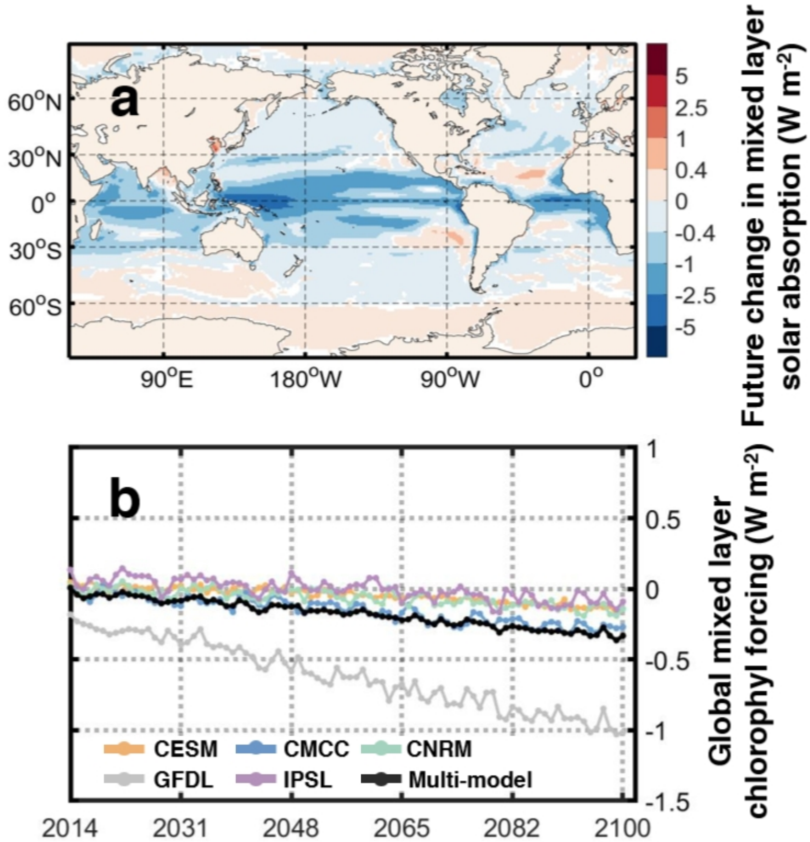

Figure 4.3: Future changes in solar absorption within the ocean surface mixed layer due to chlorophyll changes. (a) Projected multi-model mean change in mixed layer solar absorption due to chlorophyll changes, calculated as the period 2071–2100 under the SSP5-8.5 scenario minus the last 30 years of the piControl simulation. (b) Time series of global mixed layer chlorophyll forcing from five ESMs (coloured lines) and the multi-model mean (black line). Global mixed layer chlorophyll forcing (GMF) is defined as the global average anomaly of chlorophyll-induced solar absorption within the mixed layer relative to piControl.

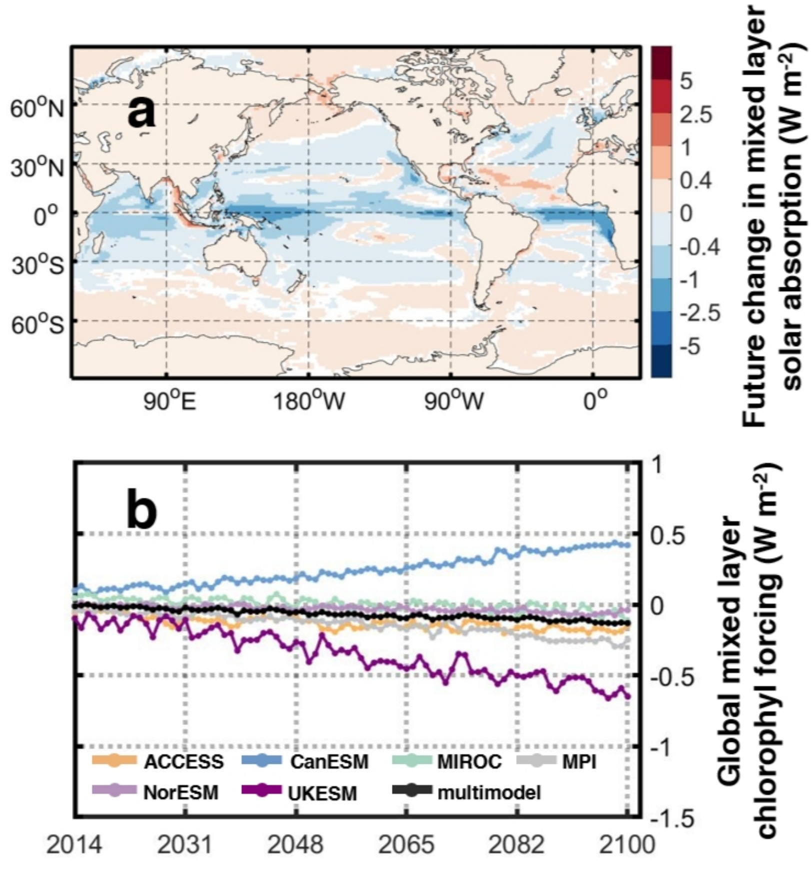

Figure 4.4: Future changes in solar absorption within the ocean surface mixed layer due to chlorophyll changes, same as in Figure 4.3 but for the ESMs that do not incorporate prognostic chlorophyll into their physical solar schemes. (a) Projected multi-model mean change in mixed layer solar absorption due to chlorophyll changes, calculated as the period 2071–2100 under the SSP5-8.5 scenario minus the last 30 years of the piControl simulation. (b) Time series of global mixed layer chlorophyll forcing from six ESMs (coloured lines) and the multi-model mean (black line). Global mixed layer chlorophyll forcing (GMF) is defined as the global average anomaly of chlorophyll-induced solar absorption within the mixed layer relative to piControl.

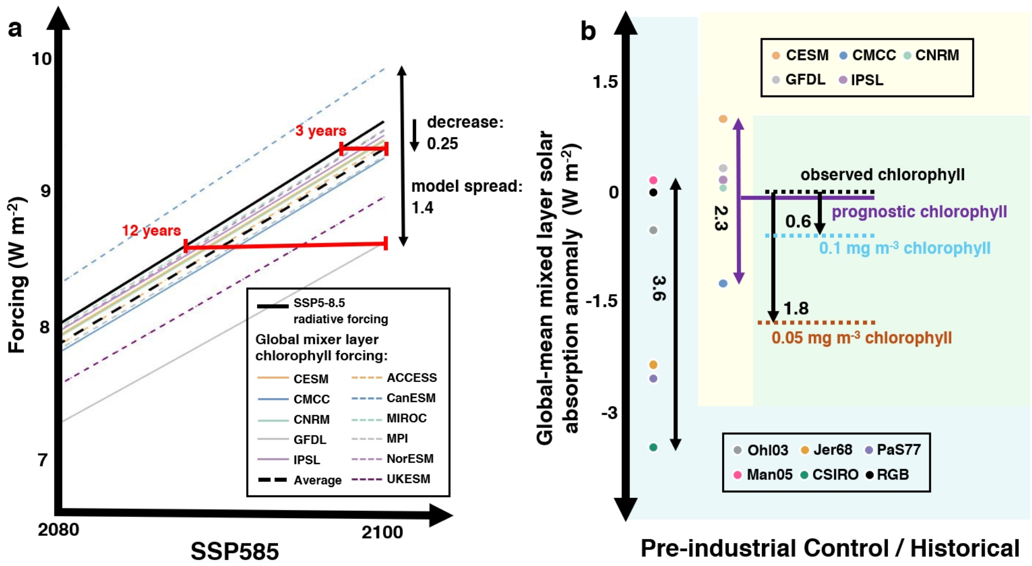

Figure 4.5: Future changes and uncertainties in the chlorophyll-induced mixed layer solar absorption in ESMs. (a) Temporal evolution of global average anomaly of chlorophyll-induced solar absorption within the mixed layer relative to piControl (global mixed layer chlorophyll forcing) under the SSP5-8.5 scenario. The black solid line shows the effective forcing under the SSP5-8.5 scenario from the reference calculation (Meinshausen et al., 2020). Coloured lines represent the sum of this reference forcing and the (negative) global mixed layer chlorophyll forcing from each ESM, and the thick black dashed line denotes the multi-model mean. The coloured solid lines correspond to the chlorophyll-induced anomalies predicted by models in Figure 4.3, while the dashed lines represent the anomalies predicted by models in Figure 4.4. The red horizontal bars represent the delay in reaching the same radiative forcing level when mixed layer chlorophyll forcing is included, shown for both the multi-model mean and GFDL. (b) Uncertainties in the multi-year mean state of global-mean mixed layer solar absorption anomaly, attributed to differences in physical solar schemes between all ESMs (light blue region), chlorophyll simulations between five ESMs as shown in Figure 4.3 (light yellow region) and chlorophyll inputs of solar schemes between all ESMs (light green region). The bar in the light blue region shows the uncertainty range caused by different physical solar schemes using the same chlorophyll input (satellite observations). The bar in the light yellow region indicates the uncertainty range from different chlorophyll simulations by five ESMs, all using the same RGB scheme. Coloured lines show anomalies due to different chlorophyll inputs using the same RGB scheme, including 1998–2007 SeaWiFS observations, contemporary multi-model mean outputs from five ESMs (historical runs) and spatially and temporally constant values of $0.05\,\mathrm{mg\,m^{-3}}$ and $0.1\,\mathrm{mg\,m^{-3}}$. The reference calculation (black dashed line at zero) uses the RGB scheme with satellite-observed chlorophyll.

4.4.2 Sources of uncertainties in modelling chlorophyll-induced solar absorption

Here we evaluate how inter-model differences in physical solar schemes and chlorophyll input data lead to a significant inter-model spread in mixed layer solar absorption, both under piControl conditions and in future climate projections. We define the global-mean mixed layer solar absorption anomaly (GMSA) as the global average anomaly of mixed layer solar absorption arising from the inter-model differences, again with land values set to zero. This section extends the analysis to all ESMs in Table 4.1.

4.4.2.1 Effect of different physical solar schemes

Six physical solar schemes are employed in current ESMs (Table 4.1). Using the global-mean reference incoming solar radiation (see Section 4.3.3) and the global-mean chlorophyll derived from the satellite observation, the range of downward solar radiation between these six physical solar schemes is $40\,\mathrm{W\,m^{-2}}$ at a depth of $10\,\mathrm{m}$ and $15\,\mathrm{W\,m^{-2}}$ at $50\,\mathrm{m}$ (Figure 4.6a). Notably these uncertainty ranges represent $\sim$50 % of the average solar radiation across the six physical solar schemes at both depths (Figure 4.6a).

Considering the spatial distributions of incoming solar radiation and chlorophyll concentrations, the range of GMSA resulting from different physical solar schemes is $3.6\,\mathrm{W\,m^{-2}}$ (Figure 4.5b), with the largest differences in the subtropical oceans (Figure 4.6b). This is because the combination of high incoming solar radiation, low chlorophyll and shallow mixed layer allows deeper solar penetration and increases the sensitivity to the choice of physical solar scheme. As a result, the inter-scheme range in solar absorption within the mixed layer reaches $11.5\,\mathrm{W\,m^{-2}}$ in these regions (Figure 4.6b).

Applying the reference incoming solar radiation and the multi-model mean chlorophyll concentrations from the SSP5-8.5 scenario to six physical solar schemes, the projected future declines in GMF show considerable inter-scheme spread. This results in an uncertainty range of 0.25–0.57 $\mathrm{W\,m^{-2}}$ (Figure 4.6c), relative to a projected decline of 0.3 $\mathrm{W\,m^{-2}}$ by the RGB scheme (Figure 4.3b). In contrast, the Jer68 and PaS77 physical solar schemes are independent of chlorophyll concentrations and thus produce a constant forcing of zero. Overall, these results show how physical solar scheme choices in ESMs affect the partitioning of solar radiation absorption between the mixed layer and the deeper ocean beneath, introducing significant uncertainties in the mixed layer heat budget and thus upper ocean stratification.

4.4.2.2 Effect of different chlorophyll inputs

Three sources of chlorophyll input are available for use in calculating solar absorption: (1) prognostic chlorophyll, (2) satellite-observed chlorophyll and (3) spatially and temporally constant chlorophyll values (Table 4.1). Inter-model differences in simulated chlorophyll introduce uncertainties of 2.3 $\mathrm{W\,m^{-2}}$ in the present-day simulations of GMSA (Figure 4.5b) and 1.4 $\mathrm{W\,m^{-2}}$ in the future projections of GMF (Figure 4.5a and Figure 4.7). The difference in prognostic chlorophyll concentrations (Figure 4.2) arises from differences such as phytoplankton growth parameterisations, nutrient limitation schemes and climate feedbacks between ESMs (Bopp et al., 2013; Laufkotter et al., 2015).

Compared with satellite observations of chlorophyll (Figure 4.8a), multi-model mean output overestimates chlorophyll in subtropical gyres, the Pacific equatorial upwelling system and the Southern Ocean, leading to overestimated solar absorption within the mixed layer in these regions (Figure 4.8b). Conversely, in coastal upwelling systems, chlorophyll concentrations are typically underestimated by ESMs, leading to negative biases in mixed layer solar absorption.

The majority of ESMs, including those not coupled to an ocean biogeochemistry model, typically use spatially and temporally constant chlorophyll concentrations such as 0.05 $\mathrm{mg\,m^{-3}}$ to calculate solar absorption (Table 4.1). This simplification

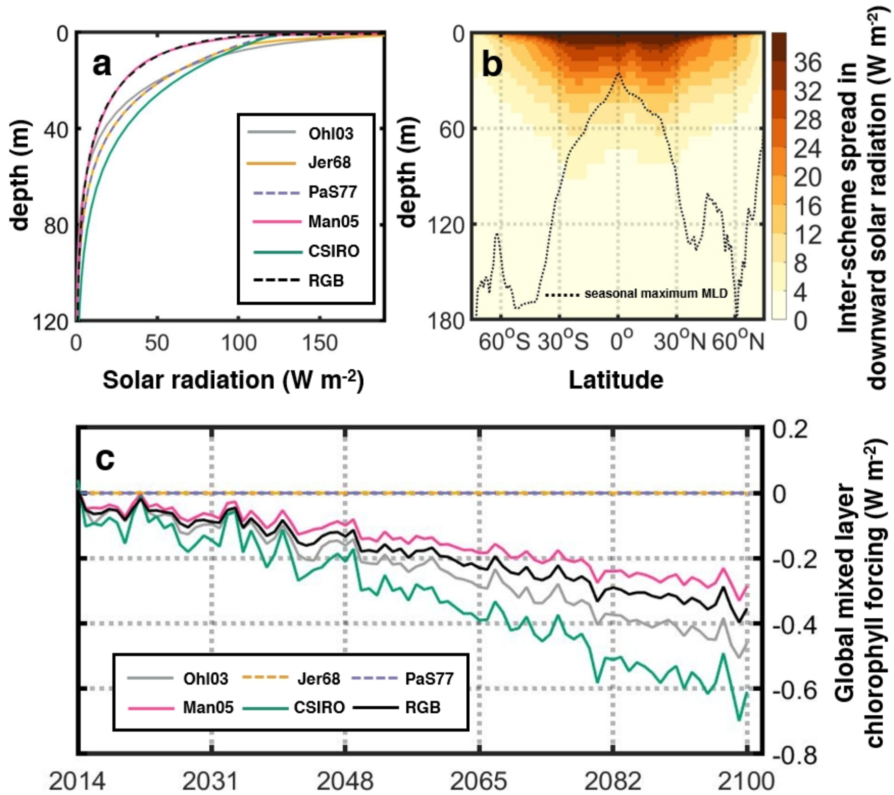

Figure 4.6: Uncertainty in solar absorption calculations in the ocean induced by different physical solar schemes. (a) Solar penetration using various solar schemes, based on the global-mean reference incoming solar radiation and satellite-observed global-mean chlorophyll. (b) Zonal mean of the spread in downward solar radiation across different physical solar schemes, based on the same reference incoming solar radiation and satellite-observed chlorophyll. The dotted line denotes the zonal mean climatological seasonal maximum MLD. (c) Annual-mean time series of global average anomaly of chlorophyll-induced solar absorption within the mixed layer relative to piControl (global mixed layer chlorophyll forcing), calculated using different physical solar schemes but the same multi-model mean chlorophyll from SSP5-8.5 scenario.

leads to a negative bias in solar absorption within the mixed layer across much of the global ocean (Figure 4.8c), resulting in a negative GMSA of $1.8\,\mathrm{W\,m^{-2}}$ (Figure 4.5b). Although some modelling groups have recently increased this prescribed chlorophyll value to $0.1\,\mathrm{mg\,m^{-3}}$ (Guiavarc'h et al., 2025), it still produces a global-scale negative bias (Figure 4.5b), and any globally uniform value will generate substantial regional biases. Although satellite-observed chlorophyll provides the most realistic representation of present-day conditions, it cannot produce self-consistent projections of future changes in mixed layer solar

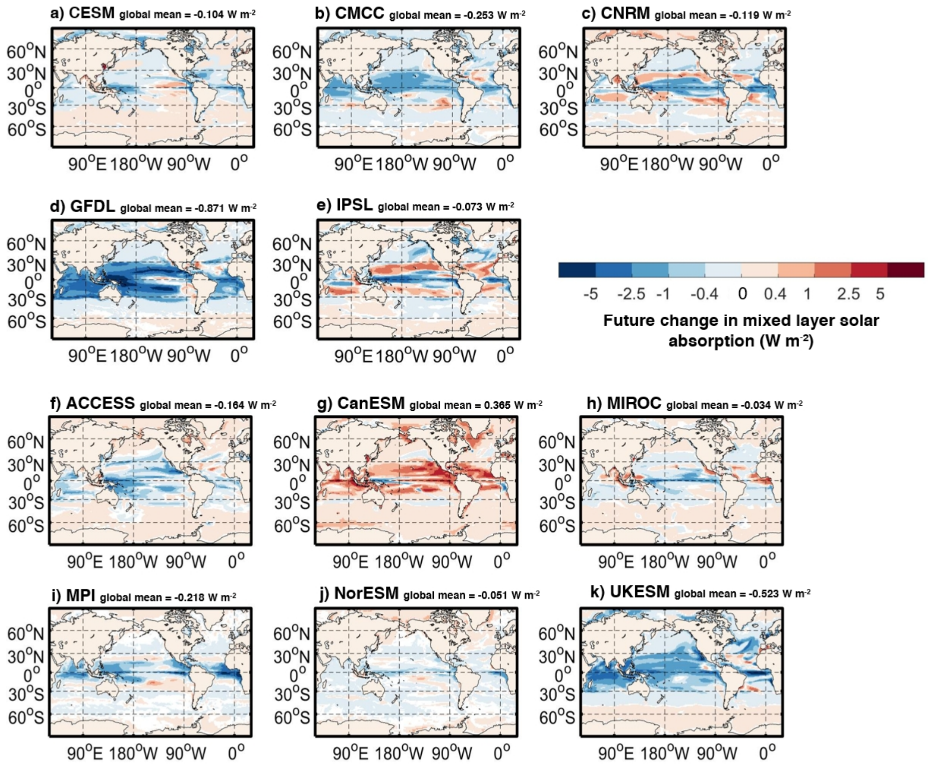

Figure 4.7: Future changes in solar absorption within the ocean surface mixed layer due to chlorophyll changes in each ESM. (a-k) Projected change in mixed layer solar absorption due to chlorophyll changes, calculated as the period 2071–2100 under the SSP5-8.5 scenario minus the last 30 years of the piControl simulation. The number shown after each panel label represents the global-mean value.

absorption.

4.5 Discussion and conclusions

Future chlorophyll decline is projected to reduce solar radiation absorption within the surface mixed layer by a global mean of $0.25\,\mathrm{W\,m^{-2}}$. This delays human-induced global surface warming by approximately 3 years, with a maximum delay of 12 years across models. Enhanced upper-ocean stratification under future climate change is expected to shoal the MLD (Capotondi et al., 2012), which is also known to decrease solar absorption within the surface ocean mixed layer. The chlorophyll-driven redistribution of solar absorption beneath the mixed layer is close to half that associated with MLD shoaling ($0.53\,\mathrm{W\,m^{-2}}$) (Figure 4.9c), and

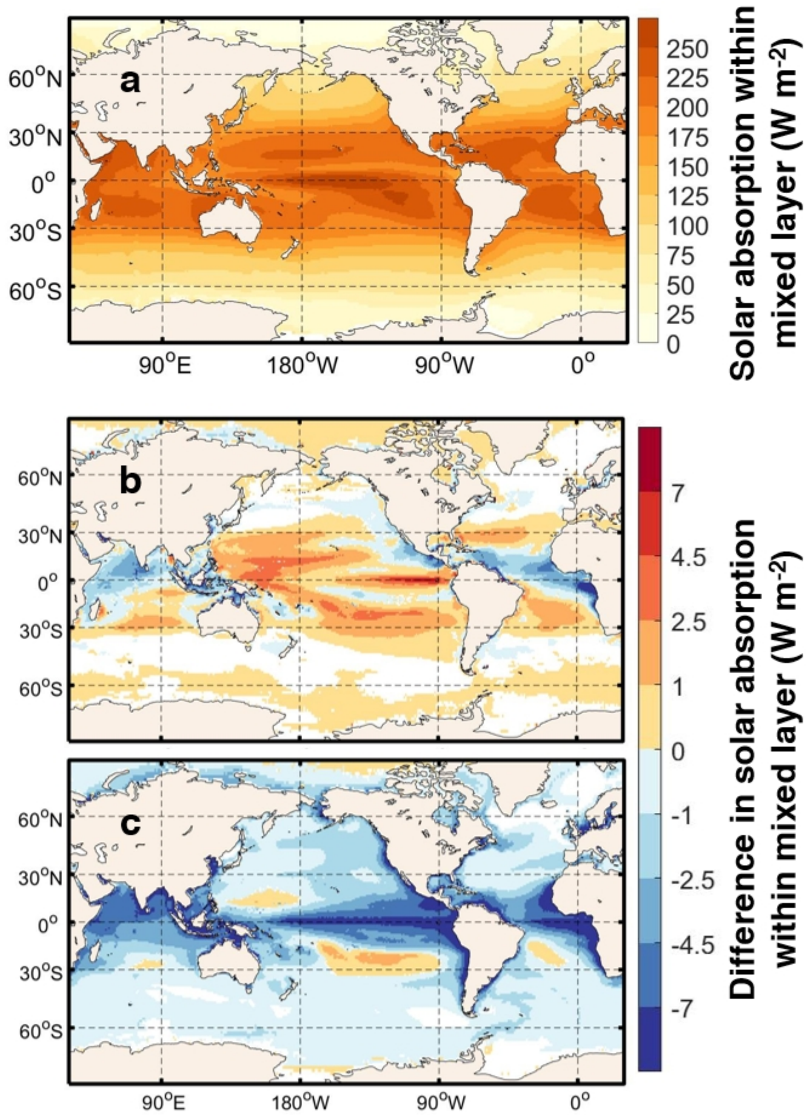

Figure 4.8: Uncertainty in mixed layer solar absorption induced by different chlorophyll data as the input of the RGB scheme. (a) Solar absorption within mixed layer using satellite-observed chlorophyll as input to the RGB scheme. (b) Difference in mixed layer solar absorption when using multi-model mean chlorophyll from contemporary historical runs as input, relative to satellite-observed chlorophyll. (c) Difference in mixed layer solar absorption when using a constant chlorophyll value of 0.05 mg m^{-3} as input, relative to satellite-observed chlorophyll. MLD is defined as the climatological mean of the seasonal maximum in all calculations, based on the multi-model mean piControl simulations.

the uncertainty introduced by inter-model spread of chlorophyll projections is comparable to that stemming from inter-model spread in MLD projections (Figures 4.9a, b and d). While MLD-induced variations in mixed layer solar absorption are routinely represented in ESMs, chlorophyll-driven changes and their radiative impacts remain largely omitted and unquantified, leading to a bias towards more rapid warming in high emission scenarios.

Future chlorophyll-driven changes in mixed layer solar absorption show large spatial variability, with decreases over the tropical and subtropical oceans being much greater than the decreases at higher latitudes (Figure 4.3a). Such tropical cooling effect and the associated reduction in the equator-to-pole temperature gradient could weaken the meridional atmospheric circulation (Seo et al., 2014; Chemke, 2021), enhance marine stratocumulus cloud cover by increasing low level stability (Cesana et al., 2019), and shift precipitation patterns by altering the global energy balance (Nicknish et al., 2023). In the western tropical Pacific, a decrease in chlorophyll concentrations reduces solar absorption within the mixed layer by up to $4\,\mathrm{W\,m^{-2}}$ (Figure 4.3a), which could modify the upper ocean heat budget and weaken the zonal gradient in equatorial Pacific SST, with resulting circulation changes and impacts.

Studies have shown that some of the heat from solar radiation penetrating below the mixed layer in subtropical gyre regions can be transported to the equatorial Pacific via subsurface meridional currents, influencing SSTs in the equatorial region (Shi et al., 2023). Therefore, some of the solar radiation that is projected to be redistributed beneath the mixed layer in future could be entrained back to the upper ocean and affect SSTs. Such an effect is mitigated though by our use of a seasonal maximum MLD. As a next step, we aim to use an ocean general circulation model to investigate the temperature responses to chlorophyll-driven changes in upper ocean solar absorption discussed in this study.

Chlorophyll-induced solar absorption is only one aspect of the complex feedback mechanisms linking phytoplankton to climate, as shifts in species composition and metabolic activities also play critical roles in regulating carbon export efficiency and greenhouse gas dynamics, thereby influencing broader climate feedback processes (Six et al., 2013; Kwiatkowski et al., 2017; Zhao et al., 2024; Silsbe et al., 2025). However, chlorophyll-induced solar absorption has hitherto been under-studied, and poorly quantified, despite being a significant mechanism that links ocean biogeochemistry and climate. Therefore, future research should prioritize improving the realism of these processes, integrating the subsequent feedback into ESMs, and quantifying their impacts on ocean physics and wider climate change.

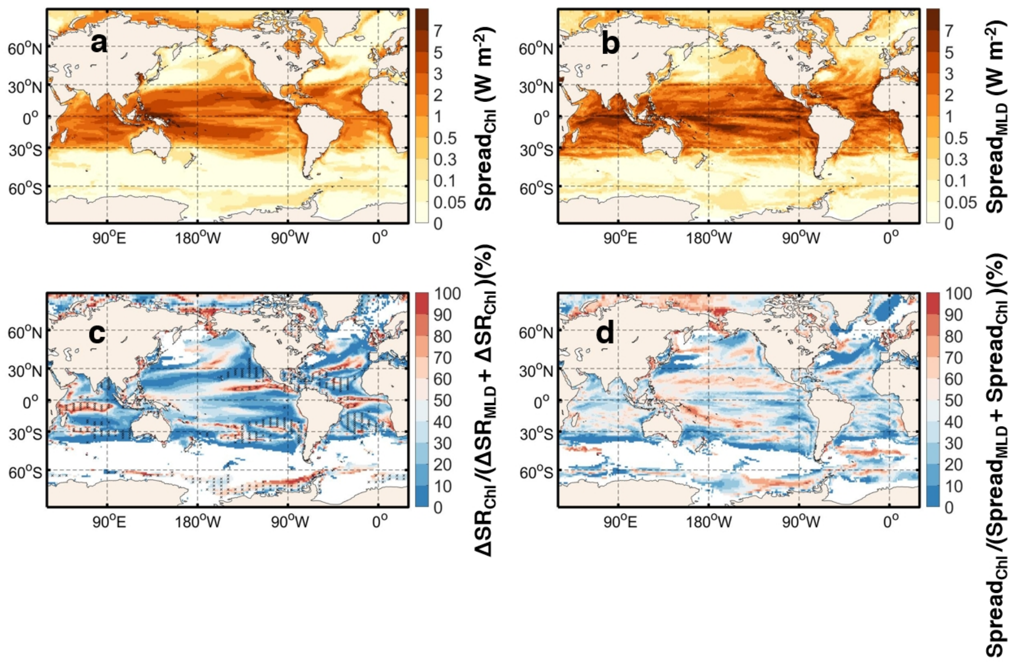

Figure 4.9: Comparison of the chlorophyll-induced and MLD-induced radiative effects in the future. (a) Inter-model spread in the future change of mixed layer solar absorption driven by chlorophyll changes ($\mathrm{Spread_{Chl}}$). (b) Inter-model spread in the future change of mixed layer solar absorption driven by MLD changes ($\mathrm{Spread_{MLD}}$). (c) Relative contribution of $\Delta\mathrm{SR_{Chl}}$ to the sum of $\Delta\mathrm{SR_{Chl}}$ and $\Delta\mathrm{SR_{MLD}}$, calculated using absolute values, expressed as $|\Delta\mathrm{SR_{Chl}}|/(|\Delta\mathrm{SR_{Chl}}|+|\Delta\mathrm{SR_{MLD}}|)\times100\%$. Values greater than 50% indicate that chlorophyll changes dominate the overall changes. $\Delta\mathrm{SR_{Chl}}$ and $\Delta\mathrm{SR_{MLD}}$ indicate the projected multi-model mean changes in mixed layer solar absorption due to future chlorophyll and MLD changes. The dotted regions indicate areas where $\Delta\mathrm{SR_{Chl}}$ and $\Delta\mathrm{SR_{MLD}}$ exhibit opposite signs. Grid points where the absolute values of both $\Delta\mathrm{SR_{Chl}}$ and $\Delta\mathrm{SR_{MLD}}$ are less than 0.05 are set to invalid values. (d) Relative contribution of $\mathrm{Spread_{Chl}}$ to the total inter-model spread, calculated as $\mathrm{Spread_{Chl}}/(\mathrm{Spread_{Chl}} + \mathrm{Spread_{MLD}}) \times 100\%$, indicating the proportion of spread arising from the differences of chlorophyll projection among models. Grid points where both $\mathrm{Spread_{Chl}}$ and $\mathrm{Spread_{MLD}}$ are less than 0.05 are set to invalid values. MLD is based on the seasonal maximum in all calculations.

Table 4.1: Overview of physical solar schemes in ESMs[1].

ESMs	Ocean physical model	Ocean biogeochemistry model	Physical solar scheme	Chlorophyll input into physical solar scheme	Source
CESM2	POP2	MARBL	Ohl03	Prognostic chlorophyll (Time-varying)	Danabasoglu et al. (2020)
CMCC-ESM2	NEMO3.6	BFM5.2	RGB scheme[2]	Prognostic chlorophyll (Time-varying)	Institution and Lovato et al. (2022)
CNRM-ESM2.1	NEMO3.6	PISCES2-gas	RGB scheme	Prognostic chlorophyll (Time-varying)	Séférian et al. (2019)
IPSL-CM6A	NEMO3.6	PISCES2	RGB scheme	Prognostic chlorophyll (Time-varying)	Boucher et al. (2020)
GFDL-ESM4.1	MOM6	COBALT2	Man05	Prognostic chlorophyll (Time-varying)	Stock et al. (2020)
EC-Earth3-ESM[3]	NEMO3.6	PISCES2	RGB scheme	$0.05\,\mathrm{mg\,m^{-3}}$ chlorophyll	Institution
UKESM1.0	NEMO3.6	MEDUSA2	RGB scheme	$0.05\,\mathrm{mg\,m^{-3}}$ chlorophyll	Institution
GISS-E2.1-G/H[3]	GO1/HYCOM	NOBM	PaS77/Jer68	PaS77/Jer68[4]	Institution and Kelley et al. (2020)
MIROC-ES2L	COCO	OECO2	PaS77	PaS77[4]	Institution
MPI-ESM1.2	MPIOM1.6	HAMOCC6	Jer68	Jer68	Institution
NorESM2	BLOM	iHAMOCC	Jer68	Jer68	Institution
ACCESS-ESM1.5	MOM5	WOMBAT	CSIRO scheme	Satellite chlorophyll (Monthly climatology)	Institution and Bi et al. (2013)
CanESM5 /CanESM5-CanOE	CanNEMO[5]	CMOC/CanOE	RGB scheme	Satellite chlorophyll (Monthly climatology)	Institution

[1] light orange indicates ESMs using prognostic and time-varying chlorophyll input to physical solar schemes, light grey indicates spatially and temporally constant chlorophyll and light magenta indicates satellite-observed and temporally constant chlorophyll.

[2] The RGB scheme refers to the physical solar scheme by Lengaigne et al. (2007), which divides incoming solar radiation into red, green, blue and infrared bands to represent wavelength-dependent solar penetration in the ocean.

[3] The results from EC-Earth3-ESM and GISS-E2-1-G/H are not included in this study due to data availability constraints.

[4] PaS77 and Jer68 do not include temporal variation in chlorophyll concentrations in their solar penetration calculations, as they use fixed attenuation coefficients based on water types.

[5] CanNEMO is based on NEMO3.4.

5

Chlorophyll decline intensifies global subsurface warming and drives an El Niño-like response in future oceans

5.1 Abstract

Upper-ocean chlorophyll modulates the vertical distribution of solar radiation and is therefore known to influence ocean physics and climate on climatological, seasonal and interannual timescales. However, the feedbacks of future chlorophyll changes on the climate system under long-term global warming remain poorly understood. Here, we use an ocean general circulation model combined with chlorophyll projections from the Coupled Model Intercomparison Project Phase 6 (CMIP6) to investigate the impacts of solar radiation redistribution induced by future chlorophyll changes. We find that the projected decline in chlorophyll under the Shared Socioeconomic Pathway 3-7.0 scenario allows more solar radiation to penetrate into the subsurface ocean, resulting in a global subsurface warming of approximately 0.05–0.2 °C, equivalent to about 1.5–8% of the subsurface warming driven by anthropogenic climate change. Future chlorophyll changes also modify the seasonal cycle of temperature, especially in the high-latitude North Atlantic. In addition, these chlorophyll changes shift the equatorial Pacific Ocean towards a more El Niño-like mean state, characterised by sea surface warming, a deepening

of the thermocline and a weakening of equatorial ocean circulation. As most current CMIP6 Earth System Models neglect the radiative effects associated with time-varying chlorophyll, our results highlight the importance of representing interactive chlorophyll-radiation feedbacks in future climate projections to improve their accuracy.

5.2 Introduction

Previous studies have demonstrated that the redistribution of solar energy induced by upper-ocean chlorophyll can influence ocean thermal structure, sea-ice feedbacks and ocean dynamics. For example, compared with an idealised optically clear ocean, the absorption of solar radiation by chlorophyll has been shown to induce a global-mean SST increase of approximately 0.5 °C and accelerate sea-ice melt (Patara et al., 2012). In addition, increased SST and enhanced sea-ice melt associated with chlorophyll modify freshwater fluxes into the ocean, altering the density structure in the high-latitude North Atlantic and impacting the strength of the AMOC (Gnanadesikan and Anderson, 2009; Patara et al., 2012). Furthermore, chlorophyll-induced solar absorption in both the surface and subsurface ocean has been shown to affect the thermal structure and intensity of equatorial and coastal upwelling (Hernandez et al., 2017; Echevin et al., 2021; Meng et al., 2024).

In addition to its influence on the mean state, chlorophyll has been shown to impact the ocean-climate system on seasonal and interannual timescales. At mid and high latitudes, the magnitude and sign of chlorophyll-induced SST responses vary with season, with surface warming of 0.1–1.5°C in spring and summer and cooling of 0.1–0.3°C in autumn and winter (Manizza et al., 2005). At the regional scale, Giddings et al. (2020) demonstrated that the radiative effect of chlorophyll is seasonally dependent in the Bay of Bengal, with its effect amplified during seasons with shallow mixed layers, leading to changes in upper-ocean temperature, air-sea fluxes and monsoon on seasonal timescales. On interannual timescales, chlorophyll variability in the eastern equatorial Pacific has been shown to influence both the magnitude (Lengaigne et al., 2007; Park et al., 2014a) and asymmetry (Timmermann and Jin, 2002; Park et al., 2014b) of the ENSO by modulating upper-ocean heat content, stratification, ocean dynamics and associated ocean-atmosphere interactions.

In contrast, the radiative effects of future chlorophyll changes under long-term anthropogenic climate change have received comparatively little attention. Projections of future chlorophyll are primarily derived from ESMs in the CMIP, which simulate changes in phytoplankton biomass and the associated chlorophyll under future climate scenarios. Due to enhanced upper-ocean stratification and other coupled physical-biogeochemical processes, most models project a decline in global-mean chlorophyll concentrations in the future (Chapter 4) (Kwiatkowski et al., 2017; Silsbe et al., 2025). Previous studies using simplified heat budget approaches have suggested that this projected chlorophyll decline would reduce solar absorption in the upper ocean and allow more solar radiation to penetrate into the subsurface ocean (Tian and Zhang, 2023). However, the implications of this altered solar radiation distribution for ocean thermal structure, dynamics and climate remain poorly understood.

Asselot et al. (2021) investigated the climatic effects of chlorophyll-induced solar absorption under a future climate change scenario using an ESM with an intermediate-complexity ocean model. They demonstrated that, compared to simulations without chlorophyll-induced solar absorption, the inclusion of this process modifies upper-ocean temperatures and air-sea heat and carbon exchanges, ultimately leading to a global-mean lower-atmospheric warming of approximately 0.7 °C. However, because their analysis focused on the background effect of chlorophyll-induced solar absorption rather than future changes in chlorophyll concentration, the oceanic and climatic impacts of the projected chlorophyll decline remain unclear.

Investigating the climatic feedbacks of future chlorophyll change is challenging, as both the simulated mean state and projected future changes of chlorophyll exhibit substantial spread across ESMs (Laufkötter et al., 2015; Kwiatkowski et al., 2017). To address these challenges, we use future chlorophyll projections from five ESMs. These time-varying chlorophyll concentrations are prescribed as external "optical" forcings in an ocean general circulation model, allowing a direct comparison between simulations that incorporate future chlorophyll changes and those in which chlorophyll is fixed at its historical state. Through this approach, we isolate and assess the impact of projected future chlorophyll decline on ocean thermal structure and dynamics, without the complication of feedbacks from the atmosphere.

5.3 Methods

5.3.1 Model description

In this study, we use NEMO, which is a hydrostatic, primitive-equation ocean general circulation model that has been extensively evaluated and widely applied in studies of large-scale ocean circulation and climate (Madec and NEMO team, 2016). In addition, it serves as the physical ocean component in several CMIP6 ESMs. The configuration of NEMO used in this study has a horizontal resolution of $2^\circ \times 2^\circ$, which is sufficient to resolve the thermal influence of future chlorophyll changes on global and basin-scale ocean processes. We employ 31 vertical levels, with a top layer thickness of 5 m and 10 levels within the upper 100 m, allowing the vertical structure of solar radiation absorption and its impacts on upper-ocean structure to be well represented.

Solar radiation penetration in the ocean is represented using the RGB physical solar scheme in NEMO (Lengaigne et al., 2007). In this scheme, incoming shortwave radiation is partitioned into infrared, red (R), green (G) and blue (B) spectral bands. The absorption of each band by chlorophyll is calculated at every vertical level, and the total absorbed radiation is then used to compute local heating rates and the ocean heat budget. By allowing chlorophyll to be prescribed from external data, NEMO enables ESM-projected future chlorophyll changes to be imposed and their modulation of solar absorption to be represented.

5.3.2 Experimental design

Two groups of numerical experiments are conducted in this study. All simulations are based on identical model configurations and atmospheric forcing. The atmospheric forcing is derived from UKESM1.0 and consists of historical forcing from 1948 to 2014, followed by forcing under the SSP3-7.0 scenario (Eyring et al., 2016) thereafter, representing a medium-to-high future climate change pathway, integrated to 2100. SSP3-7.0 is chosen here as the ocean model was already implemented with this forcing at the University of East Anglia.

The first group of experiments, referred to as CLIM_x, consists of five simulations in which prescribed chlorophyll concentrations are fixed at their historical climatological states. Specifically, climatological mean chlorophyll for the period 1948–1977, including their seasonal cycles, is derived from five CMIP6 ESMs (CESM, CMCC, CNRM, GFDL and IPSL) and prescribed in NEMO to compute solar radiation absorption. These five models are selected because they explicitly use the chlorophyll fields simulated by their biogeochemistry components to calculate solar radiation penetration. These simulations are denoted as CLIM_CESM, CLIM_CMCC, CLIM_CNRM, CLIM_GFDL and CLIM_IPSL.

The second group of experiments, referred to as FUT_x, also consists of five simulations. In these simulations, time-varying chlorophyll concentrations from the same five ESMs are prescribed, covering the historical period (1948–2014) and the future SSP3-7.0 scenario (2015–2100).

The chlorophyll data from the five CMIP6 ESMs are monthly mean outputs derived from a single ensemble member of each model (Table 2.1). These chlorophyll data are first interpolated horizontally onto the NEMO $2° \times 2°$ grid using two-dimensional linear interpolation at each original vertical level, and are then interpolated vertically onto the 31 vertical levels of NEMO using linear interpolation. The resulting four-dimensional (time-depth-longitude-latitude) chlorophyll data from the five ESMs are used to compute solar radiation penetration in NEMO.

It is important to note that the climate states simulated by individual ESMs are not temporally synchronized with each other nor with the atmospheric forcing used to drive NEMO. For example, chlorophyll anomalies in a given year from one ESM may correspond to El Niño conditions, while another ESM or the prescribed atmospheric forcing may reflect La Niña conditions. For our simulations, the atmospheric forcing is identical for each run, and we expect this atmospheric forcing to dominate over the time-varying chlorophyll and thus generate similar ENSO variability. Due to the dominance of the fixed atmospheric forcing, this experimental design does not allow an investigation of chlorophyll feedbacks on climate variability at interannual time scales.

Instead, the analysis focuses on long-term mean-state responses. Specifically, we compare 30-year means over the late 21st century (2071–2100) between FUT_x, which include projected future chlorophyll changes, and CLIM_x, in which chlorophyll is fixed at its historical state. In all comparisons between the two experiments, only results that are statistically significant at the 95% confidence level are shown.

5.4 Results

5.4.1 Subsurface warming induced by future chlorophyll decline

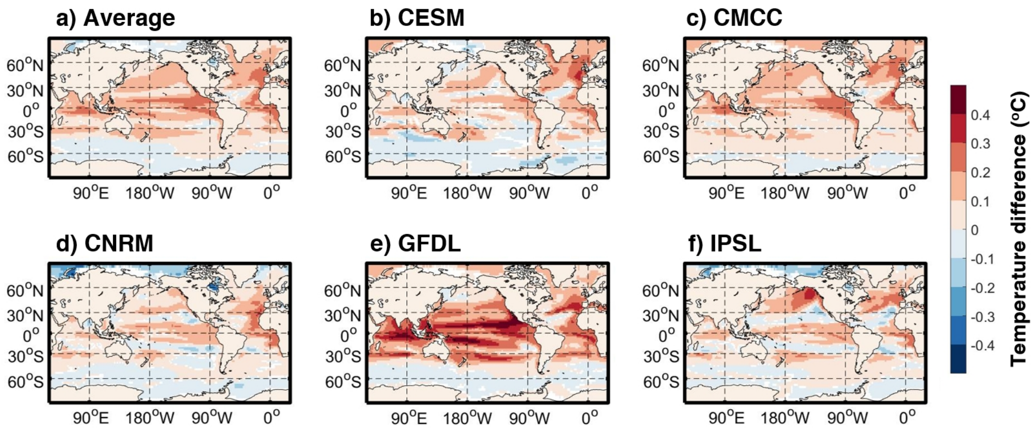

Figure 5.1: Subsurface temperature anomalies at 75 m induced by future chlorophyll changes, calculated as FUT_x minus CLIM_x and averaged in 2071–2100. Panel (a) shows the mean response across the five chlorophyll projections, while panels (b-f) show the corresponding responses to chlorophyll changes projected by individual ESMs.

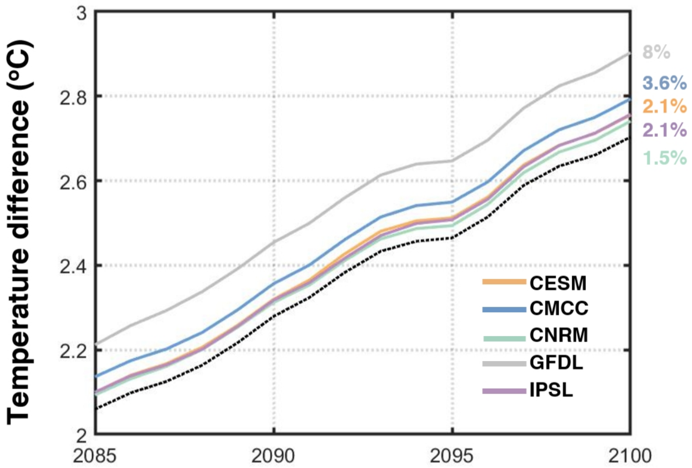

Figure 5.2: Future changes in the global mean ocean temperature at 75 m depth. The black dashed line shows the annual-mean temperature anomalies in CLIM_x ensemble mean over 2085–2100 under SSP3–7.0, relative to the 1948–1977 historical reference period. Coloured lines indicate temperature anomalies in FUT_x based on the chlorophyll projections by each ESM. Percentages indicate the fraction of chlorophyll-induced temperature changes relative to the future temperature change projected in the CLIM_x simulation.

Most ESMs consistently project a future decline in sea surface chlorophyll concentrations. Reduced chlorophyll decreases solar absorption within the surface mixed layer, allowing more solar radiation to penetrate into the subsurface ocean, in line with Chapter 4. This leads to subsurface warming at depths of 40–100 m, with a multi-model-averaged global-mean subsurface temperature increase of approximately 0.12 °C, and an inter-model spread of 0.05–0.2 °C (Figure 5.1). Based on GFDL model output, which projects the strongest future chlorophyll decline, global-mean subsurface warming reaches ∼0.2 °C, with local values exceeding 0.4 °C (Figure 5.1e), accounting for 8% of the projected anthropogenic subsurface ocean warming (Figure 5.2).

The subsurface warming associated with chlorophyll decline shows pronounced spatial variability. Vertically, the maximum warming occurs below the seasonal maximum MLD (Figure 5.3), where enhanced solar penetration leads to increased subsurface heat absorption, which is less efficiently transported back to the surface by vertical mixing. Horizontally, subsurface warming is most pronounced in the equatorial regions, eastern boundary upwelling systems and the mid- to high-latitude North Pacific and North Atlantic (Figure 5.1a).

In contrast, the impact of future chlorophyll decline on temperature at the sea surface is relatively weak, with SST changes generally below 0.05 °C at the global scale (Figure 5.4a). Reduced solar absorption within the mixed layer leads to surface cooling across most of the global ocean. However, future chlorophyll changes lead to SST increases in the equatorial upwelling zones and parts of the eastern coastal upwelling systems (Figure 5.4), reflecting the combined effects of direct radiative changes and indirect dynamical responses induced by chlorophyll changes (see Section 5.5.2).

Chlorophyll declines projected by all five ESMs consistently lead to an increase in the net downward surface heat flux due to surface cooling and the associated reduction in outgoing longwave radiation (Figure 5.5). However, the model-mean value (about 0.04 W m^{-2}) is substantially lower than estimates derived from the simplified heat-

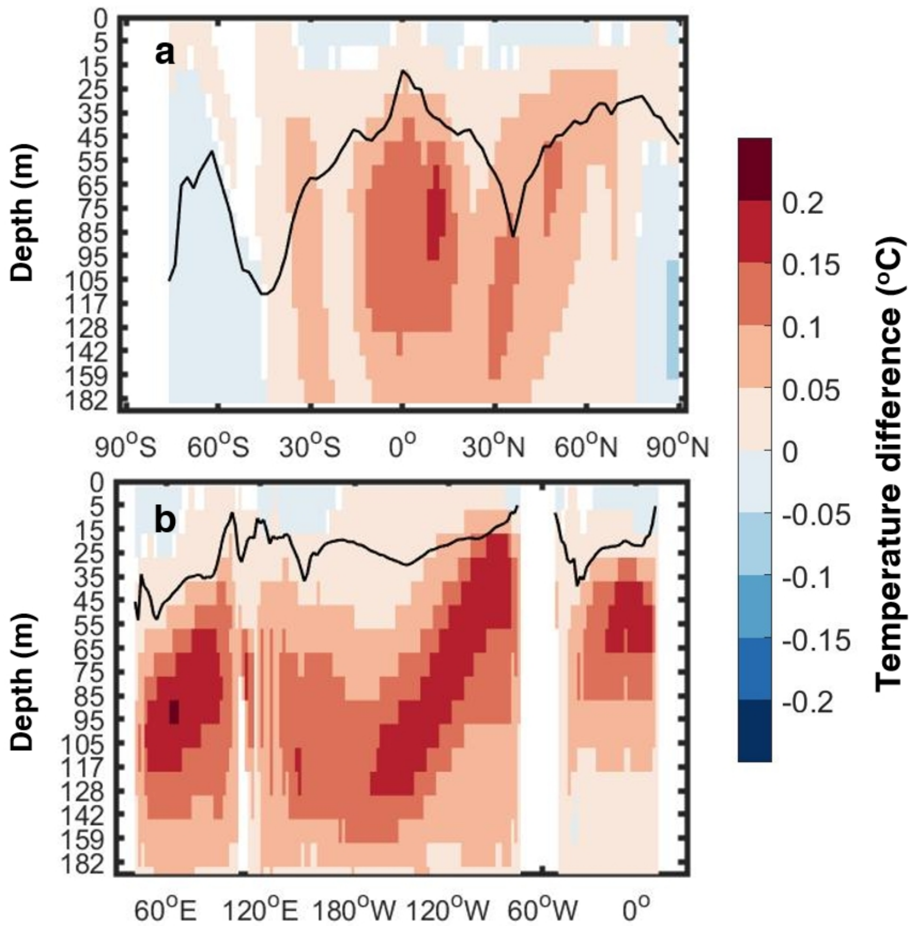

Figure 5.3: Temperature anomalies induced by future chlorophyll changes, calculated as FUT_x minus CLIM_x and averaged in 2071–2100. Panel (a) shows the global zonal mean, and panel (b) shows the meridional mean averaged between 10°S-10°N. The black lines indicate the seasonal maximum MLD, averaged in 2071–2100 of the FUT_x simulation.

budget calculation presented in Chapter 4 (0.43 W m^{-2}). This discrepancy can be partly attributed to the use of chlorophyll projections based on the SSP3-7.0 scenario here, which produces weaker chlorophyll declines and associated radiative effects than those obtained under the more extreme SSP5-8.5 scenario. In addition, in the simulations considered here, ocean dynamical and mixing processes modify the chlorophyll-induced vertical redistribution of heat in the upper ocean, thereby damping the sea surface cooling response and weakening the resulting feedbacks to the atmosphere.

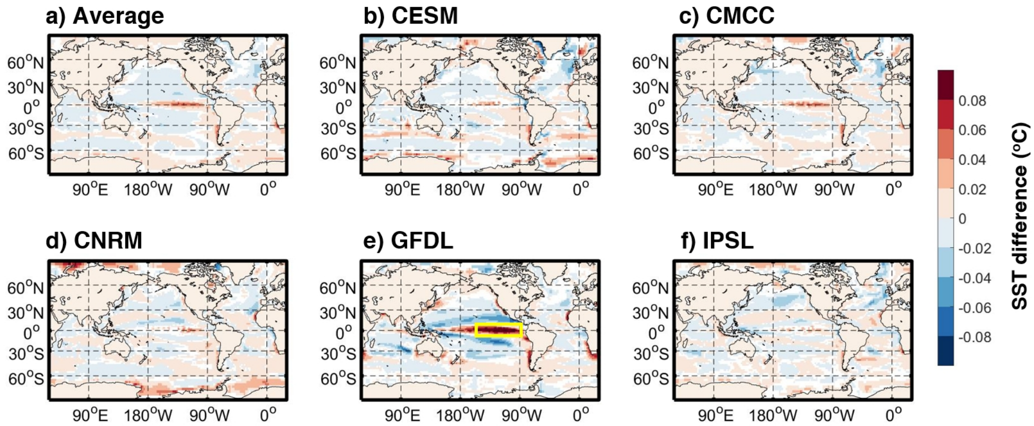

Figure 5.4: SST anomalies induced by future chlorophyll changes, calculated as FUT_x minus CLIM_x and averaged in 2071–2100. Panel (a) shows the mean response across the five chlorophyll projections, while panels (b-f) show the corresponding responses to chlorophyll changes projected by each ESM. The yellow solid box in panel (e) denotes the region (8°S-8°N, 160°W-85°W) used for the heat budget calculation shown in Figure 5.11.

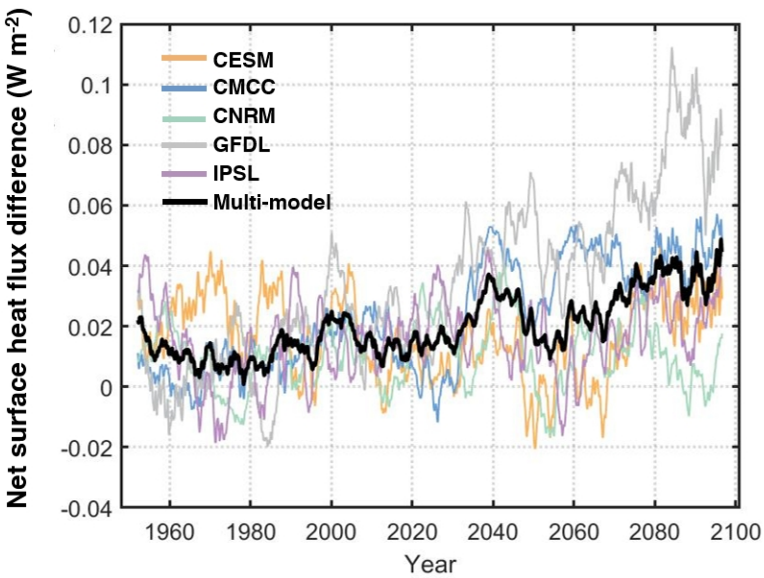

Figure 5.5: Ocean-mean differences in downward net surface heat flux at the surface induced by future chlorophyll changes, calculated as FUT_x minus CLIM_x. Coloured lines show results from individual chlorophyll projections, while the thick black line denotes the mean across the five chlorophyll projections.

5.4.2 Impacts of future chlorophyll changes on the seasonal cycle of temperature

In addition to its impact on the annual-mean ocean temperature, chlorophyll-driven solar absorption also modifies the seasonal cycle of SST. The influence of future chlorophyll decline on the SST seasonal cycle is most pronounced at high latitudes, particularly in the North Atlantic (Figure 5.6a). In this region, the decrease in the amplitude of SST seasonal cycles associated with future chlorophyll decline exceeds 0.1 °C, and reaches ∼0.2 °C in the experiment forced by CESM-projected chlorophyll changes (Figure 5.6b).

We focus on the chlorophyll changes projected by CESM as a representative example to investigate the underlying mechanisms (though simulations forced with chlorophyll declines from all models consistently show a weakening of the North Atlantic SST seasonal cycle).

The projected surface chlorophyll decline is strongest in May (Figure 5.7a). However, the corresponding SST response remains weak at this time. From June to August, as the mixed layer shoals and vertical stratification strengthens (Figure 5.7c), the additional solar radiation penetrating into the subsurface ocean due to surface chlorophyll decline is less efficiently mixed back to the surface. As a result, the surface cooling induced by chlorophyll decline is largest during boreal summer (Figure 5.7b). Subsequently, from September to the following March, deepening of the mixed layer (Figure 5.7c) entrains the excess heat stored below the mixed layer during summer back into the surface layer, leading to basin-wide warming in winter (Figure 5.7b). Together, the direct summer SST cooling associated with reduced chlorophyll and the indirect winter warming driven by vertical mixing of warmer subsurface water damp the overall amplitude of the SST seasonal cycle. Chlorophyll-induced temperature changes also affect the MLD. However, because the magnitude of subsurface warming exceeds that of surface temperature change, the mixed layer tends to deepen slightly in response to future chlorophyll decline in most months (Figure 5.7d).

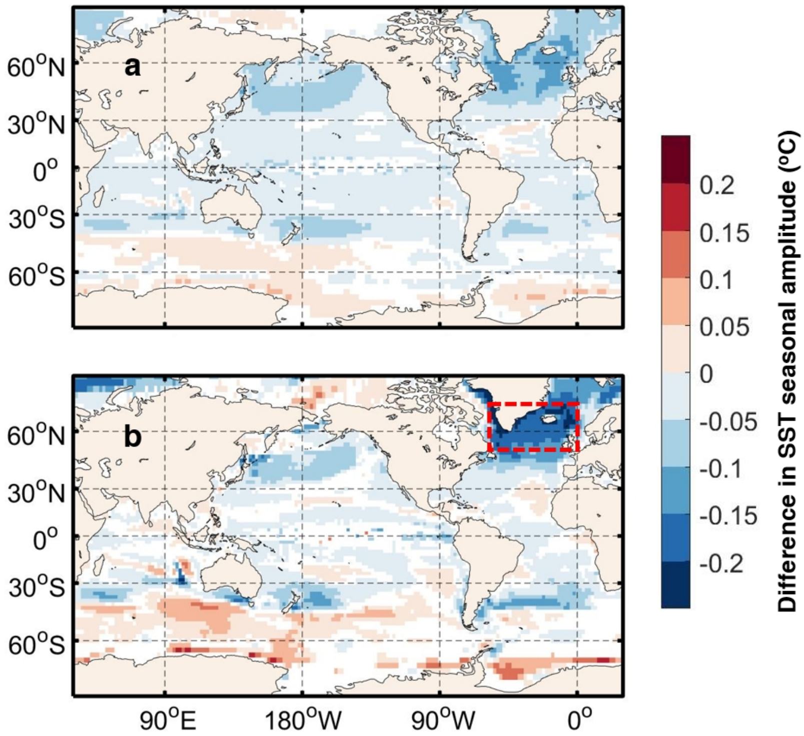

Figure 5.6: Anomalies in the amplitude of SST seasonal cycle induced by future chlorophyll changes, calculated as FUT_x minus CLIM_x and averaged in 2071–2100. Panel (a) shows the mean response across the five chlorophyll projections, while panel (b) shows the response to CESM-projected chlorophyll changes.

5.4.3 El Niño-like response to future chlorophyll decline

Future chlorophyll decline induces a zonally asymmetric SST response in the equatorial Pacific, characterised by surface warming in the eastern equatorial Pacific and cooling in the western basin (Figure 5.4). This pattern acts to amplify existing physical warm biases in the tropical Pacific mean state (Seager et al., 2019). The resulting SST anomaly pattern closely resembles El Niño-like conditions, leading to an increase in the mean Niño3.4 index of approximately 0.03–0.19 and a shift in the mean state of ENSO (Figure 5.8a). Notably, this change in Niño3.4 represents a systematic offset from the 1:1 relationship, and no statistically significant response of Niño3.4 variability to chlorophyll decline is detected.

Chlorophyll-driven subsurface warming further influences ENSO through

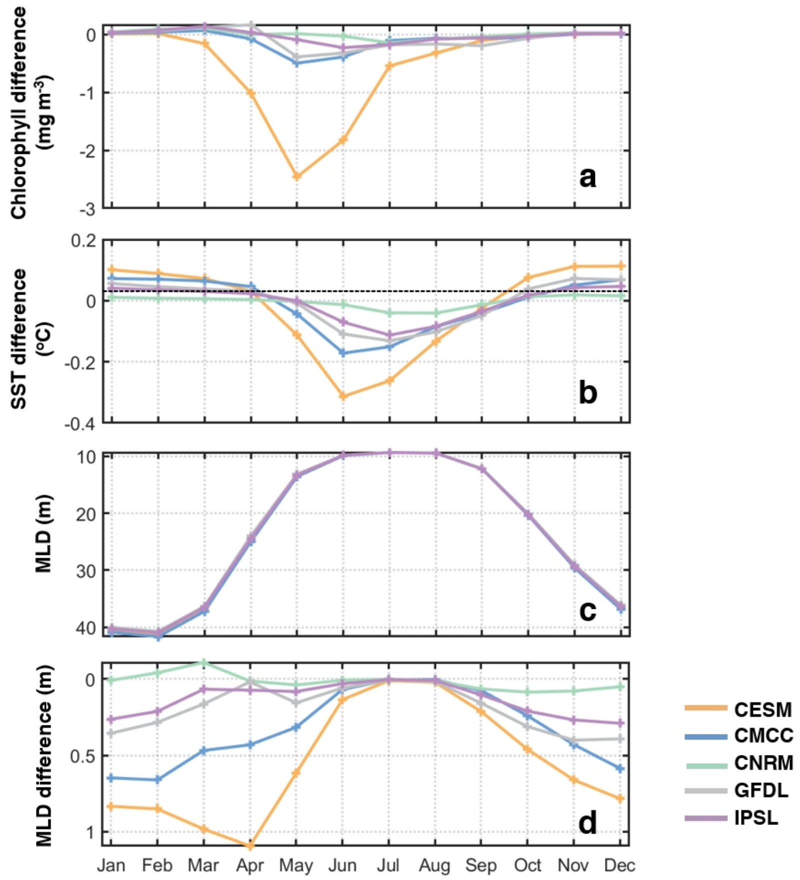

Figure 5.7: Changes in the seasonal cycle of upper-ocean properties over the high-latitude North Atlantic induced by future chlorophyll changes. (a) monthly differences in sea surface chlorophyll between 2071–2100 and 1948–1977 as projected by the five ESMs. (b) monthly SST differences of FUT_x minus CLIM_x averaged in 2071–2100, representing the SST response to projected future chlorophyll changes. (c) monthly MLD in the FUT_x averaged in 2071–2100. (d) monthly MLD differences of FUT_x minus CLIM_x averaged in 2071–2100. All quantities are averaged over the region enclosed by the red dashed box shown in Figure 5.6b.

modifications to the equatorial thermal structure. The subsurface waters of the eastern equatorial Pacific constitute the primary source of equatorial upwelling, and the depth of the 20 °C isotherm is commonly used as a proxy for ENSO-related thermocline variability. Chlorophyll-induced subsurface warming of approximately 0.2 °C (Figure 5.3b) deepens the 20 °C isotherm in the eastern equatorial Pacific by about 0.8 m (Figure 5.8b), indicating enhanced heat storage in the subsurface source waters. This subsurface warming is likely to lead to warming of the SSTs in the eastern Pacific via upwelling and mixing, and is thus favourable for a shift towards El Niño-like conditions.

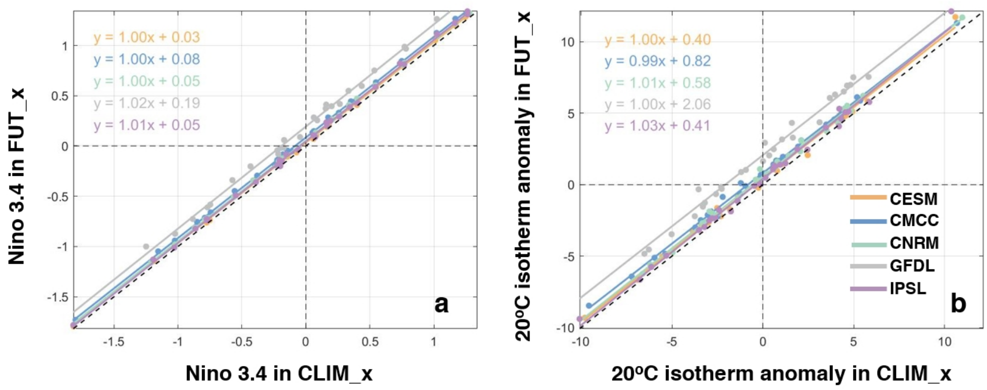

Figure 5.8: Scatter plots comparing (a) Niño 3.4 index and (b) 20°C isotherm depth anomalies between the FUT_x and CLIM_x in 2071–2100. Solid coloured lines show the linear regressions for the cases based on each chlorophyll projection with corresponding regression equations indicated, while the black dashed line denotes the 1:1 relationship.

These thermal structure changes further lead to dynamical responses in the equatorial Pacific (Figure 5.9b). In particular, future chlorophyll decline and the associated temperature changes weaken the equatorial surface currents and reduce the strength of both off-equatorial (Figure 5.9d) and along-equatorial circulations (Figure 5.9f). The resulting circulation anomalies resemble those typically associated with El Niño events (Kessler, 1995).

5.5 Discussion

5.5.1 Climatic implications of temperature changes induced by chlorophyll decline

Future chlorophyll decline reduces the absorption of incoming solar radiation in the upper ocean, leading to widespread cooling of SSTs (Figure 5.4). The resulting SST decrease weakens outgoing longwave radiation and increases the net downward heat flux at the ocean surface (Figure 5.5). In the present simulations, atmospheric forcing is prescribed, such that changes in surface heat fluxes cannot feed back onto the atmosphere. In a fully coupled atmosphere-ocean system, chlorophyll-induced

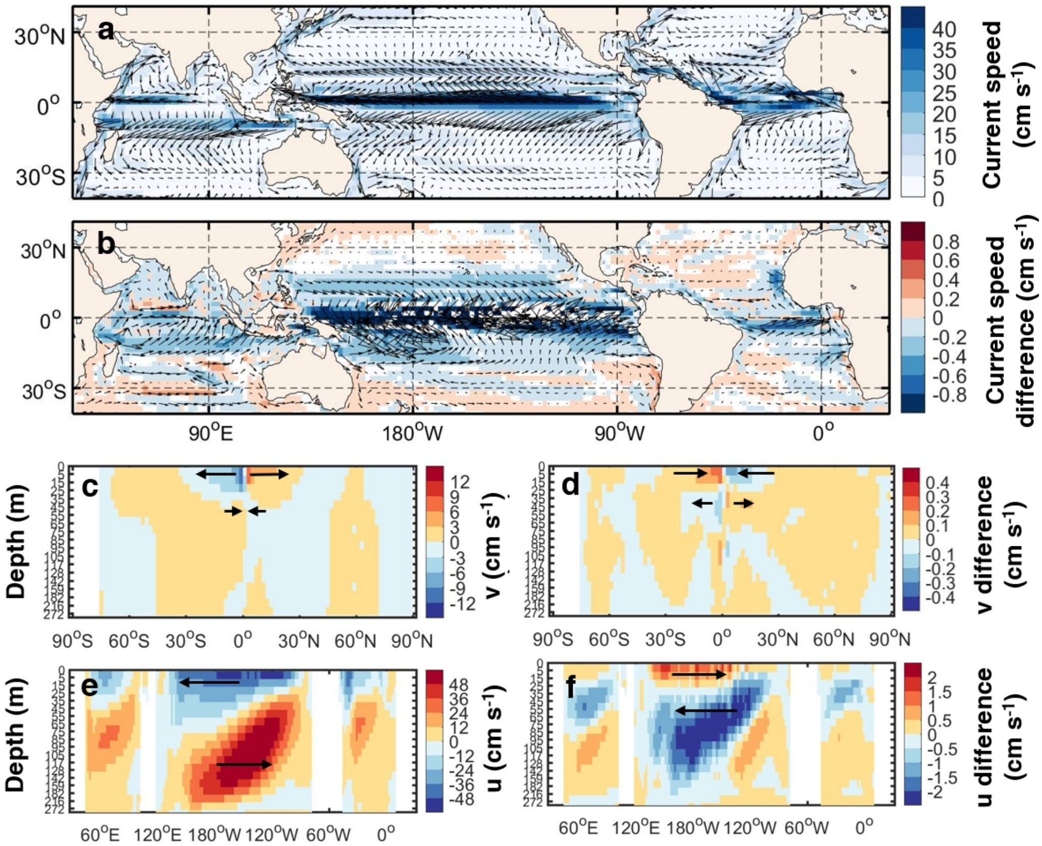

Figure 5.9: Ocean current responses to future chlorophyll changes projected by GFDL model averaged in 2071–2100. Panels (a), (c) and (e) show the simulated circulation in FUT_GFDL, including (a) surface current speed and vectors, (c) zonal-mean v velocity in the Pacific and (e) meridional-mean u velocity averaged over 5°S-5°N. Panels (b), (d) and (f) show the corresponding differences of FUT_GFDL minus CLIM_GFDL. Black arrows in (c-f) indicate the directions of current and its anomalies.

SST cooling would likely reduce near-surface air temperature and downward heat flux, thereby amplifying the surface cooling and resultant surface heat flux change induced by chlorophyll decline.

At the same time, chlorophyll decline redistributes more solar radiation downward, leading to pronounced subsurface warming and an increase in sea surface height (SSH) through thermosteric expansion. In simulations with GFDL-projected chlorophyll decline prescribed, subsurface warming between 30°S and 30°N leads to a regional-mean SSH increase of approximately 0.8 cm (Figure 5.10a). Although the weakening of equatorial currents induced by chlorophyll-driven changes in equatorial thermal structure (Figure 5.9b) would tend to reduce SSH over the

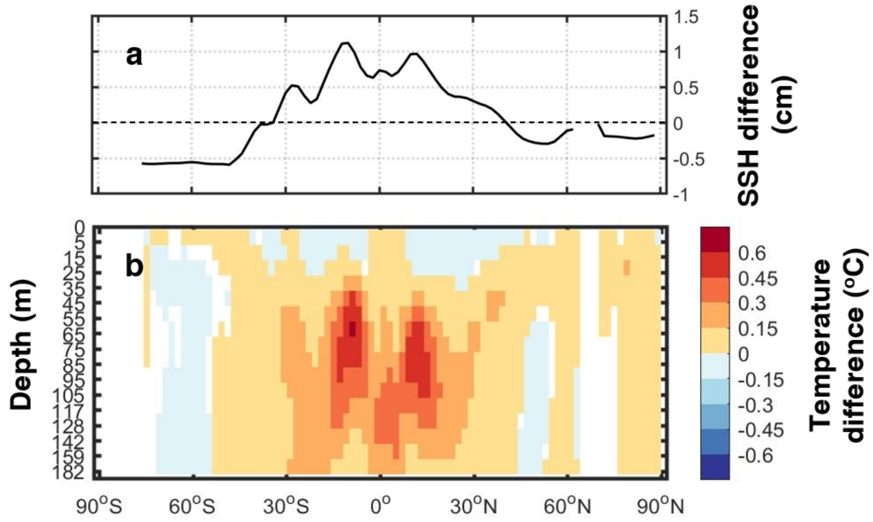

Figure 5.10: SSH responses to future chlorophyll changes projected by GFDL model. (a) SSH differences (FUT_GFDL minus CLIM_GFDL) along 175°E. (b) Zonal cross-sections of temperature differences (FUT_GFDL minus CLIM_GFDL) along 175°E. All differences are averaged in 2071–2100.

Western Pacific Warm Pool by decreasing westward mass transport (Kessler, 2006), the thermosteric expansion associated with subsurface warming (Figure 5.10b) outweighs this dynamical effect. Our results show the SSH response to chlorophyll decline is strongest over the Western Pacific Warm Pool, where subsurface warming induces an SSH increase of approximately 1.2 cm (Figure 5.10a). The Western Pacific Warm Pool plays a critical role in regulating tropical Pacific circulation and air-sea interaction, as it establishes the background pressure gradients that control equatorial and western boundary currents (McPhaden et al., 2011; Bi et al., 2013). Here, the increase in SSH driven by future chlorophyll decline over this region may therefore lead to an intensification of western boundary currents through enhanced horizontal pressure gradients, with potential implications for regional air-sea heat and momentum exchange (Figure 5.9b).

Although the subsurface warming induced by future chlorophyll decline does not occur directly at the air-sea interface and therefore does not immediately modify air-sea heat and carbon exchanges, it can nevertheless influence the atmosphere through oceanic transport processes. Using an ESM with an intermediate-complexity ocean model, Asselot et al. (2021) demonstrated that chlorophyll-induced surface warming reduces CO_2 solubility, enhances ocean-to-atmosphere CO_2 outgassing, and ultimately leads to an atmospheric warming of about 0.7 °C. Our results indicate that, under projected CMIP6 chlorophyll decline, the magnitude of subsurface temperature increase substantially exceeds that of surface temperature change, and these warmer subsurface waters can be transported towards the surface by ocean circulation and mixing. Notably, subsurface waters generally contain higher concentrations of dissolved inorganic carbon (DIC), including dissolved CO_2, primarily due to the remineralisation of sinking organic matter and their relative isolation from direct air-sea gas exchange (DeVries, 2014; Gruber et al., 2019). Therefore, the changes we find in stratification, temperature and upwelling due to future chlorophyll decline suggest a potential impact in the ocean carbon cycle. As highlighted by Asselot et al. (2024), capturing this feedback requires coupling to an atmospheric model that allows CO_2 concentrations to evolve freely, in order to fully assess the atmospheric impact of biologically mediated oceanic processes.

5.5.2 Heat budget analysis of El Niño-like temperature response

To investigate the mechanisms responsible for the El Niño-like SST response induced by future chlorophyll changes, we perform an offline heat budget analysis over the eastern equatorial Pacific. The analysis focuses on a representative box spanning the eastern equatorial Pacific (yellow solid box in Figure 5.4e) and the upper 0–30 m of the ocean. Simulations with prescribed future chlorophyll changes derived from the GFDL model are used as an example here. While simulations forced by chlorophyll changes from other models exhibit qualitatively similar El Niño-like SST responses, their amplitudes are weaker than those obtained in the GFDL-based experiment (Figure 5.4).

Because the discrete formulation of the NEMO heat budget differs from that used in the offline diagnostics, and because mixing process is simplified in the offline calculations, the diagnosed heat budget does not close exactly. Nevertheless, the residuals are small compared with the leading terms, and each diagnosed term is physically consistent with the underlying ocean circulation and thermal structure (Figure 5.11a). The heat budget analysis therefore provides useful information for interpreting the mechanisms through which future chlorophyll changes lead to El Niño-like warming in the eastern equatorial Pacific (Figure 5.4e).

The results indicate that local changes in direct radiative heating induced by chlorophyll make a negligible contribution to the upper-ocean warming in the eastern equatorial Pacific (Figure 5.11b). In contrast, nearly all of the warming is explained by changes in vertical and zonal heat transport (Figure 5.11b). The weakening of equatorial upwelling and zonal currents (Figure 5.9b) reduces both the upward supply of cold subsurface waters to the surface layer and the east-west transport of cold waters, thereby weakening the associated advective cooling (Figure 5.11c). Meanwhile, changes in the temperature field induced by chlorophyll-driven radiative effects contribute relatively less to the modifications of advective heat transport (Figure 5.11c).

The mechanism underlying the warmer equatorial Pacific upwelling associated with future chlorophyll decline is consistent with the cooling of Pacific coastal upwelling induced by increased chlorophyll shown in Chapter 3. Although equatorial upwelling is spatially more extensive than coastal upwelling, leading to a broader impact of chlorophyll-induced temperature changes (Figures 3.1b and 5.4e), the dominant contributor to the temperature response in both regions is a change in vertical advection, as indicated by the heat budget analysis. However, the physical drivers of the vertical heat advection changes differ between the two analyses. In the equatorial Pacific, the surface warming arises primarily from circulation changes. By contrast, in the Pacific coastal upwelling regions examined in Chapter 3, the temperature response is more directly controlled by chlorophyll–induced radiative heating or cooling, which generates subsurface temperature anomalies that are subsequently advected into the upper ocean

(Figure 3.10).

This difference primarily arises from the distinct regions and depth ranges over which the heat budget is calculated. In Chapter 3, the heat budget is evaluated within nearshore coastal upwelling regions, where strong upwelling allows chlorophyll-induced subsurface temperature anomalies to be efficiently transported into the upper ocean, thereby modifying advective heat transport. By contrast, the region considered here is located in the offshore open ocean and the heat budget is calculated within the upper 30 m, which lies above the subsurface warming induced by radiative effects (Figure 5.3b). However, the dominance of circulation-driven surface temperature changes is consistent with previous studies, which highlight the primary role of circulation-driven heat advection, rather than local chlorophyll-induced radiative heating or the transport of associated temperature anomalies (Sweeney et al., 2005; Park et al., 2014a; Zhang et al., 2019).

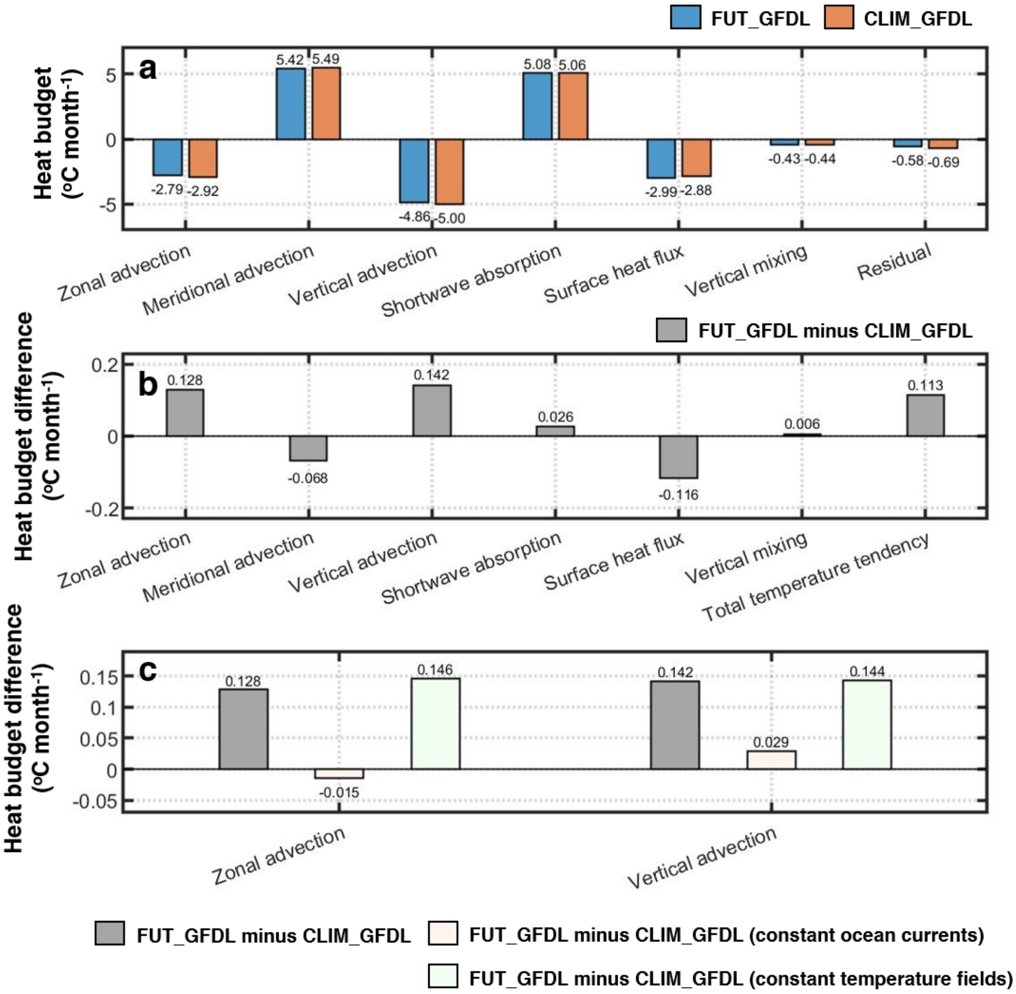

Figure 5.11: Heat budget analysis following Equation 2.1, integrated over the upper 0–30 m within the yellow solid box shown in Figure 5.4e. (a) Individual heat budget terms in the FUT_GFDL and CLIM_GFDL experiments. The rightmost bars represent residuals. (b) Differences in heat budget terms computed as FUT_GFDL minus CLIM_GFDL. (c) Grey bars indicate the differences in advective heat transport of FUT_GFDL minus CLIM_GFDL. Light red bars represent FUT_GFDL minus CLIM_GFDL assuming unchanged ocean currents (fixed at CLIM_GFDL), thereby isolating the contribution from temperature changes. Light green bars represent FUT_GFDL minus CLIM_GFDL assuming unchanged temperature fields (fixed at CLIM_GFDL), isolating the contribution from changes in ocean circulation. All terms are averaged in 2071–2100.

5.5.3 Uncertainties and limitations

This study uses future chlorophyll changes projected by multiple ESMs as prescribed “optical” forcing in NEMO, whereby chlorophyll fields are imposed to modify solar absorption in the ocean. NEMO simulations with and without these prescribed chlorophyll changes are then compared to isolate the impact of future chlorophyll decline on ocean thermal structure and dynamics. Although chlorophyll projections from five CMIP6 models are used and the responses are averaged, uncertainties remain due to model deficiencies in the representation of phytoplankton growth and mortality (Petrik et al., 2022), biases in simulated nutrient distributions (Tagliabue et al., 2021), and uncertainties in future biogeochemical projections (Kwiatkowski et al., 2017). These factors introduce uncertainty in the simulated mean state and future changes of phytoplankton biomass and chlorophyll, which may in turn affect the simulated oceanic responses to future chlorophyll decline in this study.

In addition, although our results suggest that chlorophyll-driven changes in ocean thermal structure and dynamics may feed back onto the atmosphere, this study does not include an interactive atmospheric component and therefore cannot directly quantify atmospheric responses. Instead, this work focusses on isolating and understanding the ocean thermal and dynamical responses to projected changes in chlorophyll without the complex interactions with the atmosphere, a necessary step in understanding such fully-coupled simulations.

5.6 Conclusions

In this study, we use the NEMO ocean model to compare two groups of simulations with and without changes in solar radiation absorption induced by future chlorophyll changes under anthropogenic climate forcing. The projected chlorophyll changes are derived from multiple CMIP6 ESMs. Our results demonstrate that future chlorophyll decline allows more incoming solar radiation to penetrate into the subsurface ocean, leading to pronounced subsurface warming of 0.05–0.20 °C. The magnitude of this chlorophyll-induced subsurface temperature increase reaches approximately 1.5–8% of the subsurface warming induced by anthropogenic climate change. In addition, chlorophyll-driven redistributions of solar radiation alter the seasonal cycle of upper-ocean temperature, especially in the high-latitude North Atlantic.

The oceanic response to future chlorophyll decline exhibits an El Niño-like pattern in both thermal and dynamical fields. Chlorophyll changes induce surface warming in the eastern equatorial Pacific and cooling in the western basin, shifting the mean Niño3.4 index towards an El Niño-like state by approximately 0.03–0.19. Consistent with this surface signal, the 20 °C isotherm in the eastern equatorial Pacific deepens by about 0.4–2 m, in line with the chlorophyll-induced subsurface warming. These thermal responses are accompanied by dynamical changes, including a weakening of the equatorial upwelling circulation and off-equatorial meridional circulation, which largely contribute to the El Niño-like SST pattern.

Together, these results highlight the importance of chlorophyll-induced modulation of solar radiation absorption in shaping ocean thermal structure and circulation under future climate change. They further suggest that chlorophyll-driven changes can influence sea surface height, large-scale ocean dynamics and potentially climate through ocean-atmosphere coupling. Given that most current ESMs do not use time-varying chlorophyll in their physical solar schemes, our findings therefore support the need for future ESMs to improve the representation of marine chlorophyll and to incorporate interactive, chlorophyll-dependent radiative processes in order to more realistically capture biologically mediated ocean-climate feedbacks.

6

Conclusions and future work

6.1 Summary

6.1.1 Background to the thesis

The Earth's climate system is governed by the balance between incoming solar radiation and outgoing terrestrial radiation, while the ocean acts as the primary heat reservoir by absorbing and redistributing most incoming shortwave radiation. As the dominant light-absorbing constituent in the open ocean other than water, chlorophyll strongly modulates the vertical distribution of incoming solar radiation.

Previous studies have shown that chlorophyll-induced solar absorption can alter SST, ocean stratification, circulation and sea ice, thereby influencing climate variability and air-sea heat and carbon exchange. However, how chlorophyll-induced solar absorption may change under future anthropogenic warming and, in turn, feed back onto the climate system remains poorly understood. Moreover, these effects remain incompletely represented in many ESMs, which exhibit substantial inter-model spread in the representation of chlorophyll-induced solar absorption and, in some cases, rely on overly simplified solar radiation calculations. This thesis is therefore motivated by the need to better quantify chlorophyll-induced solar absorption and its effects on ocean physics and climate, to assess the impacts of different ESM representations of this process, and to inform future improvements in its treatment within ESMs.

6.1.2 Pacific cooling and Atlantic warming responses to chlorophyll-induced solar absorption in coastal upwelling systems

Chapter 3 investigates how chlorophyll-induced solar absorption shapes upper-ocean temperature and dynamics across major eastern boundary coastal upwelling systems. We employ the NEMO ocean model coupled to the MEDUSA biogeochemistry model and perform two simulations that differ only in the chlorophyll field used by NEMO's RGB solar scheme: a control case with constant chlorophyll fixed at 0.1 mg m^{-3}, and a biologically interactive case using chlorophyll simulated by MEDUSA.

Chlorophyll-induced solar absorption leads to a cooling response in Pacific coastal upwelling regions (California, Peru and Chile) but a warming response in Atlantic coastal upwelling regions (along northwest and southwest Africa). In the Pacific, high nearshore surface chlorophyll enhances solar absorption in the upper $\sim$20 m and reduces solar penetration below, resulting in subsurface cooling that is subsequently upwelled to the surface. At the same time, heat accumulated in the near-surface layer is advected offshore, thus causing nearshore cooling accompanied by offshore warming. The associated subsurface cooling strengthens upper-ocean stratification and shoals the mixed layer. Using an offline diagnosis of net offshore transport, we show that the shallower mixed layer intensifies the geostrophic component of offshore transport, thereby increasing net offshore transport within the mixed layer and strengthening coastal upwelling. The resulting circulation anomalies amplify the existing cross-shore overturning pattern (upward-offshore-downward-onshore) and intensify the nearshore cooling effect.

In contrast, Atlantic upwelling regions exhibit low near-coast surface chlorophyll but high concentrations of chlorophyll in the subsurface chlorophyll maximum (at $\sim$60 m depth), located below the mixed layer. This vertical structure leads to enhanced absorption and heat accumulation in the subsurface offshore zone (200–1500 km from the coast), which is then transported coastward by subsurface eastward currents and subsequently upwelled, causing warming in the upper ocean near the coast (above

$\sim$80 m). Dynamically, the subsurface warming deepens the mixed layer, leading to weaker geostrophic offshore transport and reduced upwelling strength, broadly opposite to the Pacific response.

Notably, the physical responses feed back onto biogeochemistry: enhanced (weakened) upwelling in the Pacific (Atlantic) tends to increase (decrease) nearshore nutrient supply and surface chlorophyll, reinforcing the regional chlorophyll distribution and its associated radiative effects.

6.1.3 Chlorophyll-driven redistribution of solar radiation and its role in delaying future warming

Chapter 4 examines how projected future declines in ocean chlorophyll concentration modify the vertical distribution of solar radiation and thereby influence the rate of climate warming. Focusing on CMIP6 ESMs that explicitly represent chlorophyll-dependent solar absorption, we show that projected future chlorophyll decline under the SSP5-8.5 scenario reduces the absorption of solar radiation within the surface mixed layer, representing a negative radiative forcing on the upper ocean. As a global mean, approximately $0.25\,\mathrm{W\,m^{-2}}$ of solar energy is redistributed from the mixed layer into the ocean below.

By comparing with standard greenhouse-gas forcing in SSP5-8.5, the negative radiative forcing induced by future chlorophyll decline delays human-induced global warming by about 3 years on average, with a maximum delay of 12 years across models. In some models, the magnitude of this radiative effect is comparable to, or larger than, the forcing associated with projected future increases in N_2O.

We further demonstrate that differences among CMIP6 ESMs in their representations of chlorophyll-induced solar absorption introduce substantial uncertainty into climate simulations, arising from the differences in both the physical solar schemes employed and chlorophyll inputs used within these schemes. Models that rely on spatially and temporally constant chlorophyll values exhibit global-scale negative biases in mixed layer solar absorption. Meanwhile, both these models and those that use satellite-based climatological chlorophyll as input to their physical solar schemes are unable to represent the radiative effects of future chlorophyll changes under climate change, thereby biasing high-emission climate projections towards more rapid warming.

6.1.4 Subsurface warming and an El Niño-like response driven by future chlorophyll decline

Chapter 5 uses the NEMO ocean general circulation model and investigates how projected future chlorophyll decline drives large-scale changes in ocean thermal structure and circulation under anthropogenic warming. We prescribe chlorophyll output from five CMIP6 ESMs as an external "optical" forcing in the physical solar scheme of NEMO. For each chlorophyll projection, we compare a simulation with time-varying chlorophyll (historical followed by SSP3-7.0) against a control simulation in which chlorophyll is fixed to its 1948–1977 climatology, thereby isolating the physical impacts of solar redistribution induced by future chlorophyll change.

Across all five pairs of simulations with and without the radiative effects of future chlorophyll change, declining chlorophyll reduces solar absorption within the surface mixed layer and allows more solar radiation to penetrate below it, consistent with the results of Chapter 4. This redistribution of solar radiation leads to subsurface warming that peaks beneath the mixed layer (approximately 40–100 m), where the additional heat is less efficiently communicated to the surface by vertical mixing. The global-mean subsurface temperature increases are about 0.05–0.2 °C, equivalent to 1.5–8% of the subsurface warming driven by anthropogenic climate change. In contrast, the SST response is comparatively weak at the global scale, reflecting a balance between reduced mixed layer solar absorption (tending to cool the surface) and less outgoing longwave radiation, the upwelling and mixing of warmer subsurface waters (tending to warm the surface).

Future chlorophyll decline modifies the seasonal cycle of SST, particularly in the high-latitude North Atlantic. Stronger future chlorophyll decline during late spring and summer redistributes more solar radiation beneath the mixed layer, leading to summer surface cooling. During mixed layer deepening in winter, the stored subsurface heat is entrained back into the mixed layer, resulting in winter surface warming and an overall reduction in the amplitude of the SST seasonal cycle.

Future chlorophyll decline also induces an El Niño-like shift in the mean state of the equatorial Pacific, characterised by surface warming, a deepening of the 20 °C isotherm and a weakening of equatorial circulation. An offline heat budget analysis indicates that the eastern Pacific surface warming arises primarily from circulation-driven changes in vertical and zonal heat transport, rather than from direct solar absorption by chlorophyll.

6.2 Implications

Chapters 3, 4, 5 jointly analyse the representations of chlorophyll-induced solar absorption in CMIP6 ESMs, and the subsequent impacts on oceanic and climatic processes. The primary implications of this thesis therefore concern the development and application of future ESMs, and can be summarised as follows.

• This thesis provides, for the first time, a systematic analysis of how chlorophyll-induced solar radiation absorption is represented across CMIP6 ESMs (Table 4.1). Through personal communication with CMIP6 modelling groups, we compile information on the physical solar schemes employed and the chlorophyll inputs used to calculate solar penetration. This effort establishes a foundation for future intercomparison studies and uncertainty assessments of chlorophyll-radiation processes within CMIP models.

• We demonstrate that inter-model differences in representing chlorophyll-induced solar absorption introduce substantial uncertainty into the upper-ocean heat budget. Reducing these discrepancies is therefore essential for improving the realism of climate simulations and highlights the need to advance both chlorophyll simulations and the parameterisations of the chlorophyll-induced solar absorption in ESMs.

• Using multi-year mean simulations in Chapter 3, we show that replacing constant chlorophyll with more realistic chlorophyll distributions leads to contrasting thermal and dynamical responses across different coastal upwelling systems. In addition, as discussed in Section 5.5.2, the spatial extent and underlying mechanisms of chlorophyll-induced temperature changes also differ between equatorial upwelling and coastal upwelling regions. These differences imply that the chlorophyll-temperature-dynamics feedback is strongly region-dependent and should be represented realistically in ESMs to improve simulations of the mean-state climate of upwelling regions.

• In Chapter 5, simulations with the NEMO ocean model demonstrate that projected future chlorophyll decline leads to pronounced changes in subsurface ocean temperature and circulation. These changes have the potential to influence air-sea heat and carbon exchanges, atmospheric processes and the broader climate system. As most current ESMs do not incorporate time-varying chlorophyll in their solar radiation calculations, our results suggest that including interactive chlorophyll-radiation processes is necessary to improve the physical realism of future climate projections.

Chapters 4 and 5 show that chlorophyll-induced radiative effects exert a significant influence on ocean thermal structure and dynamics, with implications for both climate change and climate variability. Chlorophyll should therefore be regarded as a key variable with physical feedbacks in understanding and representing ocean-climate interactions.

• We show that the radiative forcing induced by future chlorophyll declines can be comparable in magnitude to some greenhouse-gas radiative forcings, and can delay surface warming and lead to subsurface warming under climate change scenarios. This demonstrates that marine biological processes can directly redistribute energy within the upper ocean, thereby modifying the vertical structure and timing of climate warming, in addition to their established roles in regulating the magnitude of climate change through primary production and carbon cycling.

• In the equatorial Pacific, future chlorophyll decline drives the ocean thermal structure and circulation towards a more El Niño-like mean state. This indicates that temporal variations in chlorophyll can not only influence the amplitude but also the background state of climate variability. Therefore, future projections of climate variability should take into account the radiative effects associated with chlorophyll changes.

Our results further suggest that chlorophyll-induced modulation of solar absorption not only affects ocean physical processes, but may also feed back onto marine biogeochemical cycles through changes in light conditions and nutrient transport via stratification and ocean dynamics. This two-way coupling highlights the importance of considering physical-biogeochemical interactions when studying marine ecosystem dynamics.

• We show that spatial variability in chlorophyll can alter the depth to which light penetrates by several tens of metres. As a result, within this depth range, the calculation of photosynthetically available radiation in biogeochemical models depends critically on an accurate representation of chlorophyll-induced solar absorption in the upper ocean. Future biogeochemical modelling work should therefore prioritise improving the representation of chlorophyll-induced light attenuation to more realistically simulate in-ocean light conditions for phytoplankton.

• In the Pacific coastal upwelling regions, chlorophyll-induced radiative effects enhance upwelling, increasing nutrient supply to the surface and promoting phytoplankton growth, thereby amplifying the existing high surface chlorophyll concentrations. In the Atlantic upwelling regions, weakened upwelling leads to reduced surface chlorophyll, allowing increased light penetration into the subsurface and strengthening the subsurface chlorophyll maximum. These contrasting responses collectively reinforce the pre-existing spatial distribution of chlorophyll. Under future climate change, chlorophyll-driven surface and subsurface temperature responses also modify upper-ocean stratification, with potential implications for nutrient supply and biological productivity. Accurately simulating marine biogeochemical cycles therefore requires an integrated representation of the two-way coupling between ocean physics and marine biogeochemistry.

6.3 Future work

6.3.1 Interannual variability of chlorophyll-induced solar absorption in coastal upwelling regions

In Chapter 3, we investigate the impacts of chlorophyll-induced solar absorption on ocean temperature and dynamics in coastal upwelling regions based on multi-year mean simulations. However, chlorophyll concentrations in these regions exhibit pronounced interannual variability (Thomas et al., 2009; Demarcq, 2009), highlighting the need to investigate the radiative effects associated with chlorophyll variability on interannual timescales in future work. Such radiative effects may influence interannual variations in upwelling temperature and intensity, thereby modifying air-sea heat and momentum exchange. These changes may further affect local cloud conditions and potentially contribute to remote climate variability, such as ENSO (Chiang and Vimont, 2004; Qu et al., 2014). Furthermore, interannual variability in ocean physical processes associated with chlorophyll-driven radiative effects can influence nutrient supply and temperatures, thereby modulating phytoplankton growth, with implications for coastal marine ecosystems and fisheries (Messié et al., 2023). Therefore, we present below some preliminary results from an ongoing analysis aimed at extending this work to interannual timescales. Specifically, we analyse 100 years of data from the piControl simulation of UKESM1.0 to explore the interannual variability of chlorophyll-driven solar

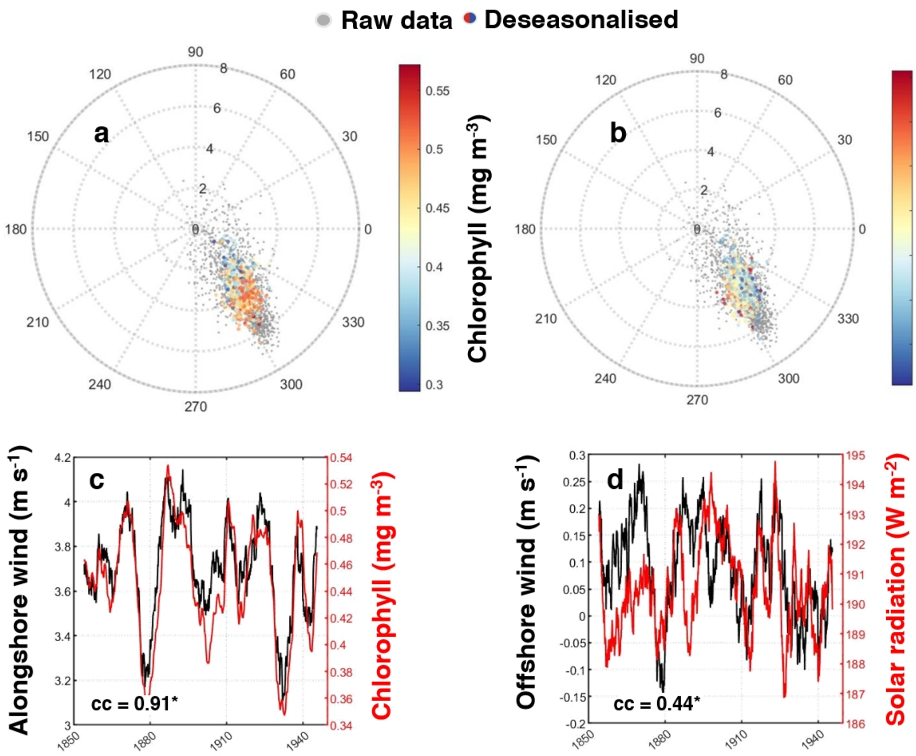

Figure 6.1: Interannual variations of chlorophyll-induced solar absorption during 1850–1949, illustrated using the regionally averaged California coastal upwelling region shown in Figure 3.1. (a) Wind rose diagram, where grey dots represent monthly wind and coloured dots represent deseasonalised wind, with colour indicating deseasonalised chlorophyll concentration. (b) As in (a), but with colour showing deseasonalised incoming solar radiation. (c) Time series of deseasonalised alongshore wind and chlorophyll concentration. (d) Time series of deseasonalised offshore wind and incoming solar radiation. Here, 'cc' denotes the correlation coefficient, and '*' indicates statistical significance at the 0.05 level.

absorption.

Using the California coastal upwelling system as an example (Figure 3.1), we propose the hypothesis that the interannual variability of chlorophyll-induced solar absorption is primarily controlled by the alongshore and offshore components of the wind field. First, stronger alongshore winds enhance offshore Ekman transport, leading to intensified coastal upwelling and increased upward transport of nutrients. This process promotes phytoplankton growth and results in higher surface chlorophyll concentrations (Figures 6.1a and c). Second, stronger offshore winds enhance the advection of dry continental air, which reduces cloud cover over coastal upwelling regions and allows more incoming solar radiation to reach the ocean surface (Figures 6.1b and d). As a consequence, higher wind speeds (in both alongshore and offshore directions) can exert two impacts: an 'alongshore wind-upwelling-chlorophyll' impact and an 'offshore wind-cloud-solar radiation' impact. Together, these processes jointly regulate the strength of chlorophyll-induced solar absorption in the surface ocean.

However, these two effects do not operate consistently across all coastal upwelling systems (Table 6.1). This likely reflects the influence of additional regional processes. For example, in the northwestern African coastal upwelling region, mineral dust transported from land can directly attenuate incoming solar radiation (Foltz and McPhaden, 2008; Song et al., 2018), such that dry air advection does not necessarily increase surface incoming solar radiation through cloud reduction. Furthermore, the impact of wind direction on cloud cover may depend on the details of the regional climatological circulation patterns in both the atmosphere and ocean, which shape the background conditions for air–sea coupling (Abrahams et al., 2021). These complexities indicate that the mechanisms controlling interannual variability in chlorophyll-induced solar absorption are regionally dependent. Future studies are therefore encouraged to further explore the underlying drivers of variability in chlorophyll-induced radiative effects and associated temperature responses, and to assess the hypotheses proposed here.

6.3.2 The necessity of using an atmosphere-ocean coupled model

In Chapters 4 and 5, we use CMIP6 model output and the NEMO ocean model to assess oceanic responses to future chlorophyll decline. The use of an ocean-only modelling framework has provided valuable insights into the underlying physical mechanisms, allowing the direct impacts of chlorophyll-induced radiative effects on ocean temperature, stratification and dynamics to be isolated.

Previous studies focusing on the eastern equatorial Pacific, based on present-day simulations, have shown that the magnitude of the thermal and dynamical responses to chlorophyll-induced solar absorption depends on whether the ocean model is coupled to the atmosphere (Anderson et al., 2009; Jochum et al., 2010; Park et al., 2014a), as well as on the strength of ocean-atmosphere coupling (Tian et al., 2021a). These results suggest that the oceanic responses to future chlorophyll decline may be modulated by atmospheric processes through air-sea coupling, and may in turn influence air-sea heat and carbon exchanges and atmospheric circulation, as discussed in Section 5.5.1.

While this thesis focuses on isolating oceanic processes, extending this work using fully coupled ocean-atmosphere models would be useful and scientifically interesting. For example, future studies could employ a coupled modelling framework with one experiment in which chlorophyll is prescribed at a historical climatological level and another in which chlorophyll is allowed to decline under future climate conditions, as in Chapter 5. Comparing these experiments would help to quantify the atmospheric response to the radiative effects associated with chlorophyll decline and to assess how the oceanic responses identified here manifest under future climate change.

6.3.3 Future improvements in Earth system models

This thesis shows that, within CMIP6, only a few ESMs use simulated chlorophyll to modulate solar absorption. As a fundamental step forward, we therefore encourage a broader adoption of time-varying, modelled chlorophyll fields in the calculation of solar radiation within ESMs, in order to represent biologically mediated radiative effects more realistically. In addition, targeted sensitivity experiments using different chlorophyll fields would help to better quantify uncertainties associated with these radiative effects.

We further highlight that current ESMs exhibit substantial biases in their simulations of the climatological mean state of chlorophyll, as well as a large inter-model spread in future chlorophyll projections. These deficiencies introduce considerable uncertainty into assessments of chlorophyll-driven radiative effects. Future research may therefore focus on improving the representation of chlorophyll dynamics in ESMs, or on combining process-based biogeochemical models with data-driven approaches, such as neural networks or machine learning-based parameterisations (Yuval and O'Gorman, 2020; Watt-Meyer et al., 2024), to enhance the predictive skill of chlorophyll simulations and reduce uncertainties in future climate projections.

Finally, in some coastal regions, other optically active constituents, such as CDOM and NAP, can contribute to solar absorption at a magnitude comparable to or even larger than that of chlorophyll (Nelson and Siegel, 2013; Pefanis et al., 2020). Accounting for these components in future modelling studies will be essential for achieving more realistic simulations of coastal ocean radiative processes and their associated physical and biogeochemical responses.

Table 6.1: Correlations between alongshore/offshore wind speed and other environmental variables in major eastern boundary coastal upwelling regions.

Variable pair	**California**	**Peru**	**Chile**	**NW Africa**	**SW Africa**
Offshore wind & cloud coverage	−0.46*	−0.79*	−0.50*	−0.08	−0.50*
Alongshore wind & cloud coverage	−0.21	0.52*	−0.31*	−0.24	0.02
Offshore wind & solar radiation	0.44*	0.76*	0.50*	0.18	0.53*
Alongshore wind & solar radiation	0.20	−0.40	0.18	0.15	0.15
Offshore wind & upwelling	0.70*	−0.29	0.40	0.25	0.37*
Alongshore wind & upwelling	0.92*	0.49*	0.74*	0.88*	0.43*
Offshore wind & chlorophyll	0.51*	−0.13	0.18	0.31*	−0.11
Alongshore wind & chlorophyll	0.91*	0.11	0.68*	0.70*	0.07

Note: Correlations are calculated using deseasonalised monthly data over 1850–1949. '*' indicates statistical significance at the 0.05 level.

Bibliography

Abrahams, A., Schlegel, R. W., and Smit, A. J. (2021). Variation and change of upwelling dynamics detected in the world's Eastern Boundary Upwelling Systems. *Frontiers in Marine Science*, 8:626411.

Anderson, W., Gnanadesikan, A., and Wittenberg, A. (2009). Regional impacts of ocean color on tropical Pacific variability. *Ocean Science*, 5(3):313–327.

Asselot, R., Holden, P. B., Lunkeit, F., and Hense, I. (2024). A missing link in the carbon cycle: phytoplankton light absorption under RCP emission scenarios. *Earth System Dynamics*, 15(4):875–891.

Asselot, R., Lunkeit, F., Holden, P. B., and Hense, I. (2021). The relative importance of phytoplankton light absorption and ecosystem complexity in an Earth System Model. *Journal of Advances in Modeling Earth Systems*, 13(5):2020MS002110.

Asselot, R., Lunkeit, F., Holden, P. B., and Hense, I. (2022). Climate pathways behind phytoplankton-induced atmospheric warming. *Biogeosciences*, 19(1):223–239.

Babin, M., Stramski, D., Ferrari, G. M., Claustre, H., Bricaud, A., Obolensky, G., and Hoepffner, N. (2003). Variations in the light absorption coefficients of phytoplankton, nonalgal particles, and dissolved organic matter in coastal waters around Europe. *Journal of Geophysical Research: Oceans*, 108(C7):3211.

Behrenfeld, M. J., O'Malley, R. T., Boss, E. S., Westberry, T. K., Graff, J. R., Halsey, K. H., Milligan, A. J., Siegel, D. A., and Brown, M. B. (2016). Revaluating ocean warming impacts on global phytoplankton. *Nature Climate Change*, 6(3):323–330.

Bi, D., Marsland, S. J., Uotila, P., O'farrell, S., Fiedler, R., Sullivan, A., Griffies, S. M., Zhou, X., and Hirst, A. C. (2013). ACCESS-OM: the ocean and sea-ice core of the ACCESS coupled model. *Australian Meteorological and Oceanographic Journal*, 63(1):213–232.

Bopp, L., Resplandy, L., Orr, J. C., Doney, S. C., Dunne, J. P., Gehlen, M., Halloran, P., Heinze, C., Ilyina, T., Séférian, R., Tjiputra, J., and Vichi, M. (2013). Multiple stressors of ocean ecosystems in the 21st century: Projections with CMIP5 models. *Biogeosciences*, 10(10):6225–6245.

Boucher, O., Servonnat, J., Albright, A. L., Aumont, O., Balkanski, Y., Bastrikov, V., Bekki, S., Bonnet, R., Bony, S., Bopp, L., Braconnot, P., Brockmann, P., Cadule, P., Caubel, A., Cheruy, F., Codron, F., Cozic, A., Cugnet, D., D'Andrea, F., Davini, P., de Lavergne, C., Denvil, S., Deshayes, J., Devilliers, M., Ducharne, A., Dufresne, J. L., Dupont, E., Éthé, C., Fairhead, L., Falletti, L., Flavoni, S., Foujols, M. A., Gardoll, S., Gastineau, G., Ghattas, J., Grandpeix, J. Y., Guenet, B., Lionel, E. G., Guilyardi, E., Guimberteau, M., Hauglustaine, D., Hourdin, F., Idelkadi, A., Joussaume, S., Kageyama, M., Khodri, M., Krinner, G., Lebas, N., Levavasseur, G., Lévy, C., Li, L., Lott, F., Lurton, T., Luyssaert, S., Madec, G., Madeleine, J. B., Maignan, F., Marchand, M., Marti, O., Mellul, L., Meurdesoif, Y., Mignot, J., Musat, I., Ottlé, C., Peylin, P., Planton, Y., Polcher, J., Rio, C., Rochetin, N., Rousset, C., Sepulchre, P., Sima, A., Swingedouw, D., Thiéblemont, R., Traore, A. K., Vancoppenolle, M., Vial, J., Vialard, J., Viovy, N., and Vuichard, N. (2020). Presentation and evaluation of the IPSL-CM6A-LR climate model. *Journal of Advances in Modeling Earth Systems*, 12(7):e2019MS002010.

Bricaud, A., Babin, M., Morel, A., and Claustre, H. (1995). Variability in the chlorophyll-specific absorption coefficients of natural phytoplankton: Analysis and parameterization. *Journal of Geophysical Research: Oceans*, 100(C7):13321–13332.

Bricaud, A., Morel, A., and Prieur, L. (1981). Absorption by dissolved organic matter of the sea (yellow substance) in the UV and visible domains. *Limnology and Oceanography*, 26(1):43–53.

Brient, F. and Bony, S. (2012). Interpretation of the positive low-cloud feedback predicted by a climate model under global warming. *Climate Dynamics*, 40(9-10):2415–2431.

Buckley, M. W. and Marshall, J. (2016). Observations, inferences, and mechanisms of the Atlantic Meridional Overturning Circulation: A review. *Reviews of Geophysics*, 54(1):5–63.

Capotondi, A., Alexander, M. A., Bond, N. A., Curchitser, E. N., and Scott, J. D. (2012). Enhanced upper ocean stratification with climate change in the CMIP3 models. *Journal of Geophysical Research: Oceans*, 117(4):2011JC007409.

Cesana, G., Genio, D. A. D., Ackerman, S. A., Kelley, M., Elsaesser, G., Fridlind, M. A., Cheng, Y., and Yao, M. S. (2019). Evaluating models response of tropical low clouds to SST forcings using CALIPSO observations. *Atmospheric Chemistry and Physics*, 19(5):2813–2832.

Chavez, F. P. and Messié, M. (2009). A comparison of eastern boundary upwelling ecosystems. *Progress in Oceanography*, 83(1-4):80–96.

Chelton, D. B., Schlax, M. G., and Samelson, R. M. (2011). Global observations of nonlinear mesoscale eddies. *Progress in Oceanography*, 91(2):167–216.

Chemke, R. (2021). Future changes in the Hadley circulation: The role of ocean heat transport. *Geophysical Research Letters*, 48(4):e2020GL091372.

Chiang, J. C. H. and Vimont, D. J. (2004). Analogous Pacific and Atlantic meridional modes of tropical atmosphere–ocean variability. *Journal of Climate*, 17(21):4143–4158.

Coakley, J. A. (2003). Reflectance and albedo, surface. In *Encyclopedia of Atmospheric Sciences*, pages 1914–1923. Elsevier.

Currie, J. C., Lengaigne, M., Vialard, J., Kaplan, D. M., Aumont, O., Naqvi, S. W. A., and Maury, O. (2013). Indian Ocean Dipole and El Niño/Southern Oscillation impacts on regional chlorophyll anomalies in the Indian Ocean. *Biogeosciences*, 10:6677–6698.

Dai, M., Luo, Y. W., Achterberg, E. P., Browning, T. J., Cai, Y., Cao, Z., Chai, F., Chen, B., Church, M. J., Ci, D., Du, C., Gao, K., Guo, X., Hu, Z., Kao, S. J., Laws, E. A., Lee, Z., Lin, H., Liu, Q., Liu, X., Luo, W., Meng, F., Shang, S., Shi, D., Saito, H., Song, L., Wan, X. S., Wang, Y., Wang, W. L., Wen, Z., Xiu, P., Zhang, J., Zhang, R., and Zhou, K. (2023). Upper ocean biogeochemistry of the oligotrophic North Pacific Subtropical Gyre: From nutrient sources to carbon export. *Reviews of Geophysics*, 61(3):2022RG000800.

Danabasoglu, G., Lamarque, J. F., Bacmeister, J., Bailey, D. A., DuVivier, A. K., Edwards, J., Emmons, L. K., Fasullo, J., Garcia, R., Gettelman, A., Hannay, C., Holland, M. M., Large, W. G., Lauritzen, P. H., Lawrence, D. M., Lenaerts, J. T., Lindsay, K., Lipscomb, W. H., Mills, M. J., Neale, R., Oleson, K. W., Otto-Bliesner, B., Phillips, A. S., Sacks, W., Tilmes, S., van Kampenhout, L., Vertenstein, M., Bertini, A., Dennis, J., Deser, C., Fischer, C., Fox-Kemper, B., Kay, J. E., Kinnison, D., Kushner, P. J., Larson, V. E., Long, M. C., Mickelson, S., Moore, J. K., Nienhouse, E., Polvani, L., Rasch, P. J., and Strand, W. G. (2020). The Community Earth System Model Version 2 (CESM2). *Journal of Advances in Modeling Earth Systems*, 12(2):e2019MS001916.

Demarcq, H. (2009). Trends in primary production, sea surface temperature and wind in upwelling systems (1998–2007). *Progress in Oceanography*, 83(1–4):376–385.

DeVries, T. (2014). The oceanic anthropogenic CO_2 sink: Storage, air–sea fluxes, and transports over the industrial era. *Global Biogeochemical Cycles*, 28(7):631–647.

Dinesh, A. S., Sachan, D., Kumar, P., Dvornikov, A. Y., and Sein, D. V. (2025). Phytoplankton-light feedback delayed the appearance of permanent marine heatwave state in the indian ocean: insights from a regional earth system model. *Climate Dynamics*, 63(4):181.

Ding, H., Alexander, M. A., and Jacox, M. G. (2021). Role of geostrophic currents in future changes of coastal upwelling in the California current system. *Geophysical Research Letters*, 48(3):e2020GL090768.

Du, T., Wang, S., Jing, Z., Wu, L., Zhang, C., and Zhang, B. (2024). Future changes in coastal upwelling and biological production in eastern boundary upwelling systems. *Nature Communications*, 15(1):6238.

Duntley, S. Q. (1942). The visibility of submerged objects. *Journal of the Optical Society of America*, 32(1):61–70.

Durack, P. J., Gleckler, P. J., Purkey, S. G., Johnson, G. C., Lyman, J. M., and Boyer, T. P. (2018). Ocean warming: From the surface to the deep in observations and models. *Oceanography*, 31(2):41–51.

Echevin, V., Hauschildt, J., Colas, F., Thomsen, S., and Aumont, O. (2021). Impact of chlorophyll shading on the Peruvian upwelling system. *Geophysical Research Letters*, 48(19):2021GL094429.

Eyring, V., Bony, S., Meehl, G. A., Senior, C. A., Stevens, B., Stouffer, R. J., and Taylor, K. E. (2016). Overview of the Coupled Model Intercomparison Project Phase 6 (CMIP6) experimental design and organization. *Geoscientific Model Development*, 9(5):1937–1958.

Ferreira, A., Brotas, V., Palma, C., Borges, C., and Brito, A. C. (2021). Assessing phytoplankton bloom phenology in upwelling-influenced regions using ocean color remote sensing. *Remote Sensing*, 13(4):1–27.

Foltz, G. R. and McPhaden, M. J. (2008). Impact of saharan dust on tropical north atlantic SST. *Journal of Climate*, 21(19):5048–5060.

Font, E., Swart, S., Vinayachandran, P. N., and Queste, B. Y. (2025). On mode water formation and erosion in the Arabian Sea: forcing mechanisms, regionality, and seasonality. *Ocean Science*, 21(4):1349–1368.

Giddings, J., Matthews, A. J., Klingaman, N. P., Heywood, K. J., Joshi, M., and Webber, B. G. (2020). The effect of seasonally and spatially varying chlorophyll on Bay of Bengal surface ocean properties and the south Asian monsoon. *Weather and Climate Dynamics*, 1(2):635–655.

Gnanadesikan, A. and Anderson, W. G. (2009). Ocean water clarity and the ocean general circulation in a coupled climate model. *Journal of Physical Oceanography*, 39(2):314–332.

Griffies, S. M., Biastoch, A., Böning, C., Bryan, F., Danabasoglu, G., Chassignet, E. P., England, M. H., Gerdes, R., Haak, H., Hallberg, R. W., Hazeleger, W., Jungclaus, J., Large, W. G., Madec, G., Pirani, A., Samuels, B. L., Scheinert, M., Gupta, A. S., Severijns, C. A., Simmons, H. L., Tréguier, A.-M., Winton, M., Yeager, S., and Yin, J. (2009). Coordinated ocean-ice reference experiments (COREs). *Ocean Modelling*, 26(1-2):1–46.

Groeskamp, S., Griffies, S. M., Iudicone, D., Marsh, R., Nurser, A. J. G., and Zika, J. D. (2019). The water mass transformation framework for ocean physics and biogeochemistry. *Annual Review of Marine Science*, 11(1):271–305.

Gruber, N., Clement, D., Carter, B. R., Feely, R. A., van Heuven, S., Hoppema, M., Ishii, M., Key, R. M., Kozyr, A., Lauvset, S. K., Lo Monaco, C., Mathis, J. T., Murata, A., Olsen, A., Perez, F. F., Sabine, C. L., Tanhua, T., and Wanninkhof, R. (2019). The oceanic sink for anthropogenic CO_2 from 1994 to 2007. *Science*, 363(6432):1193–1199.

Guiavarc'h, C., Storkey, D., Blaker, A. T., Blockley, E., Megann, A., Hewitt, H., Bell, M. J., Calvert, D., Copsey, D., Sinha, B., Moreton, S., Mathiot, P., and An, B. (2025). GOSI9: UK Global Ocean and Sea Ice configurations. *Geoscientific Model Development*, 18(2):377–403.

Hernandez, O., Jouanno, J., Echevin, V., and Aumont, O. (2017). Modification of sea surface temperature by chlorophyll concentration in the Atlantic upwelling systems. *Journal of Geophysical Research: Oceans*, 122(7):5367–5389.

Hilt, M., Auclair, F., Benshila, R., Bordois, L., Capet, X., Debreu, L., Dumas, F., Jullien, S., Lemarié, F., Marchesiello, P., Nguyen, C., and Roblou, L. (2020).

Numerical modelling of hydraulic control, solitary waves and primary instabilities in the strait of Gibraltar. *Ocean Modelling*, 151:101642.

Hu, Z. Z., Huang, B., and Pegion, K. (2008). Low cloud errors over the southeastern Atlantic in the NCEP CFS and their association with lower-tropospheric stability and air-sea interaction. *Journal of Geophysical Research: Atmospheres*, 113(12):D12114.

Huan, Y., Sun, D., Wang, S., Zhang, H., Qiu, Z., Bilal, M., and He, Y. (2021). Remote sensing estimation of phytoplankton absorption associated with size classes in coastal waters. *Ecological Indicators*, 121:107198.

Iudicone, D., Madec, G., and McDougall, T. J. (2008). Water-mass transformations in a neutral density framework and the key role of light penetration. *Journal of Physical Oceanography*, 38(7):1357–1376.

Jerlov, N. G. (1968). *Optical Oceanography*. Elsevier Science.

Jing, Z., Wang, S., Wu, L., Wang, H., Zhou, S., Sun, B., Chen, Z., Ma, X., Gan, B., and Yang, H. (2023). Geostrophic flows control future changes of oceanic eastern boundary upwelling. *Nature Climate Change*, 13(2):148–154.

Jochum, M., Yeager, S., Lindsay, K., Moore, K., and Murtugudde, R. (2010). Quantification of the feedback between phytoplankton and ENSO in the community climate system model. *Journal of Climate*, 23(11):2916–2925.

Kang, X., Zhang, R.-H., Gao, C., and Zhu, J. (2017). An improved ENSO simulation by representing chlorophyll-induced climate feedback in the NCAR Community Earth System Model. *Scientific Reports*, 7(1):17123.

Kelley, M., Schmidt, G. A., Nazarenko, L. S., Bauer, S. E., Ruedy, R., Russell, G. L., Ackerman, A. S., Aleinov, I., Bauer, M., Bleck, R., Canuto, V., Cesana, G., Cheng, Y., Clune, T. L., Cook, B. I., Cruz, C. A., Genio, A. D. D., Elsaesser, G. S., Faluvegi, G., Kiang, N. Y., Kim, D., Lacis, A. A., Leboissetier, A., LeGrande, A. N., Lo, K. K., Marshall, J., Matthews, E. E., McDermid, S., Mezuman, K., Miller, R. L., Murray, L. T., Oinas, V., Orbe, C., García-Pando, C. P., Perlwitz,

J. P., Puma, M. J., Rind, D., Romanou, A., Shindell, D. T., Sun, S., Tausnev, N., Tsigaridis, K., Tselioudis, G., Weng, E., Wu, J., and Yao, M. S. (2020). GISS-E2.1: configurations and climatology. *Journal of Advances in Modeling Earth Systems*, 12(8):e2019MS002025.

Kessler, W. S. (1995). The 1991–1993 El Niño in the central Pacific. *Deep-Sea Research Part II*, 42(2–3):295–333.

Kessler, W. S. (2006). The circulation of the eastern tropical Pacific: A review. *Progress in Oceanography*, 69(2–4):181–217.

Koltermann, K. P., Gouretski, V. V., and Jancke, K. (2011). Hydrographic Atlas of the World Ocean Circulation Experiment (WOCE), Volume 3: Atlantic Ocean.

Kuhlbrodt, T., Jones, C. G., Sellar, A., Storkey, D., Blockley, E., Stringer, M., Hill, R., Graham, T., Ridley, J., Blaker, A., Calvert, D., Copsey, D., Ellis, R., Hewitt, H., Hyder, P., Ineson, S., Mulcahy, J., Siahaan, A., and Walton, J. (2018). The low-resolution version of HadGEM3 GC3.1: development and evaluation for global climate. *Journal of Advances in Modeling Earth Systems*, 10(11):2865–2888.

Kwiatkowski, L., Bopp, L., Aumont, O., Ciais, P., Cox, P. M., Laufkotter, C., Li, Y., and Seferian, R. (2017). Emergent constraints on projections of declining primary production in the tropical oceans. *Nature Climate Change*, 7(5):355–357.

Lambert, J. H. (1760). *Photometria sive de mensura et gradibus luminis*. Eberhard Klett, Augsburg.

Large, W. G., McWilliams, J. C., and Doney, S. C. (1994). Oceanic vertical mixing: A review and a model with a nonlocal boundary layer parameterization. *Reviews of Geophysics*, 32(4):363–403.

Laufkötter, C., Vogt, M., Gruber, N., Aita, M. N., Lima, I. D., Seferian, R., Bopp, L., Buitenhuis, E. T., Doney, S. C., Dunne, J. P., Hashioka, T., John, J. G., Le Quéré, C., Seibel, B., Totterdell, I., Vichi, M., and Völker, C. (2015). Drivers and uncertainties of future global marine primary production in marine ecosystem models. *Geoscientific Model Development*, 8(23):531–551.

Laufkotter, C., Vogt, M., Gruber, N., Aita-Noguchi, M., Aumont, O., Bopp, L., Buitenhuis, E., Doney, S. C., Dunne, J., Hashioka, T., Hauck, J., Hirata, T., John, J., Le Quéré, C., Lima, I. D., Nakano, H., Seferian, R., Totterdell, I., Vichi, M., and Volker, C. (2015). Drivers and uncertainties of future global marine primary production in marine ecosystem models. *Biogeosciences*, 12(23):6955–6984.

Laufkötter, C., Vogt, M., Gruber, N., Aumont, O., Bopp, L., Doney, S. C., Dunne, J. P., Hauck, J., John, J. G., Lima, I. D., Seferian, R., and Völker, C. (2016). Projected decreases in future marine export production: The role of the carbon flux through the upper ocean ecosystem. *Biogeosciences*, 13(13):4023–4047.

Lee, S., Chae, J. Y., Park, J.-H., Kim, Y. T., Kang, B., Shin, C. W., and Ha, H. K. (2024). Remote impacts of low-latitude oceanic climate on coastal upwelling in a marginal sea of the northwestern Pacific. *Regional Studies in Marine Science*, 69:103344.

Lee, Z., Darecki, M., Carder, K., Davis, C., Stramski, D., and Rhea, W. (2005). Diffuse attenuation coefficient of downwelling irradiance: An evaluation of remote-sensing methods. *Journal of Geophysical Research: Oceans*, 110(C2):C02017.

Lengaigne, M., Madec, G., Bopp, L., Menkes, C., Aumont, O., and Cadule, P. (2009). Bio-physical feedbacks in the Arctic Ocean using an Earth system model. *Geophysical Research Letters*, 36:L21602.

Lengaigne, M., Menkes, C., Aumont, O., Gorgues, T., Bopp, L., André, J. M., and Madec, G. (2007). Influence of the oceanic biology on the tropical Pacific climate in a coupled general circulation model. *Climate Dynamics*, 28(5):503–516.

Lewis, M., Carr, M.-E., Feldman, G., Esaias, W., and McClain, C. (1990). Influence of penetrating solar radiation on the heat budget of the equatorial Pacific ocean. *Nature*, 347(6293):543–545.

Lim, H.-G., Park, J.-Y., and Kug, J.-S. (2018). Impact of chlorophyll bias on the tropical Pacific mean climate in an Earth system model. *Climate Dynamics*, 51(7–8):2681–2694.

Löptien, U., Eden, C., Timmermann, A., and Dietze, H. (2009). Effects of biologically induced differential heating in an eddy-permitting coupled ocean-ecosystem model. *Journal of Geophysical Research: Oceans*, 114:C06011.

Lorente, P., García-Sotillo, M., Amo-Baladrón, A., Aznar, R., Levier, B., Sánchez-Garrido, J. C., Sammartino, S., de Pascual-Collar, A., Reffray, G., Toledano, C., and Álvarez Fanjul, E. (2019). Skill assessment of global, regional, and coastal circulation forecast models: Evaluating the benefits of dynamical downscaling in IBI (Iberia–Biscay–Ireland) surface waters. *Ocean Science*, 15(4):967–996.

Lovato, T., Peano, D., Butenschön, M., Materia, S., Iovino, D., Scoccimarro, E., Fogli, P. G., Cherchi, A., Bellucci, A., Gualdi, S., Masina, S., and Navarra, A. (2022). CMIP6 simulations with the CMCC Earth System Model (CMCC-ESM2). *Journal of Advances in Modeling Earth Systems*, 14(3):e2021MS002814.

Ma, J., Liu, H., Lin, P., and Zhan, H. (2015). Effects of the interannual variability in chlorophyll concentrations on sea surface temperatures in the east tropical Indian Ocean. *Journal of Geophysical Research: Oceans*, 120(10):7015–7027.

Ma, J., Yang, Q., Liu, H., Lin, P., and Liu, J. (2022). Effects of ocean chlorophyll on the mode water subduction rate in the northwestern and central Pacific Ocean. *Frontiers in Marine Science*, 9:814053.

Madec, G. and NEMO team (2016). NEMO ocean engine, version 3.6 stable.

Manizza, M., Le Quéré, C., Watson, A. J., and Buitenhuis, E. T. (2005). Bio-optical feedbacks among phytoplankton, upper ocean physics and sea-ice in a global model. *Geophysical Research Letters*, 32(5):L05603.

Manizza, M., Le Quéré, C., Watson, A. J., and Buitenhuis, E. T. (2008). Ocean biogeochemical response to phytoplankton-light feedback in a global model. *Journal of Geophysical Research: Oceans*, 113(10):C10010.

Marzeion, B., Timmermann, A., Murtugudde, R., and Jin, F.-F. (2005). Biophysical feedbacks in the tropical Pacific. *Journal of Climate*, 18(1):58–70.

McPhaden, M. J., Lee, T., and McClurg, D. (2011). El Niño and its relationship to changing background conditions in the tropical Pacific Ocean. *Geophysical Research Letters*, 38(15):L15709.

Meinshausen, M., Nicholls, Z. R., Lewis, J., Gidden, M. J., Vogel, E., Freund, M., Beyerle, U., Gessner, C., Nauels, A., Bauer, N., Canadell, J. G., Daniel, J. S., John, A., Krummel, P. B., Luderer, G., Meinshausen, N., Montzka, S. A., Rayner, P. J., Reimann, S., Smith, S. J., Berg, M. V. D., Velders, G. J., Vollmer, M. K., and Wang, R. H. (2020). The shared socio-economic pathway (SSP) greenhouse gas concentrations and their extensions to 2500. *Geoscientific Model Development*, 13(8):3571–3605.

Meng, S., Gong, X., Yu, Y., Yao, X., Gong, X., Lu, K., Zhang, C., Shi, J., Yu, X., and Gao, H. (2021). Strengthened ocean-desert process in the north pacific over the past two decades. *Environmental Research Letters*, 16(2):024034.

Meng, S., Webber, B. G., Stevens, D. P., Joshi, M., Palmieri, J., and Yool, A. (2024). Diverse responses of upper ocean temperatures to chlorophyll-induced solar absorption across different coastal upwelling regions. *Geophysical Research Letters*, 51(19):2024GL109714.

Mercado, J. M. and Gómez-Jakobsen, F. (2022). Seasonal variability in phytoplankton light absorption properties: Implications for the regional parameterization of the chlorophyll a specific absorption coefficients. *Continental Shelf Research*, 232:104614.

Messié, M., Sherlock, R. E., Huffard, C. L., Pennington, J. T., Choy, C. A., Michisaki, R. P., Gomes, K., Chavez, F. P., Robison, B. H., and Smith Jr., K. L. (2023). Coastal upwelling drives ecosystem temporal variability from the surface to the abyssal seafloor. *Proceedings of the National Academy of Sciences*, 120(13):e2214567120.

Messié, M. and Chavez, F. P. (2015). Seasonal regulation of primary production in eastern boundary upwelling systems. *Progress in Oceanography*, 134:1–18.

Mobley, C. D. (1994). *Light and water: Radiative transfer in natural waters.* Academic Press, San Diego.

Morel, A. (1988). Optical modeling of the upper ocean in relation to its biogenous matter content (case I waters). *Journal of Geophysical Research: Oceans*, 93(C9):10749–10768.

Morel, A. and Berthon, J.-F. B. (1989). Surface pigments, algal biomass profiles, and potential production of the euphotic layer: Relationships reinvestigated in view of remote-sensing applications. *Limnology and Oceanography*, 34(8):1545–1562.

Morel, A. and Maritorena, S. (2001). Bio-optical properties of oceanic waters: A reappraisal. *Journal of Geophysical Research: Oceans*, 106(C4):7163–7180.

Murtugudde, R., Beauchamp, J., Mcclain, C. R., Lewis, M., and Busalacchi, A. J. (2002). Effects of penetrative radiation on the upper tropical ocean circulation. *Journal of Climate*, 15(5):470–486.

Nakamoto, S., Kumar, S. P., Oberhuber, J. M., Ishizaka, J., Muneyama, K., and Frouin, R. (2001). Response of the equatorial Pacific to chlorophyll pigment in a mixed layer isopycnal ocean general circulation model. *Geophysical Research Letters*, 28(10):2021–2024.

Nalli, N. R., Minnett, P. J., and van Delst, P. (2008). Emissivity and reflection model for calculating unpolarized isotropic water surface-leaving radiance in the infrared. I: Theoretical development and calculations. *Applied Optics*, 47(21):3701–3721.

Nelson, N. B. and Siegel, D. A. (2013). The global distribution and dynamics of chromophoric dissolved organic matter. *Annual Review of Marine Science*, 5:447–476.

Nicknish, P. A., Chiang, J. C. H., Hu, A., and Boos, W. R. (2023). Regional tropical rainfall shifts under global warming: An energetic perspective. *Environmental Research: Climate*, 2(1):015007.

Oglethorpe, K., Castro, B. F., Spingys, C. P., Naveira Garabato, A. C., and Williams, R. G. (2025). The role of mesoscale eddy stirring and microscale turbulence in sustaining biological production in the subtropical gyres. *Global Biogeochemical Cycles*, 39(9):e2024GB008180.

Ohlmann, J. C. (2003). Ocean radiant heating in climate models. *Journal of Climate*, 16(9):1337–1351.

Ohlmann, J. C. and Siegel, D. A. (2000). Ocean radiant heating. Part II: Parameterizing solar radiation transmission through the upper ocean. *Journal of Physical Oceanography*, 30(8):1849–1865.

O'Neill, B. C., Tebaldi, C., van Vuuren, D. P., Eyring, V., Friedlingstein, P., Hurtt, J. C., Kriegler, E., Lamarque, J.-F., Lowe, J. A., Meehl, G., Moss, R., Riahi, K., and Sanderson, B. M. (2016). The scenario model intercomparison project (ScenarioMIP) for CMIP6. *Geoscientific Model Development Discussions*, 9:3461–3482.

O'Reilly, J. E., Maritorena, S., Mitchell, B. G., Siegel, D. A., Carder, K. L., Garver, S. A., Kahru, M., and McClain, C. (1998). Ocean color chlorophyll algorithms for SeaWiFS. *Journal of Geophysical Research: Oceans*, 103(C11):24937–24953.

Parida, C., Lotliker, A. A., Roy, R., and Vinayachandran, P. N. (2022). Radiant heating rate associated with chlorophyll dynamics in upper ocean of southern bay of Bengal: A case study during bay of Bengal boundary layer experiment. *Deep-Sea Research Part II: Topical Studies in Oceanography*, 196:105026.

Park, J.-Y. and Kug, J.-S. (2014). Marine biological feedback associated with indian ocean dipole in a coupled ocean/biogeochemical model. *Climate Dynamics*, 42(1-2):329–343.

Park, J.-Y., Kug, J. S., Bader, J., Rolph, R., and Kwon, M. (2015). Amplified Arctic warming by phytoplankton under greenhouse warming. *Proceedings of the National Academy of Sciences of the United States of America*, 112(19):5921–5926.

Park, J.-Y., Kug, J. S., and Park, Y. G. (2014a). An exploratory modeling study on bio-physical processes associated with ENSO. *Progress in Oceanography*, 124:28–41.

Park, J.-Y., Kug, J.-S., Seo, H., and Bader, J. (2014b). Impact of bio-physical feedbacks on the tropical climate in coupled and uncoupled GCMs. *Climate Dynamics*, 43(7–8):1811–1827.

Patara, L., Vichi, M., Masina, S., Fogli, P. G., and Manzini, E. (2012). Global response to solar radiation absorbed by phytoplankton in a coupled climate model. *Climate Dynamics*, 39(7-8):1951–1968.

Patil, P. A., Adhikari, A., and Menon, H. B. (2023). Bio-optical complexity and radiant heating rates in the coastal waters of eastern Arabian Sea. *Science of the Total Environment*, 884:163838.

Patti, B., Guisande, C., Vergara, A. R., Riveiro, I., Maneiro, I., Barreiro, A., Bonanno, A., Buscaino, G., Cuttitta, A., Basilone, G., and Mazzola, S. (2008). Factors responsible for the differences in satellite-based chlorophyll a concentration between the major global upwelling areas. *Estuarine, Coastal and Shelf Science*, 76(4):775–786.

Paulsen, H., Ilyina, T., Jungclaus, J., Six, K., and Stemmler, I. (2018). Light absorption by marine cyanobacteria affects tropical climate mean state and variability. *Earth System Dynamics*, 9(4):1283–1300.

Paulson, C. A. and Simpson, J. J. (1977). Irradiance measurements in the upper ocean. *Journal of Physical Oceanography*, 7(6):952–956.

Pefanis, V., Losa, S. N., Losch, M., Janout, M. A., and Bracher, A. (2020). Amplified Arctic surface warming and sea ice loss due to phytoplankton and colored dissolved material. *Geophysical Research Letters*, 47(21):e2020GL088795.

Petrik, C. M., Luo, J. Y., Heneghan, R. F., Everett, J. D., Harrison, C. S., and Richardson, A. J. (2022). Assessment and constraint of mesozooplankton in CMIP6 Earth system models. *Global Biogeochemical Cycles*, 36(11):e2021GB007367.

Poole, H. H. and Atkins, W. R. G. (1929). Photo-electric measurements of submarine illumination throughout the year. *Journal of the Marine Biological Association of the United Kingdom*, 16(1):297–324.

Pope, R. M. and Fry, E. S. (1997). Absorption spectrum (380–700 nm) of pure water II. Integrating cavity measurements. *Applied Optics*, 36(33):8710–8723.

Qu, X., Hall, A., Klein, S. A., and Caldwell, P. M. (2014). On the spread of changes in marine low cloud cover in climate model simulations of the 21st century. *Climate Dynamics*, 42(9-10):2603–2626.

Richter, I. (2015). Climate model biases in the eastern tropical oceans: Causes, impacts and ways forward. *Wiley Interdisciplinary Reviews: Climate Change*, 6(3):345–358.

Ryan-Keogh, T. J., Tagliabue, A., and Thomalla, S. J. (2025). Global decline in net primary production underestimated by climate models. *Communications Earth and Environment*, 6(1):975–978.

Seager, R., Cane, M., Henderson, N., Lee, D., Abernathey, R., and Zhang, H. (2019). Strengthening tropical Pacific zonal sea surface temperature gradient consistent with rising greenhouse gases. *Nature Climate Change*, 9(7):517–522.

Sellar, A. A., Jones, C. G., Mulcahy, J. P., Tang, Y., Yool, A., Wiltshire, A., O'Connor, F. M., Stringer, M., Hill, R., Palmiéri, J., Woodward, S., de Mora, L., Kuhlbrodt, T., Rumbold, S. T., Kelley, D. I., Ellis, R., Johnson, C. E., Walton, J., Abraham, N. L., Andrews, M. B., Andrews, T., Archibald, A. T., Berthou, S., Burke, E., Blockley, E., Carslaw, K., Dalvi, M., Edwards, J., Folberth, G. A., Gedney, N., Griffiths, P. T., Harper, A. B., Hendry, M. A., Hewitt, A. J., Johnson, B., Jones, A., Jones, C. D., Keeble, J., Liddicoat, S., Morgenstern, O., Parker, R. J., Predoi, V., Robertson, E., Siahaan, A., Smith, R. S., Swaminathan, R., Woodhouse, M. T., Zeng, G., and Zerroukat, M. (2019). UKESM1: Description and evaluation of the U.K. Earth System Model. *Journal of Advances in Modeling Earth Systems*, 11(12):4513–4558.

Seo, K. H., Frierson, D. M., and Son, J. H. (2014). A mechanism for future changes in Hadley circulation strength in CMIP5 climate change simulations. *Geophysical Research Letters*, 41(14):5251–5258.

Shell, K. M., Frouin, R., Nakamoto, S., and Somerville, R. C. J. (2003). Atmospheric response to solar radiation absorbed by phytoplankton. *Journal of Geophysical Research*, 108(D15):4445.

Shi, Q., Zhang, R.-H., and Tian, F. (2023). Impact of the deep chlorophyll maximum in the equatorial Pacific as revealed in a coupled ocean GCM-ecosystem model. *Journal of Geophysical Research: Oceans*, 128(4):2022JC018631.

Silsbe, G. M., Fox, J., Westberry, T. K., and Halsey, K. H. (2025). Global declines in net primary production in the ocean color era. *Nature Communications*, 16(1):5821.

Six, K. D., Kloster, S., Ilyina, T., Archer, S. D., Zhang, K., and Maier-Reimer, E. (2013). Global warming amplified by reduced sulphur fluxes as a result of ocean acidification. *Nature Climate Change*, 3(11):975–978.

Smith, R. C. and Baker, K. S. (1978). The bio-optical state of ocean waters and remote sensing. *Limnology and Oceanography*, 23(2):247–259.

Song, Q., Zhang, Z., Yu, H., Kato, S., Yang, P., Colarco, P., Remer, L. A., and Ryder, C. L. (2018). Net radiative effects of dust in the tropical North Atlantic based on integrated satellite and in situ observations. *Atmospheric Chemistry and Physics*, 18(15):11303–11322.

Sosik, H. M. and Mitchell, B. G. (1995). Light absorption by phytoplankton, photosynthetic pigments and detritus in the California Current System. *Deep-Sea Research Part I*, 42(10):1717–1748.

Stock, C. A., Dunne, J. P., Fan, S., Ginoux, P., John, J., Krasting, J. P., Laufkötter, C., Paulot, F., and Zadeh, N. (2020). Ocean biogeochemistry in GFDL's Earth System Model 4.1 and its response to increasing atmospheric CO2. *Journal of Advances in Modeling Earth Systems*, 12(10):e2019MS002043.

Sweeney, C., Gnanadesikan, A., Griffies, S. M., Harrison, M. J., Rosati, A. J., and Samuels, B. L. (2005). Impacts of shortwave penetration depth on large-scale ocean circulation and heat transport. *Journal of Physical Oceanography*, 35(6):1103–1119.

Séférian, R., Nabat, P., Michou, M., Saint-Martin, D., Voldoire, A., Colin, J., Decharme, B., Delire, C., Berthet, S., Chevallier, M., Sénési, S., Franchisteguy, L., Vial, J., Mallet, M., Joetzjer, E., Geoffroy, O., Guérémy, J. F., Moine, M. P., Msadek, R., Ribes, A., Rocher, M., Roehrig, R., y Mélia, D. S., Sanchez, E., Terray, L., Valcke, S., Waldman, R., Aumont, O., Bopp, L., Deshayes, J., Éthé, C., and Madec, G. (2019). Evaluation of CNRM Earth System Model, CNRM-ESM2-1: role of earth system processes in present-day and future climate. *Journal of Advances in Modeling Earth Systems*, 11(12):4182–4227.

Tagliabue, A., Kwiatkowski, L., Bopp, L., Butenschön, M., Cheung, W. W. L., Lengaigne, M., and Vialard, J. (2021). Persistent uncertainties in ocean net primary production from CMIP models. *Frontiers in Climate*, 3(11):738224.

Talley, L. D. (2007). Hydrographic Atlas of the World Ocean Circulation Experiment (WOCE), Volume 2: Pacific Ocean.

Talley, L. D., Pickard, G. L., Emery, W. J., and Swift, J. H. (2011). *Descriptive Physical Oceanography: An Introduction*. Academic Press, Boston, 6 edition.

Thomas, A., Brickley, P., and Weatherbee, R. (2009). Interannual variability in chlorophyll concentrations in eastern boundary upwelling systems. *Progress in Oceanography*, 83(1-4):386–392.

Tian, F. and Zhang, R.-H. (2023). Increasing shortwave penetration through the bottom of the oceanic mixed layer in a warmer climate. *Journal of Geophysical Research: Oceans*, 128(7):e2022JC019587.

Tian, F., Zhang, R.-H., and Wang, X. (2021a). Coupling ocean–atmosphere intensity determines ocean chlorophyll-induced SST change in the tropical Pacific. *Climate Dynamics*, 56(11-12):3775–3795.

Tian, F., Zhang, R.-H., Wang, X., and Zhi, H. (2021b). Rectified effects of interannual chlorophyll variability on the tropical Pacific climate revealed by a hybrid coupled physics-biology model. *Journal of Geophysical Research: Oceans*, 126(6):e2021JC017263.

Timmermann, A. and Jin, F. (2002). Phytoplankton influences on tropical climate. *Geophysical Research Letters*, 29(23):2002GL015434.

Trenberth, K. E. and Fasullo, J. T. (2010). Tracking Earth's energy. *Science*, 328(5976):316–317.

Trenberth, K. E., Fasullo, J. T., and Balmaseda, M. A. (2014). Earth's energy imbalance. *Journal of Climate*, 27(9):3129–3144.

Turner, A. G., Joshi, M., Robertson, E. S., and Woolnough, S. J. (2012). The effect of Arabian Sea optical properties on SST biases and the South Asian summer monsoon in a coupled GCM. *Climate Dynamics*, 39(3-4):811–826.

Wang, X., Murtugudde, R., Hackert, E. C., and Marañón, E. (2013). Phytoplankton carbon and chlorophyll distributions in the equatorial Pacific and Atlantic: A basin-scale comparative study. *Journal of Marine Systems*, 109–110:138–148.

Watt-Meyer, O., Brenowitz, N. D., Clark, S. K., Henn, B., Kwa, A., McGibbon, J., Perkins, W. A., Harris, L., and Bretherton, C. S. (2024). Neural network parameterization of subgrid-scale physics from a realistic geography global storm-resolving simulation. *Journal of Advances in Modeling Earth Systems*, 16(2):e2023MS003668.

Wetzel, P., Maier-Reimer, E., Botzet, M., Jungclaus, J., Keenlyside, N., and Latif, M. (2006). Effects of ocean biology on the penetrative radiation in a coupled climate model. *Journal of Climate*, 19(16):3973–3987.

Whalen, C. B., Talley, L. D., and MacKinnon, J. A. (2012). Spatial and temporal variability of global ocean mixing inferred from Argo profiles. *Geophysical Research Letters*, 39(18):L18612.

Witte, C. R., Subramaniam, A., and Zappa, C. J. (2024). An improved bio-physical parameterization for ocean radiant heating in conditions of near-surface stratification. *Journal of Geophysical Research: Oceans*, 129(11):2024JC021049.

Wood, R. (2012). Stratocumulus clouds. *Monthly Weather Review*, 140(8):2373–2423.

Yang, K., Meyer, A., Strutton, P. G., and Fischer, A. M. (2023). Global trends of fronts and chlorophyll in a warming ocean. *Communications Earth and Environment*, 4(1):489.

Yasunaka, S., Ono, T., Sasaoka, K., and Sato, K. (2022). Global distribution and variability of subsurface chlorophyll a concentrations. *Ocean Science*, 18(1):255–268.

Yool, A., Palmiéri, J., Jones, C. G., Mora, L. D., Kuhlbrodt, T., Popova, E. E., Nurser, A. J. G., Hirschi, J., Blaker, A. T., Coward, A. C., Blockley, E. W., and Sellar, A. A. (2021). Evaluating the physical and biogeochemical state of the global ocean component of UKESM1 in CMIP6 historical simulations. *Geoscientific Model Development*, 14(6):3437–3472.

Yool, A., Popova, E. E., and Anderson, T. R. (2011). MEDUSA-1.0: a new intermediate complexity plankton ecosystem model for the global domain. *Geoscientific Model Development*, 4(2):381–417.

Yool, A., Popova, E. E., and Anderson, T. R. (2013). MEDUSA-2.0: An intermediate complexity biogeochemical model of the marine carbon cycle for climate change and ocean acidification studies. *Geoscientific Model Development*, 6(5):1767–1811.

Yu, J.-Y. and Mechoso, C. R. (1999). Links between annual variations of Peruvian stratocumulus clouds and of SST in the eastern equatorial Pacific. *Journal of Climate*, 12(11):3305–3318.

Yuval, J. and O'Gorman, P. A. (2020). Stable machine-learning parameterization of subgrid processes for climate modeling at a range of resolutions. *Nature Communications*, 11:3295.

Zhang, M. and Bretherton, C. (2008). Mechanisms of low cloud-climate feedback in idealized single-column simulations with the Community Atmospheric Model, version 3 (CAM3). *Journal of Climate*, 21(18):4859–4878.

Zhang, Q., Liu, B., Li, S., and Zhou, T. (2023). Understanding models' global sea surface temperature bias in mean state: From CMIP5 to CMIP6. *Geophysical Research Letters*, 50(4):e2022GL100888.

Zhang, R.-H. (2015). A hybrid coupled model for the Pacific ocean–atmosphere system. Part I: Description and basic performance. *Advances in Atmospheric Sciences*, 32(3):301—-318.

Zhang, R.-H., Busalacchi, A. J., Wang, X., Ballabrera-Poy, J., Murtugudde, R. G., Hackert, E. C., and Chen, D. (2009). Role of ocean biology-induced climate feedback in the modulation of El Niño-Southern Oscillation. *Geophysical Research Letters*, 36(3):L03708.

Zhang, R.-H., Chen, D., and Wang, G. (2011). Using satellite ocean color data to derive an empirical model for the penetration depth of solar radiation (Hp) in the Tropical Pacific ocean. *Journal of Atmospheric and Oceanic Technology*, 28(7):944–965.

Zhang, R.-H., Tian, F., and Wang, X. (2018a). A new hybrid coupled model of atmosphere, ocean physics, and ocean biogeochemistry to represent biogeophysical feedback effects in the tropical Pacific. *Journal of Advances in Modeling Earth Systems*, 10(8):1901–1923.

Zhang, R.-H., Tian, F., and Wang, X. (2018b). Ocean chlorophyll-induced heating feedbacks on ENSO in a coupled ocean physics-biology model forced by prescribed wind anomalies. *Journal of Climate*, 31(5):1811–1832.

Zhang, R.-H., Tian, F., Zhi, H., and Kang, X. (2019). Observed structural relationships between ocean chlorophyll variability and its heating effects on the ENSO. *Climate Dynamics*, 53(9-10):5165–5186.

Zhao, H., Manizza, M., Lozier, M. S., and Cassar, N. (2025). Greener green and bluer blue: Ocean poleward greening over the past two decades. *Science*, 388(6753):1337–1340.

Zhao, J., Zhang, Y., Bie, S., Bilsback, K. R., Pierce, J. R., and Chen, Y. (2024). Changes in global DMS production driven by increased CO2 levels and its impact on radiative forcing. *npj Climate and Atmospheric Science*, 7(1):18.